UNIVERSITEIT GENT

FACULTEIT DIERGENEESKUNDE
approved by EAEVE

Thoracic cardiovascular CT angiography in dogs

Procedure, anatomical and functional assessment and impact of anesthetic protocol

RANDI DREES

Thesis submitted in fulfilment of the requirements for the degree of Doctor in Veterinary Science (PhD), Faculty of Veterinary Medicine, Ghent University

2015

Promotor: Prof. Dr. J.H. Saunders

Department of Veterinary Medical Imaging
Faculty of Veterinary Medicine
Ghent University

Funding sources:
The project was supported by the Clinical and Translational Science Award (CTSA) program, previously through the National Center for Research Resources (NCRR) grant 1UL1RR025011, and now by the NIH National Center for Advancing Translational Sciences (NCATS), grant 9U54TR000021 and Dr. Johnson was supported by the Clinical and Translational Science Award (CTSA) program, through the NIH National Center for Advancing Translational Sciences (NCATS), grant UL1TR000427.

TABLE OF CONTENTS

TABLE OF CONTENTS 5
LIST OF ABBREVIATIONS 9
CHAPTER 1 13
Computed Tomographic Angiography (CTA) of The Thoracic Cardiovascular System In Companion Animals 13
Summary 14
Introduction 15
General considerations regarding CT units in cardiovascular imaging 17
ECG-gated image acquisition in cardiac CT 21
Image Contrast 23
Contrast medium administration 25
Methodology for angiographic applications 25
Factors affecting contrast enhancement 26
Calculation of the arrival time of the bolus in the vascular bed 32
Digital imaging software 35
Clinical considerations in thoracic MDCTA protocols in companion animals 35
References 47
CHAPTER 2 61
Scientific aims 61
CHAPTER 3 65
Pulmonary angiography with 64 Multidetector Row Computed Tomography in Normal Dogs 65

Table of contents

Summary....66
Introduction....67
Material and methods:....68
Results....72
Discussion....79
References....84
CHAPTER 4....89
64-Multi-Detector Computed Tomographic Angiography of the Canine Coronary Arteries....89
Summary....90
Introduction....91
Material and methods....93
Results....98
Discussion....110
References:....116
CHAPTER 5....121
Effect of two different anesthetic protocols on 64-MDCT coronary angiography in dogs....121
Summary....122
Introduction....124
Material and methods....126
Results....132
Discussion....141
References....149
CHAPTER 6....155
Quantitative planar and volumetric cardiac measurements using 64 MDCT and 3T MRI versus standard 2D and M-mode echocardiography: Does anesthetic protocol matter?....155
Summary....156

Table of contents

Introduction 158
Material and Methods 160
Results 173
Discussion 197
References 206
CHAPTER 7 229
General discussion 229
References 247
Summary 257
Samenvatting 263
CURRICULUM VITAE 269
Publications 272
Oral presentations at national or international meetings 277
thank you note 282

List of abbreviations

LIST OF ABBREVIATIONS

ALARA	as low as reasonable achievable
Ao	aorta
AoDiam	aortic diameter
AV	right azygos vein
bpm	beats per minutes
B-Mode	brightness mode
BT	brachiocephalic trunk
BW	bandwidth
C	carina
CT	computed tomography
CTA	computed tomographic angiography
CrVC	cranial vena cava
CVC	caudal vena cava
dAO	descending aorta
dFOV	display field of view
E	esophagus
ECG	electrocardiogram
EDV	end diastolic volume
EF	ejection fraction
epiEDV	epicardial end diastolic left ventricular volume
epiESV	epicardial end systolic left ventricular volume
ESV	end systolic volume
ETL	echo train length
ECG	electrocardiogram
FOV	field of view
FS	fractional shortening
h	hour
HU	Hounsfield Units
i.v. or IV	intravenous
IVS	interventricular septum

IVSd	diastolic interventricular septal thickness
IVSs	systolic interventricular septal thickness
kVP	kilovolt peak
L	left
LA	left atrium
LADiam	left atrial diameter
Lau	left auricle
lb/in^2	pounds per square inch
LIVP	left interventricular paraconal branch of the left coronary artery
LcdPV	left caudal pulmonary vein
LCA	left coronary artery
LCX	left circumflex coronary artery branch
LLOA	lower level of agreement
LPA	left pulmonary artery
LS	left subclavian artery; or septal branch of the left coronary artery
LV	left ventricle
LVEDV	left ventricular end diastolic volume
LVEF	left ventricular ejection fraction
LVESV	left ventricular end systolic volume
LVIDd	diastolic left ventricular internal diameter
LVIDs	systolic left ventricular internal diameter
LVM	left ventricular mass
LVmassD	left ventricular end diastolic mass
LVmassS	left ventricular end systolic mass
LVPWd	diastolic left ventricular posterior wall thickness
LVPWs	systolic left ventricular posterior wall thickness
LVSV	left ventricular stroke volume
mA	milliampere
mm	millimeter
M-Mode	motion-mode
MDCT	multidetector-row computed tomography

MDCTA	multidetector-row computed tomographic angiography
mgI	milligram iodine
mi	minute
MIP	maximum intensity reconstruciton
ml	milliliter
MPA	main pulmonary artery
MPR	multiplanar reconstruction
NEX	number of excitations
PA	pulmonary artery
PADIAM	pulmonary artery diameter
PSI	pounds per square inch
PV	pulmonary vein
R	right
RA	right atrium
ROI	region of interest
ROIs	regions of interest
RPA	right pulmonary artery
RV	right ventricle
RVEF	right ventricular ejection fraction
RVEDV	right ventricular end diastolic volume
RVESV	right ventricular end systolic volume
RVSV	right ventricular stroke volume
RVOT	right ventricular outflow tract
s	second
SD	standard deviation
SD-CTA	single detector computed tomographic angiography
sFOV	scan field of view
SSFP	steady state free precision
SV	stroke volume
Tarr	time to arrival
TE	time to echo
Tpeak	time to peak
TR	time to repetition

List of abbreviations

ULOA	upper level of agreement
RCa	right coronary artery
RcdPV	right caudal pulmonary vein
RPA	right pulmonary artery
RV	right ventricle
RVEDV	right ventricular end diastolic volume
RVESV	right ventricular end systolic volume
VPS	views per second
2D	two dimensional
3D	three dimensional

CHAPTER 1

Computed Tomographic Angiography (CTA) of The Thoracic Cardiovascular System In Companion Animals

Randi Drees[1], Christopher J François[2], Jimmy H Saunders[3]

[1]Department of Veterinary Clinical Sciences and Services, Royal Veterinary College, University of London, North Mymms, Hatfield, Herts AL9 7TA, UK;
[2]UW-Madison, School of Medicine and Public Health, Department of Radiology, 600 Highland Avenue, Madison, WI 53792, USA;
[3]UGent, Faculty of Veterinary Medicine, Salisburylaan 133, 9820 Merelbeke, Belgium

Adapted from: *American Journal of Veterinary Research* 2008;69:631-638.

Summary

Computed tomographic angiography (CTA) of the thoracic cardiovascular system is offering new diagnostic opportunities in companion animal patients with the increasing availability of multidetector-row computed tomographic (MDCT) units in veterinary facilities. Optimal investigation of the systemic, pulmonary and coronary circulation provides unique challenges due to the constant movement of the heart, the small size of several of the structures of interest and the dependence of angiographic quality on various contrast bolus design and patient factors. Technical and practical aspects of thoracic cardiovascular CTA are reviewed in light of the currently available veterinary literature and future opportunities given utilizing MDCT in companion animal patients with suspected thoracic cardiovascular disease.

Introduction

Until recently, computed tomography (CT) applications for the thorax were mostly limited to morphologic evaluation of the chest wall, mediastinum, vessels and lung parenchyma for differentiating normal from pathological conditions in companion animals[1-9]. With the increased availability of multi-detector-row CT (MDCT) scanners with up to 320 detector rows that allow image acquisition with high temporal and spatial resolution, the utilization of this modality will likely rise for evaluating the thoracic cardiovascular system in companion animals and has been used in initial case reports and studies[10-24].

Thoracic cardiovascular structures of clinical interest in companion animals that may potentially benefit from the evaluation using MDCT are the heart including the coronary arteries, aorta, cranial and caudal vena cava and pulmonary arteries. Many of these structures are considerably smaller in the companion animal patient compared to the adult human patient and spatial resolution has to be optimized similar to pediatric conditions.[11, 12, 25, 26]

It remains to be proven which clinical diagnostic merits will be generated by the use of CT over traditional methods including standard radiographs, echocardiography, standard selective or nonselective angiography and scintigraphic techniques for cardiovascular imaging in companion animal patients, acknowledging that companion animal patients will likely have to be anesthetized or heavily sedated to undergo these CT exams. Sedation or anesthesia may potentially alter

the physiologic pattern seen in currently used awake imaging techniques, specifically echocardiography. In addition, the normal heart rate of companion animals ranges between 80-120bpm, which is considerably higher than the adult human target heart rate of less than 65bpm during image acquisition. This may pose similar challenges with regards to the temporal resolution as that seen in children[25-28].

This manuscript aims to review the technical and practical challenges and opportunities encountered in cross-sectional cardiovascular imaging using MDCT in companion animals.

General considerations regarding CT units in cardiovascular imaging

CT units and parameters of image acquisition

Almost all modern CT units utilize the rotate-rotate geometry that is the hallmark of 3rd generation CT and which was enabled by introduction of the slip ring technology[29, 30]. Third generation CT units consist of a rotating gantry on which an x-ray source is mounted opposite to x-ray detectors. As the patient is moved through the gantry on the patient table, a helical data set is acquired. This has allowed for generation of data sets with higher temporal and spatial resolution than the older generation CTs could deliver[31].

Addition of the multi-detector-row feature has furthered those advantages over single-detector-row CT units that still find application in veterinary medicine due to their relatively low cost in acquisition and maintenance[32]. For example, using a 64-MDCT unit with a detector width of 0.625mm, images over 40mm length of the patient will be acquired during one gantry rotation (0.625mm x 64 = 40mm), where as on a 16-MDCT unit this would only be a length of 10mm (0.625mmx 16 = 10mm)[29, 33]. Even though initial studies of cardiac MDCT were conducted using 4 detector-row units, the current state of the art in human cardiopulmonary CTA is performed using 64- to 320 detector-row units[34-37].

The 360° gantry (or tube) rotation time is approximating 5 rotations per second (0.2s rotation time) in modern MDCT units. Additionally newer reconstruction algorithms allow for generation of high quality

images with a data set acquired from less than a 360° gantry rotation (usually 180° plus the fan angle), further increasing the speed of data acquisition[29].

A newer approach to increase the temporal resolution introduced dual source CT units[38, 39]. In this configuration two x-ray sources and their respective opposing detectors are mounted 90° apart on the gantry. This can further half the degrees of gantry rotation or tube rotation time needed to acquire a similar amount of data compared to using a single source unit and may reduce the need for beta blockers to reduce the heart rate and allow for non-gated acquisitions in cardiovascular application in people and companion animals.[29, 40, 41]

In helical CT scanning, the "pitch" determines the speed at which the patient on the table will be moved through the rotating gantry. It is defined as patient table travel per complete gantry rotation and divided by the collimation of the x-ray beam in the z-axis. For multi-detector-row units pitch is calculated by multiplying the number of active channels by the width of the detector surface assigned to each channel[29, 31]. This parameter is selected prior to the scan and for cardiac applications a higher heart rate necessitates a higher pitch to avoid motion artifact.[29, 37, 42]

Helical acquisition commonly used retrospectively EKG gated exams in human patients with physiological high heart rates, such as pediatric patients, or patients with tachyarrhytmias and has been applied in dogs[12, 43]; whereas axial acquisition used in prospectively EKG gated

exams has been shown to deliver accurate and comparable results at a much lower radiation dose in adult human patients with an upper limit heart rate of 75bpm[44]. The use of ionizing radiation is a specific concern in human and especially pediatric computed tomography[45] and may need further investigation as these exams become more commonplace in companion animal patients, as the use of x-rays is to be kept as low as possible (ALARA).

The matrix size, detector geometry and spatial reconstruction algorithm determine spatial resolution[29, 33].

The matrix is commonly set to 512x512 pixels inherently to the software. The scan field of view (sFOV) is usually defined to the maximum achievable by the length of the detector array along the x/y-plane or fan angle to enable for retrospective reconstructions from the entire scan volume. Tight setting of the display field of view (dFOV) around the anatomy in question will increase the in-plane resolution by minimizing the size of the individual pixels and reducing volume-averaging artifact[29, 33].

The external thoracic boundaries are commonly chosen for evaluation of the pulmonary arteries and a reduction of the dFOV to include the heart and proximal portion of the great vessels only for cardiac applications such as coronary artery evaluation will increase the in-plane resolution for these small structures.

In MDCT units, the lower limit of slice thickness depends on the height of the individual detector rows along the z-axis, commonly ranging from 0.5-1.25mm, where binning of detectors in one channel can be

used to vary slice thickness independent of detector height. Slice thickness determines the size of the voxel and hence the third dimension of the spatial resolution: the thinner the slice thickness, the higher the spatial resolution in the z-direction[29, 31].

Regardless of the CT unit used, trade off to the thin slice thickness is always increased image noise as less photons contribute to the image data composition compared to thicker slice thickness with unchanged mA settings. This may be balanced by increasing the tube output resulting in higher radiation dose to the patient[29, 46].

The raw data collected in the detectors can be spatially reconstructed with different strategies. Filtered back-projection, Fourier-based reconstruction kernels or filters as well as iterative reconstruction techniques allow for increased spatial resolution compared to previously used simple back-projection strategies. Newer iterative reconstruction algorithms can also be used to improve the signal to noise ratio from low dose protocols eliminating need for increased patient dose[29, 47]. On standard units these techniques are usually inherent to the software installed by the manufacturer and may not be adjustable on the user surface.

Magnetic resonance imaging is the alternative cross-sectional modality to assess cardiac morphology and function. Different to CTA no radiation is used to generate the image but the patient is placed in a strong magnetic field (typically 1.5-3T) and protons inherent in the tissues and intravascular fluid are used to generate images referenced to the patients ECG. Different imaging sequences are used to highlight

different tissue or blood volume and flow characteristics with or without the use of MRI specific contrast media. Typical sequences for evaluation of the myocardium are balanced steady state free precession sequences that bear vendor specific names and are acquired in different planes aligned similar to the echocardiographic planes, capturing images of the heart throughout the cardiac cycle focusing on a specific section of the anatomy or including the entire heart. As different planes are acquired different to the single transverse acquisition in CTA the MRI typically takes longer then the CTA exam, total length of the exam depending on number of sequences used. Also, veterinary patients need to undergo general anesthesia to lay still on the table during the longer exam time and the noise generated by the MRI unit during the sequence acquisition, where as for CTA sedation can be possible.

ECG-gated image acquisition in cardiac CT

As the heart is constantly moving throughout the cardiac cycle, ECG-gating techniques are required to link the image acquisition to a specific phase in the cardiac cycle. The ECG leads are placed on the companion animal patient's footpads or chest and the CT unit registers the reading, usually the ECG trace is also displayed on the operator console.

Two types of cardiac ECG gating are used: prospective and retrospective ECG gating[29, 31, 48].

In prospective ECG gating, image acquisition is only triggered during a certain phase of the cardiac cycle, commonly in the end diastolic phase where the heart is mostly motionless (Figure 1).

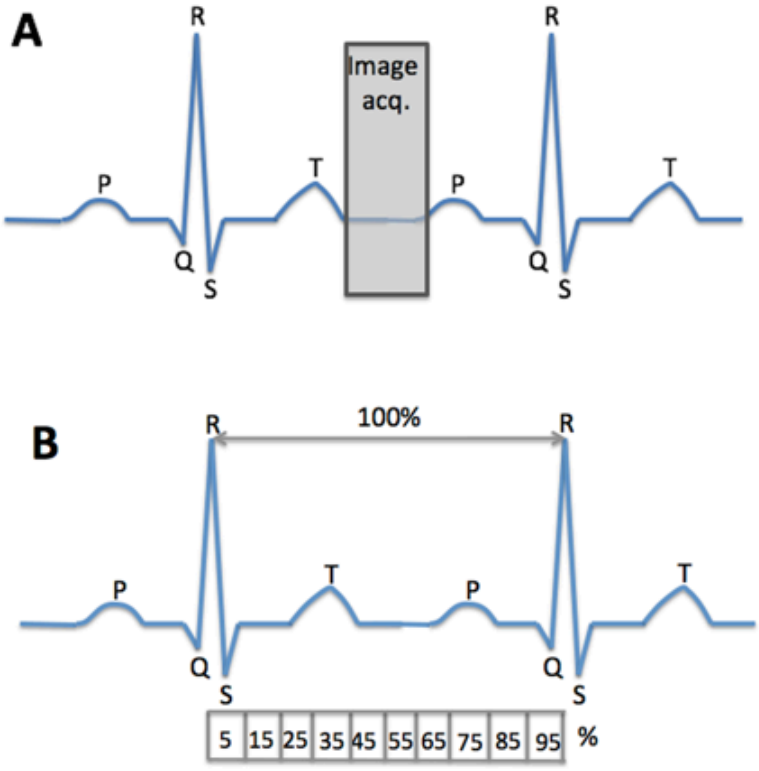

Figure 1: ECG-gating strategies in cardiac CT: Using prospective gating (A) images are acquired over a predefined portion of one or more cardiac cycles, commonly end diastolic. Using retrospective gating (B) images are acquired over one or several full cardiac cycles and are retrospectively segmented into different phases of the cycle (commonly 5-10% intervals).

This is favored for morphological evaluations as adequate image quality is provided at a lower radiation dose relative to retrospective ECG gating approaches[44]. The shortcoming of prospective gating is that not a full cycle dataset is acquired. In patients with an irregular heart rhythm prospective gating may lead to acquisition of an incomplete data set,

that may necessitate repeating the scan and contrast injection[31]. Furthermore, in patients with higher heart rates, the optimal phase of the cardiac cycle to image the coronary arteries may not occur during diastole or may be different for different coronary arteries, then a retrospective approach may be preferred[44, 40].

In retrospective ECG gating, image acquisition is triggered over the whole length of one or more cardiac cycles[36]. The data set can then retrospectively be separated out into different phases of the cardiac cycle (usually in 5-10% intervals) and cardiac function and as well morphology can be evaluated in the different phases of the cardiac cycle or images be displayed to show the beating heart over the entire cardiac cycle (Figure 1). As these retrospectively gated data sets contain information in the x-, y- and z- axis (3D) of the patient as well a temporal component, they are described as 4D studies and require specific viewing software to display the time dimensional component[49].

The disadvantage of retrospective gating is a higher radiation dose delivered to the patient compared to prospective gating[44]. Newer technologies allow for dose modulation during the cardiac cycle where the regular mA (200mA) is used during the end diastole but reduced throughout the remainder of the cardiac cycle[31, 50].

Image Contrast

Iodine is most commonly used as intravascular contrast medium in cardiothoracic CT. The amount of iodine present in the organ or vessel determines the attenuation value depicted in the image[29]. Generally the

magnitude of intravascular contrast is considered adequate between 250-300HU but this remains to be under discussion especially for coronary imaging in humans as attenuation >300HU may obscure calcified plaques[51, 52].

Newer technologies take advantage of the predominance of the photoelectric effect in lower kVp settings in acquiring images using two kVp settings (commonly 80/140 or 100/140kVp) at the same time using dual source units or rapid kilovoltage switching in single source units. This is used to enable material decomposition, that is the analysis of scanned tissue within one voxel based on the different interactions at different kilovoltage settings and is used to identify calcium components, which can be important in coronary plaque imaging[53, 54].

Lower kVp settings may further be exploited especially in small companion animal patients to reduce radiation dose and increase contrast due to the predominance of the photoelectric effect.

Where the HU are inherent to the acquired data set, spatial reconstruction kernels or algorithms can be chosen by the operator to favor the display of certain structures such as lung, vessels or parenchyma of the heart. These reconstruction algorithms commonly have vendor specific intuitive names such as “lung”, “detail” etc[29, 33]; for cardiovascular applications a medium frequency reconstruction kernel is commonly chosen. On the viewing station the display can then be further adjusted by setting the window width and window level.

Contrast medium administration

Methodology for angiographic applications

In standard CT applications, iodinated contrast medium at a dose of 600-800mgI/kg is used to enhance parenchyma and vessels within the first 3min after intravenous injection[55].

For angiographic applications iodinated contrast medium is used to opacify the vascular bed in question and image acquisition has to be timed with bolus arrival and duration in that specific vascular bed. For thoracic exams commonly either the right side of the heart and pulmonary arterial tree or the left side of the heart including the coronary arteries or aorta is to be investigated in separate exams. In human medicine, a newer approach termed 'triple rule out' exam, aims to investigate the coronary arteries, aorta, pulmonary arteries and adjacent intrathoracic structures with a single exam and contrast injection in patients with acute chest pain but the usefulness of this approach is still discussed[56, 57].

The bolus of contrast medium is reportedly ideally injected through the right cephalic vein, which results in fewer artifacts compared to the left vein in humans[58]. It will then move through the afferent cranial vena cava into the right atrium and ventricle, through the main pulmonary artery and its branches, capillary bed and return through the pulmonary veins to the left atrium and ventricle before entering the systemic circulation in the first pass. Even though a defined bolus is injected, admixture of the contrast medium with the blood in the

vascular system will cause dilution that increases after the first pass and flatten the bolus peak further downstream. The advancement of the contrast bolus in the vascular system is governed by the hemodynamic state of the patient but the rapidly automatically injected bolus can disturb the given hemodynamics in the system especially in the venous bed starting at the injection site[51].

Factors affecting contrast enhancement

Based on extensive experimental work in animal and human subjects, the principal factors affecting contrast enhancement in CT are the patient, the contrast medium and the specific CT-scan parameters[51, 59-63].

The main patient factors to consider for optimal contrast enhancement are body size (weight and length) and cardiac output (circulation time). Other factors such as age, gender, venous access, renal function and pathological conditions such as hepatic cirrhosis and portal hypertension have been investigated in human patients[60] but have only received limited attention in companion animals[20].

Body weight greatly influences the magnitude of vascular and parenchymal contrast enhancement. Using a fixed dose of contrast medium, the magnitude of contrast enhancement will decrease proportionally with the patient's weight. Often a simple linear 1:1 scale is used for calculation of the dose of iodine given for a certain body weight which may be of limited accuracy specifically in patients with obese body habitus as the body fat is not contributing to dilute the

contrast medium in the blood pool and excess amount of contrast medium may be given in obese patients[51].

Body surface area as used in chemotherapeutic dosing in people and companion animals as well as lean body weight were determined better adjustment parameters than total body weight in people achieving more consistent contrast enhancement with less inter-patient variability[62].

The cardiovascular output determines the circulation time (how fast the contrast bolus is advanced through the system). Time of contrast bolus arrival (Tarr) and time to peak enhancement (Tpeak) in all organs are linearly correlated with cardiac output. Hence decreased cardiac output results in delayed contrast arrival and peak enhancement as well as slower clearance of the contrast medium from the circulation resulting in a need to individualize scan delay for each organ or vascular bed using a test bolus or bolus tracking technique (see further) [51, 64].

Contrast medium factors to consider are injection duration (contrast medium volume divided by the injection rate), injection rate, injection bolus shaping, contrast medium concentration and saline flush.

Injection duration: the injection duration is critical for magnitude of contrast enhancement. At a given injection rate, a longer injection duration results in a larger contrast volume and larger iodine dose delivered, it will therefore increase the magnitude of contrast enhancement proportionally to injection duration[51]. The injection

duration is the most important factor to determine scan timing because Tpeak in an organ or vessel is directly related to the injection duration: increased injection duration will delay the time to maximum enhancement, consequentially Tpeak will increase and a longer scan delay may have to be applied. Prolonged injection durations are used to maintain enhancement throughout the entire scan duration and can be used when a larger dose of iodine is needed (i.e. large patient) but the injection rate and contrast medium concentration cannot be increased. Alternatively, shorter injection duration (low volume or high injection rate) will result in earlier arterial peak and parenchymal enhancement[51].

The optimal injection duration is determined by the scanning conditions and the clinical purpose of the exam.

Injection rate: When increasing the injection rate (ml/s) with fixed injection duration the total volume of contrast will increase as will the magnitude of vascular and parenchymal enhancement. Using a fixed volume of contrast and increasing the injection rate, the injection duration will be shortened as well as the time to peak enhancement.[51] High injection rates also result in longer intervals between arterial and parenchymal enhancement that could be utilized for multiphasic imaging. The increased injection rate reduces the temporal window available for CT scanning and precise timing as well as fast image acquisition provided by MDCT units are needed. High injection rates may also cause retrograde reflux of contrast medium through the right atrium into the caudal vena cava even in the absence of cardiac disease

that may induce artifacts. Commonly used injection rates for the thoracic cardiovascular system in people range between 2-5ml/s, somewhat depending on catheter bore size[51, 62, 64], where the higher end rates may not be applicable in small companion animal patients.

Injection bolus shaping: For conventional CT exams, an i.v. bolus of 100% contrast medium is commonly used, applied with an automated injector, termed constant or uniphasic rate injection. Adjusting the shape of the bolus profile can be achieved by utilizing a biphasic injection rate. In this case the automated injector is programmed to deliver a fast followed by a slow constant-rate injection. This will prolong the injection duration without increasing the contrast medium volume. A variation to this protocol is to utilize two different contrast medium concentrations: undiluted higher concentrated followed by the injection of lower concentrated or diluted contrast medium. The latter is commonly achieved using simultaneous injection of saline and undiluted contrast from a dual barrel automatic injector. This has been proven useful in cardiac CTA, improving right ventricular chamber enhancement and reducing the artifact from the dense undiluted contrast medium bolus tail in the cranial vena cava[51, 64].

The intravascular bolus profile will also be differently shaped depending on the bolus design: the uniphasic-rate injection will cause the time enhancement curve to progressively increase and peak shortly after completion of the injection without a true plateau phase. The biphasic injection on the other hand results in a double peaked arterial contrast enhancement. A more advanced technique uses a multiphasic,

exponentially decelerated injection to further improve the uniformity of the bolus profile[65].

Concentration of the contrast medium: With MDCT, high iodine concentrations (>350mgI/ml) are commonly used, reflecting the need for a high injection rate to achieve good arterial contrast. Using a fixed injection volume, rate and duration, a higher concentrated contrast medium will result in a higher peak contrast enhancement and a wider temporal window for the CT scan at a given enhancement level. Also, it may allow using a lower volume, which may be advantageous in smaller patients but then only a shorter temporal window will be available. Overall, lower concentrated contrast media have however lower viscosity and allow for faster injection and may be useful if no saline flush is used as less high density artifact may result from the tail of the bolus in the cranial vena cava[64].

Saline flush: Using a saline flush will advance the tail of the injected contrast medium bolus into the central blood volume but also flush the contrast medium out of the injection tubing and peripheral veins that would otherwise remain unused or cause artifact. The bolus geometry will be improved as the bolus is kept 'tighter' with less dispersion of intravascular contrast medium. Also, increased hydration of the patient may reduce contrast-induced nephrotoxicity. The maximal contrast savings are equal to the volume of contrast medium retained in the injector tubing (±10ml) and the volume that remains in the peripheral venous space between the cephalic vein and cranial vena cava (12-20ml in humans) which is patient size dependent. Distinct values have not

been established in companion animals but are expected to be at the lower level and below volumes reported in humans (estimated total of 20-30ml)[17, 64].

A practical formula to calculate the needed injection volume in MDCT angiography is given in the following: Contrast volume = (scan time + diagnostic delay) x injection rate. A diagnostic delay or time to peak enhancement of 4-6 seconds for the main pulmonary artery[11], 5 seconds for the right pulmonary artery[13] and 6-11 seconds for the base of the aorta has been reported in dogs[11, 12] so that a typical diagnostic of 4-6 seconds may ensure sufficient contrast of the entire vasculature of interest.

Nonionic contrast media may be preferred in companion animals based on the lower incidence of adverse reactions as well as alterations in hemodynamic and biochemical parameters.[66-69] Where as an iodine dose of 600-800mgI/kg has been advised companion animal patients[55] and anecdotally a maximal injection volume of 60ml is used in some institutions, no maximal dose or volume limit is available for companion animals. The LD50 for intravenous injection of iohexol is reported at 24.2gI/kg in mice and 15.0gI/kg in rats.[70] Individual patient considerations with regards to the hemodynamic and renal function are recommended to determine the individual maximal contrast medium dose and volume, also with regards to possible repeat injections.

CT scanning factors such as scan duration, scan direction, multiphasic acquisitions and inherent scan delays play a significant role in enabling to acquire the contrast enhanced images in the temporal window given by the bolus chosen and those need to be taken into consideration when designing the contrast bolus. Once the scan field is determined based on acquired localizer images, the scan duration is usually displayed on the user surface and the injection duration will need to be adjusted to maintain adequate enhancement during the scan time. Usually CT scans are acquired in the direction analogous to the contrast bolus propagation, exceptions are made in longer scan durations given with low-number-detector-row units where breathing motion may not be avoided such as in pulmonary CTA, then a scan direction from caudal to cranial would be preferable[51, 64].

Calculation of the arrival time of the bolus in the vascular bed

The arrival time of the bolus in the vascular bed of interest depends on the individual patients' circulatory time as discussed above. Two basic methods are used to individualize the bolus delivery: test bolus injection or bolus tracking methods[54]. Both measure the time to arrival (Tarr) or time to peak enhancement (Tpeak) over a preselected region of interest chosen by the operator. A slice including a representative vessel is repetitively scanned (cine scan) following the injection of contrast medium and contrast enhancement can be visually traced or measured over time by placing a region of interest (ROI) over the vessel of interest.

For the test bolus method, a small bolus, in companion animals often 1/3 of the planned dose for the diagnostic scan or a minimum of 2-4ml is used to determine Tarr and Tpeak, lower doses may be possible. Based on the speed of the image acquisition of the cine scan, Tarr or Tpeak can be calculated and the resulting time will be used as a scan delay for diagnostic acquisition after injecting the full bolus. The test bolus method provides additional testing of the integrity of the venous access system. If a very short injection duration (<10s) is used the test bolus technique may be more appropriate as there may not be sufficient time for the bolus tracking method to trigger the scan during peak enhancement. The smaller volume of the test bolus will however have a slightly different bolus profile than the larger volume of the diagnostic bolus[51, 64, 71].

For the bolus tracking methods the full diagnostic bolus is injected and either manually or at a set threshold, the diagnostic scan is triggered (Figure 2).

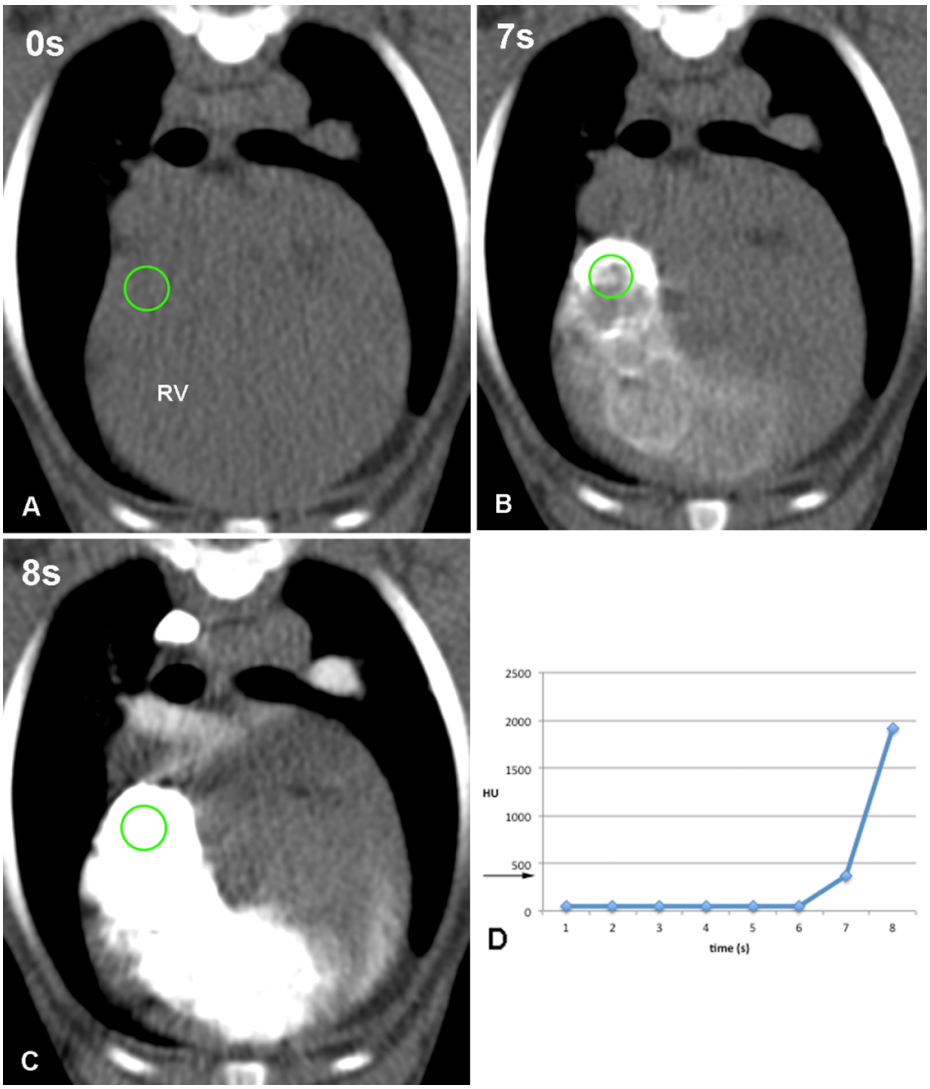

Figure 2: Scan timing can either be performed using a test bolus or (semi-) automated bolus tracking software. Below the contrast bolus arrival is shown in right ventricle of a dog (0, 7, 8s after contrast injection, A-C) and tracking of the respective Hounsfield units over the cine scan is shown in the diagram (D). Immediate scan trigger after the enhancement has reached a predefined threshold value (black arrow) would depict the bolus highlighting the pulmonary arterial system, delaying scan trigger would depict the bolus highlighting the left heart and aorta. RV = Right ventricle; HU = Hounsfield units. Contrast bolus: 15ml 300mgI/ml followed by 5ml saline flush, 2ml/s at 325PSI.

These methods are considered more efficient and practical than the test bolus methods by some. Nevertheless, care must be taken as there may be an additional inherent delay of a few seconds until the diagnostic scan will start after the trigger button is pressed. This relates to table translation time to the start point of the diagnostic scan that may be different from the location of the cine scan or might be inherent to the software[64, 71].

Digital imaging software

Evaluating thoracic cardiovascular cross-sectional studies digital imaging software with multiplanar (MPR), maximum intensity (MIP) and 3D reconstruction capability is helpful for evaluation and communication of the complex anatomy[72]. Retrospectively gated 4D cardiac studies additionally require specific software to display in the 4th dimension and open source[49] as well as commercial products are available. Furthermore the evaluation of the coronary arteries is commonly done using specific vessel track functions in curved multi-planar reconstruction applications[73, 74].

Clinical considerations in thoracic MDCTA protocols in companion animals

Until now, the gold standard for evaluation of cardiac function and morphology in companion animals has been echocardiography using

2D, 3D and Doppler-examinations. 3D and 4D CT studies will likely be able to supply global anatomical and functional assessment of the heart and associated vessels in companion animals.
For CTA purposes the left heart, aorta and coronary arteries must be considered as one entity due to their circulatory proximity; the same is true for the right heart and pulmonary arterial tree. Hence typically the exam is tailored to evaluate either the pulmonary or systemic circulation. For evaluation of both the the left (left heart, aorta, coronary arteries) and right (right heart, pulmonary arterial tree) circulations three phasic injection protocols are used to ensure adequate opacification of the vessels in both vascular beds.

Even though the normal cardiac anatomy as provided from MDCT exams in companion animals has not been described (Figure 3 and 4),

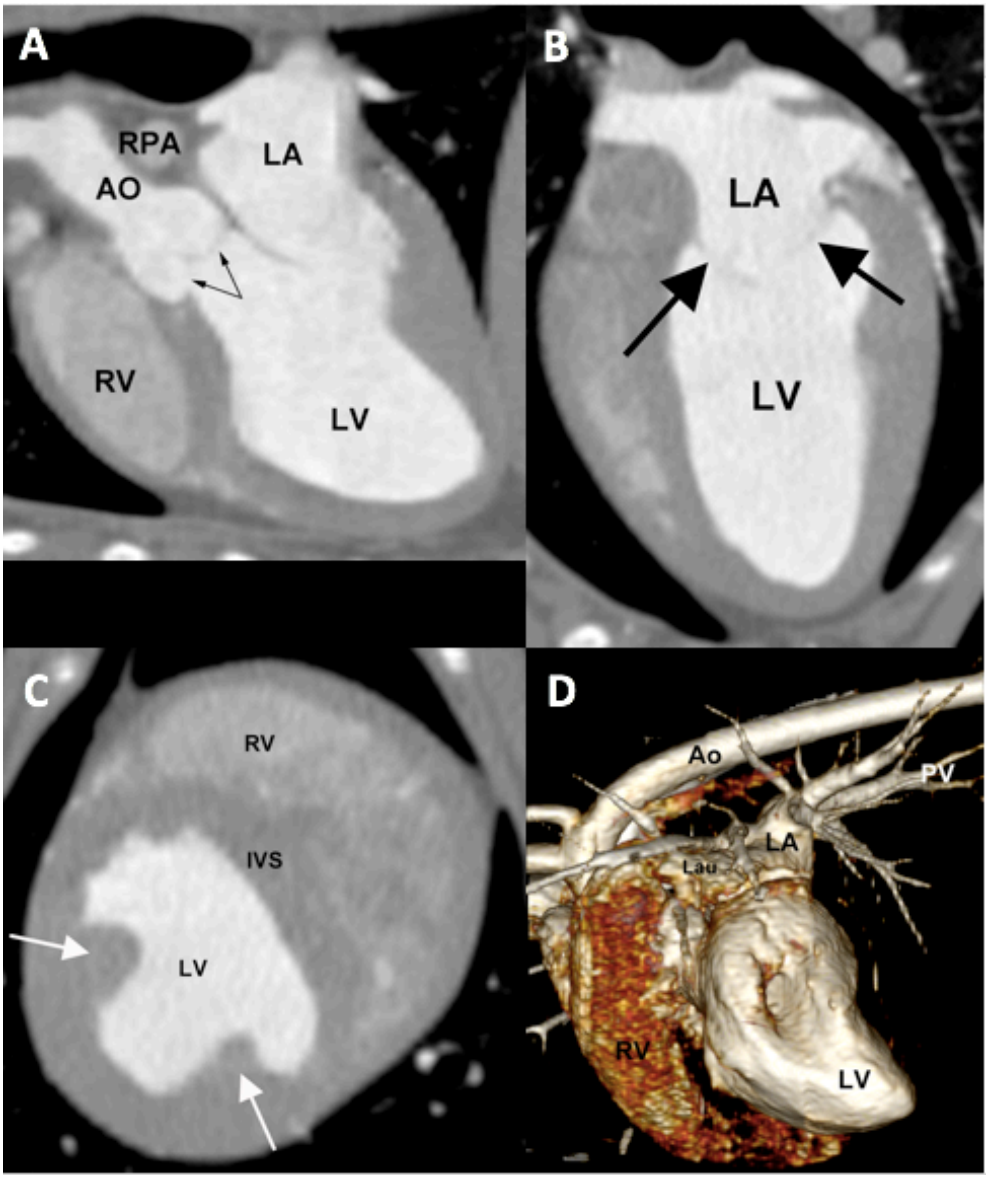

Figure 3: Multiplanar reconstructions allow viewing of the cardiac anatomy of the dog in different planes, mimicking planes currently viewed in echocardiography. Sagittal three chamber view (A), oblique transverse plane 2-chamber view (B) and dorsal plane short axis view (C). The aortic and mitral valve leaflets can be seen as slender filling defects in the sagittal three-chamber (thin black arrows) and two-chamber view (large black arrows) respectively. The papillary muscles are seen in the transverse plane (white arrows). A three dimensional

volume rendered image (D) is showing the left atrium (LA), ventricle (LV) and aorta (AO) from the left side highlighted by the contrast bolus, a lesser amount of contrast is present in the right ventricle (RV). RPA = right pulmonary artery, IVS = interventricular septum, Lau = left auricle, PV = pulmonary veins.

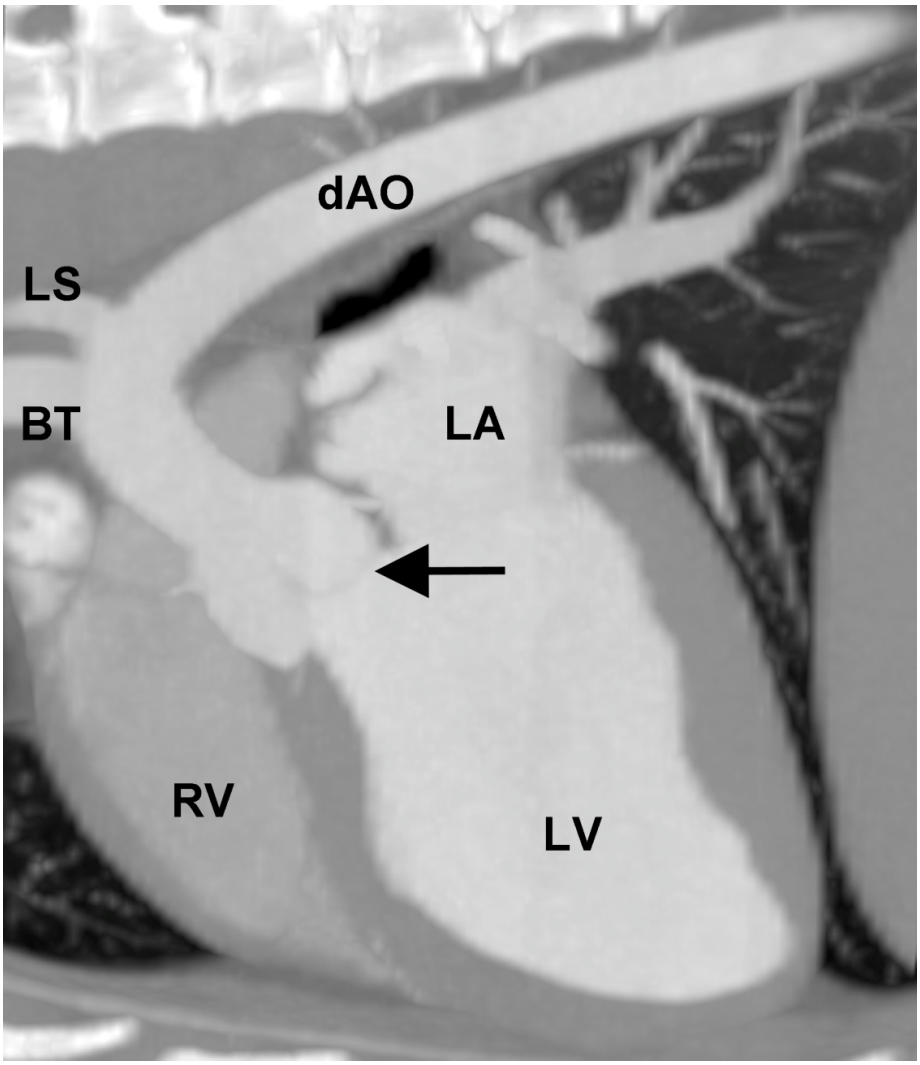

Figure 4: The aorta and its branches of a normal dog viewed in a sagittal plane three chamber view. The aortic valves (black arrows) can be seen as thin filling defects in the contrast pool along the root of the aorta. dAO = descending aorta, LS = left subclavian artery, BT = brachiocephalic trunk, RV = right ventricle, LV = left ventricle, LA = left atrium

Several reports focus on the diagnosis of congenital or acquired cardiovascular alterations or mass lesions involving the heart using this modality, such as an aberrant left subclavian artery, peripheral pulmonary artery stenosis, a complicated persistent patent ductus arteriosus or tumors or granulomas involving the heart of dogs[14, 15, 19, 75-77].

At this time, few recent studies are evaluating the use of MDCT for functional or anatomical evaluation of the heart specifically for the application in dogs in an experimental setting[22-24, 43]. As the companion animal patients will mostly need to undergo anesthesia or heavy sedation for these exams, functional alterations depending on the drug regiment used will have to be taken into consideration. In one study using 10 beagle dogs premedication with levomethadone and diazepam was used for premedication followed by induction with propofol to effect and maintenance on inhaled isoflurane. Using this protocol a mean heart rate of 95 ± 13.73bpm resulted in blurred margins in 7/10 studies that hampered the evaluation of the endocardial borders in dogs but overall the image quality was rated as good[43]. It has been shown in adult humans that image quality can be improved by pharmaceutical reduction and regulation of the heart rate using beta-blockers and/or calcium channel blockers for cardiac exams using 16- through 320-MDCT units in humans, targeting a heart of less than 65 beats per minutes (bpm) during image acquisition[78-81].

To enhance depiction of small vessels, vasodilators are commonly given in adult human patients to evaluate for stenotic coronary artery disease[82]. In children the use of vasodilators is usually unnecessary because in these patients the examination is targeted to the evaluation of the coronary artery origins and proximal coronary arteries, for which vasodilation may not be necessary[27, 28,24, 25].

In companion animals, anatomical evaluation of the normal coronary artery branches has been the primary focus using 64-MDCT in dogs (Figure 5)[12].

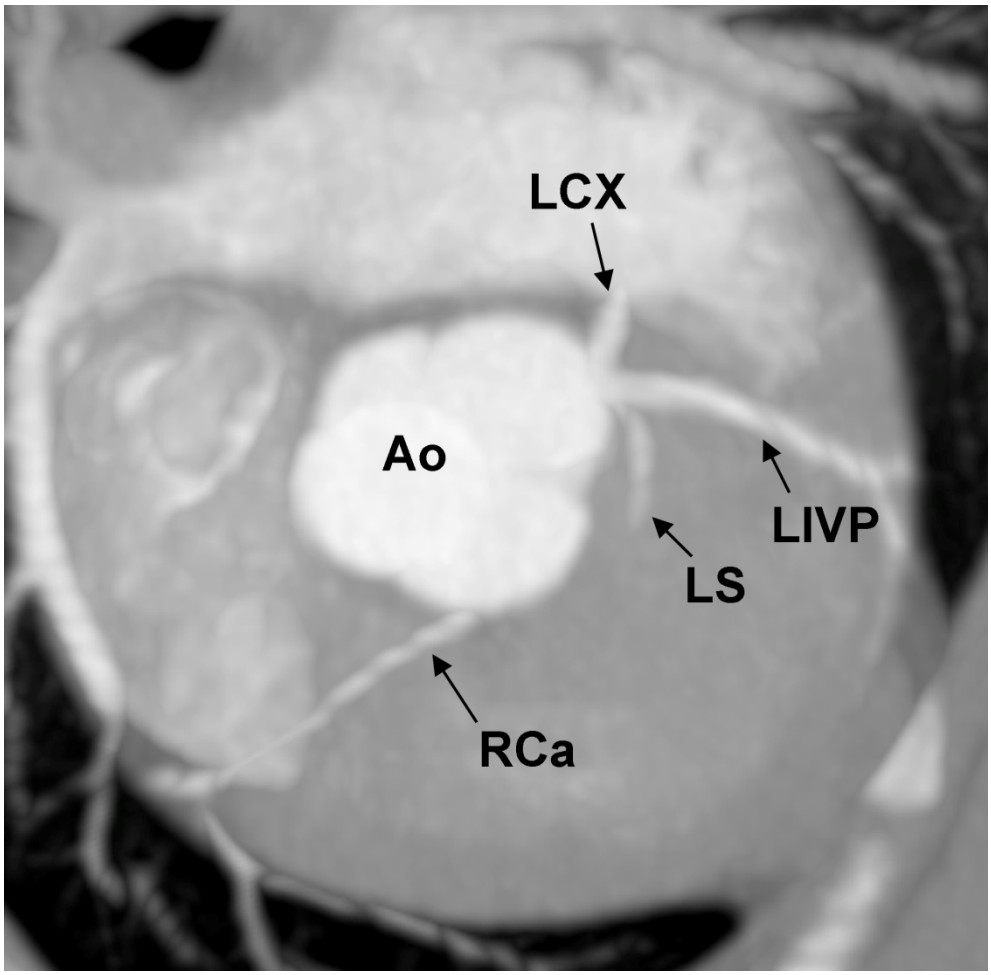

Figure 5: The coronary arteries are depicted in a dorsal short axis plane at the root of the aorta using a maximum intensity projection (MIP) in a dog. The three branches of the left and the single branch of the right coronary artery can be seen arising from the aorta (Ao) in the regular anatomical position. LXC = left circumflex branch, LIVP = left interventricular paraconal branch, LS = left sepal branch, RCa = right coronary artery

In this study, the use of nitroprusside as an arteriolar and venous dilator showed no significant effect on visualized coronary artery length or diameter, also the use of esmolol, a β-1 adrenergic receptor

antagonist, did not yield successful down-regulation of the heart rate yet image quality was rated overall as good to excellent[12].

Beta-blockers are commonly given in human adult and pediatric patients to lower the heart rate to improve image quality especially for the coronary arteries[27, 80].

Coronary artery depiction on units of less than 64-MDCT remains to be investigated in companion animal patients, those units may be easier accessible in veterinary clinics[82, 83].

The role of coronary arterial perfusion in patients with cardiomyopathy or infarcts remains to be further investigated in companion animals using MDCT.

In humans, MDCT has been deemed useful to evaluate valvular function based on planimetry and morphology especially when initial echocardiography yields suboptimal images[84, 85]. In dogs, one publication describes the position of the pulmonic valve but without functional or morphological evaluation[11].

Evaluation of the aorta or its branches has not been specifically targeted using MDCTA in dogs but several case reports of vascular ring anomalies exist[14, 15].

3D or 4D depiction of the heart and the great vessels will likely be helpful for surgical guidance in complex congenital cardiovascular anomalies.

There is no veterinary study on the evaluation of the right heart and ventricle beyond an initial anatomical description[11].

Several reports have been published describing the technique, contrast enhancement pattern as well as pathologies for pulmonary angiography in dogs (Figure 6).

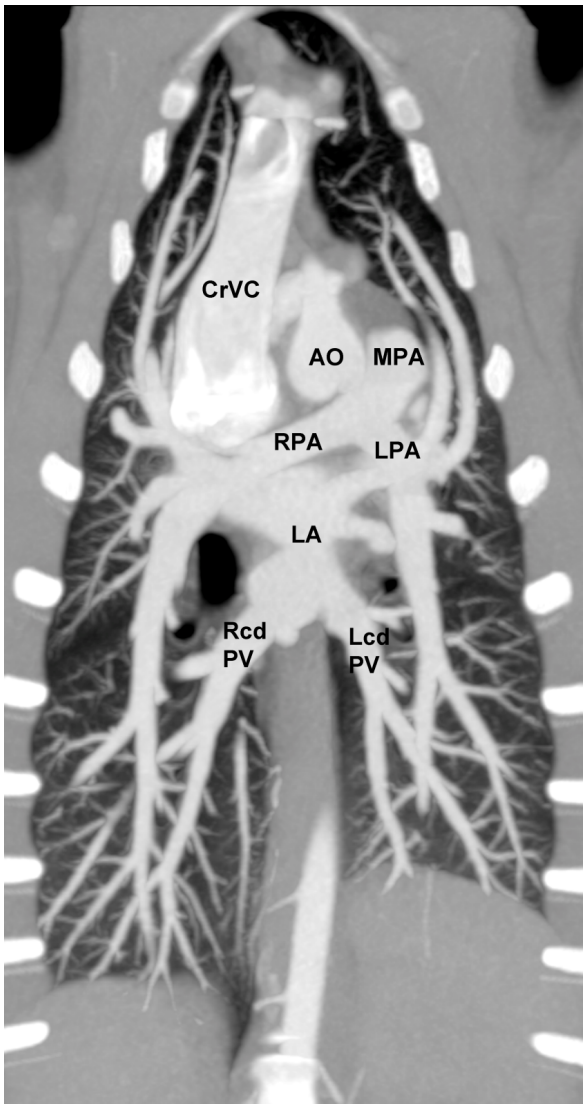

Figure 6: Dorsal plane maximal intensity projection (MIP) showing the pulmonary arterial and venous tree as provided in a triple-rule out study by using a prolonged injection duration in a dog using a 64-MDCT unit. CrVC = cranial vena cava, AO = aorta, MPA = main pulmonary artery, RPA = right pulmonary artery, LPA = left pulmonary artery, LA = left atrium (very dorsal aspect), RcdPV = right caudal pulmonary vein, LcdPV = left caudal pulmonary vein.

Pulmonary 16-MDCTA has been described in 5 healthy beagles using a helical pitch of 1.4 and a dose of 400mgI/kg of contrast medium producing good to excellent enhancement with a peak enhancement at 8s in the majority of the dogs[13].

In another canine study using a 16-MDCT, the effect of contrast medium injection duration on pulmonary artery peak enhancement magnitude and time to peak enhancement on different weight groups in dogs[20], mirroring previously performed research by Bae et al.[51]. This study also concluded that the injection duration is a key feature in the injection protocols and that adjustment of injection duration to scan duration appears beneficial in companion animals that commonly present with a variety of weights and sizes[20]. Pulmonary arterial anatomy as well as the effect of slice thickness for detection of pulmonary artery branches was evaluated using 64-MDCT; a slice thickness of 0.625mm allowed for detection of significantly more segments than larger reconstructions[11]. Pulmonary MDCTA has been successfully used in experimental disease settings to describe the changes associated in the early patent phase of dirofilariasis in one dog[16] and to describe pulmonary emboli observed after long-term administration of ivermectin in dogs with experimental heartworm infection[17]. A case report describes the features of peripheral pulmonary arterial stenosis using a 8-MDCT[19].

The incidence of pulmonary arterial embolism following different hip replacement techniques was also successfully evaluated using pulmonary MDCTA in dogs[18].
Further evaluation of the use of pulmonary MDCT angiography in clinical companion animals with clinical signs suggestive of pulmonary thromboembolism is desirable.

In summary the application of MDCT will likely offer new opportunities to evaluate the anatomy and function of the heart and associated great vessels as well as the pulmonary arterial system in companion animals, yet the need for advanced CT units as well as scanner software might limit this modality to selected institutions at the time. While first reports have established concepts in image acquisition and evaluation for pulmonary and cardiac CTA, a detailed review of the pulmonary, coronary and cardiac CTA anatomy with respect to the technical parameters of image acquisition is currently not available. For the evaluation of the pulmonary vasculature this will lay the foundation for utilizing this modality in clinical studies in patients with suspected congenital or acquired anatomical alterations of the pulmonary arteries for accurate interventional treatment planning and follow up, in the clinical workup of patients with suspected pulmonary thromboembolism. The evaluation of the coronary arteries is currently performed only very limited in veterinary patients relying on depiction of the ostia in echocardiography and possible fluoroscopic two dimensional localization of the vessels in cases of suspected aberrant

coronary artery anatomy or post mortem exams. CTA will likely give more detailed and global diagnostic access to evaluate the anatomy and also patency of these small vessels that are currently not routinely evaluated, possibly giving further insight also the etiology of ischemic disease for example in cats. For cardiac applications including the great vessels the CTA studies are expected to provide comprehensive anatomical evaluation especially in patients with congenital anomalies with need for surgical planning, where echocardiography does not provide the global overview. Similarly, patients with acquired disease such as mitral valve disease are to be assessed pre and post surgical procedures.

In addition, influence of drug regimens used for sedation or anesthesia on cardiac rate and function need to be considered in using this modality for functional evaluations. The use of CTA will likely gain importance in patients with acquired myocardial disease once the use of the modality is further established, allowing for accurate assessment of left and right ventricular systolic function as well as providing global overview of the thoracic vascular system and myocardium.

References

1. Armbrust LJ, Biller DS, Bamford A, Chun R, Garrett LD, Sanderson MW. Comparison of three-view thoracic radiography and computed tomography for detection of pulmonary nodules in dogs with neoplasia. *Journal of the American Veterinary Medical Association*. 2012;240: 1088-1094.

2. Prather AB, Berry CR, Thrall DE. Use of radiography in combination with computed tomography for the assessment of noncardiac thoracic disease in the dog and cat. *Veterinary radiology & ultrasound : the official journal of the American College of Veterinary Radiology and the International Veterinary Radiology Association*. 2005;46: 114-121.

3. Schuller S, Fredericksen M, Schroder H, Meyer-Lindenberg A, Hewicker-Trautwein M, Nolte I. [Computer tomographic differentiation of intrathoracic neoplasms and inflammation in the dog]. *Berl Munch Tierarztl Wochenschr*. 2005;118: 76-84.

4. Marolf AJ, Gibbons DS, Podell BK, Park RD. Computed tomographic appearance of primary lung tumors in dogs. *Veterinary radiology & ultrasound : the official journal of the American College of Veterinary Radiology and the International Veterinary Radiology Association*. 2011;52: 168-172.

5. Reetz JA, Buza EL, Krick EL. CT features of pleural masses and nodules. *Veterinary radiology & ultrasound : the official journal of the American College of Veterinary Radiology and the International Veterinary Radiology Association*. 2012;53: 121-127.

6. Henninger W. Use of computed tomography in the diseased feline thorax. *The Journal of small animal practice*. 2003;44: 56-64.

7. Petite AF, Kirberger RM. Mediastinum. In: Schwarz T, Saunders J (eds): *Veterinary Computed Tomography*. Chichester: Wiley-Blackwell, 2011;249-260.

8. Saunders J, Vignoli M, Gielen I. Thoracic Boundaries. In: Schwarz T, Saunders J (eds): *Veterinary Computed Tomography*. Chichester: Wiley-Blackwell, 2011;285-296.

9. Mai W. Pleura. In: Schwarz T, Saunders J (eds): *Veternary Computed Tomography*. Chichester: Wiley & Sons Ltd, 2011;279-284.

10. d'Anjou ME, Schwarz T. Heart and Vessels. In: Schwarz T, Saunders J (eds): *Veterinary Computed Tomography*. Chichester: Wiley-Blackwell, 2011;229-242.

11. Drees R, Frydrychowicz A, Keuler NS, Reeder SB, Johnson R. Pulmonary angiography with 64-multidetector-row computed tomography in normal dogs. *Veterinary radiology & ultrasound : the official journal of the American College of Veterinary Radiology and the International Veterinary Radiology Association*. 2011;52: 362-367.

12. Drees R, Frydrychowicz A, Reeder SB, Pinkerton ME, Johnson R. 64-multidetector computed tomographic angiography of the canine coronary arteries. *Veterinary radiology & ultrasound : the official journal of the American College of Veterinary Radiology and the International Veterinary Radiology Association*. 2011;52: 507-515.

13. Habing A, Coelho JC, Nelson N, Brown A, Beal M, Kinns J. Pulmonary angiography using 16 slice multidetector computed

tomography in normal dogs. *Veterinary radiology & ultrasound : the official journal of the American College of Veterinary Radiology and the International Veterinary Radiology Association*. 2011;52: 173-178.

14. Bottorff B, Sisson DD. Hypoplastic aberrant left subclavian artery in a dog with a persistent right aortic arch. *J Vet Cardiol*. 2012;14: 381-385.

15. Pownder S, Scrivani PV. Non-selective computed tomography angiography of a vascular ring anomaly in a dog. *J Vet Cardiol*. 2008;10: 125-128.

16. Seiler GS, Nolan TJ, Withnall E, Reynolds C, Lok JB, Sleeper MM. Computed tomographic changes associated with the prepatent and early patent phase of dirofilariasis in an experimentally infected dog. *Veterinary radiology & ultrasound : the official journal of the American College of Veterinary Radiology and the International Veterinary Radiology Association*. 2010;51: 136-140.

17. Takahashi A, Yamada K, Kishimoto M, Shimizu J, Maeda R. Computed tomography (CT) observation of pulmonary emboli caused by long-term administration of ivermectin in dogs experimentally infected with heartworms. *Vet Parasitol*. 2008;155: 242-248.

18. Tidwell SA, Graham JP, Peck JN, Berry CR. Incidence of pulmonary embolism after non-cemented total hip arthroplasty in eleven dogs: computed tomographic pulmonary angiography and pulmonary perfusion scintigraphy. *Veterinary surgery : VS*. 2007;36: 37-42.

19. Tyner D, Reese D, Maisenbacher H. Computed tomography angiography of bilateral peripheral pulmonary arterial stenoses in a dog. *J Vet Cardiol*. 2011;13: 57-62.

20. Makara M, Dennler M, Kuhn K, Kalchofner K, Kircher P. Effect of contrast medium injection duration on peak enhancement and time to peak enhancement of canine pulmonary arteries. *Veterinary radiology & ultrasound : the official journal of the American College of Veterinary Radiology and the International Veterinary Radiology Association*. 2011;52: 605-610.

21. Kirberger RM, Stander N, Cassel N, Pazzi P, Mukorera V, Christie J, et al. Computed tomographic and radiographic characteristics of aortic lesions in 42 dogs with spirocercosis. *Veterinary radiology & ultrasound : the official journal of the American College of Veterinary Radiology and the International Veterinary Radiology Association*. 2013;54: 212-222.

22. Lee M, Park N, Lee S, Lee A, Jung J, Kim Y, et al. Comparison of echocardiography with dual-source computed tomography for assessment of left ventricular volume in healthy Beagles. *American journal of veterinary research*. 2013;74: 62-69.

23. Henjes CR, Hungerbuhler S, Bojarski IB, Nolte I, Wefstaedt P. Comparison of multi-detector row computed tomography with echocardiography for assessment of left ventricular function in healthy dogs. *American journal of veterinary research*. 2012;73: 393-403.

24. Park N, Lee M, Lee A, Lee S, Song S, Jung J, et al. Comparative study of cardiac anatomic measurements obtained by

echocardiography and dual-source computed tomography. *J Vet Med Sci*. 2012;74: 1597-1602.

25. Frush DP. Technique of pediatric thoracic CT angiography. *Radiol Clin North Am*. 2005;43: 419-433.

26. Frush DP, Herlong JR. Pediatric thoracic CT angiography. *Pediatr Radiol*. 2005;35: 11-25.

27. Rigsby CK, deFreitas RA, Nicholas AC, Leidecker C, Johanek AJ, Anley P, et al. Safety and efficacy of a drug regimen to control heart rate during 64-slice ECG-gated coronary CTA in children. *Pediatr Radiol*. 2010;40: 1880-1889.

28. Jin KN, Park EA, Shin CI, Lee W, Chung JW, Park JH. Retrospective versus prospective ECG-gated dual-source CT in pediatric patients with congenital heart diseases: comparison of image quality and radiation dose. *Int J Cardiovasc Imaging*. 2010;26 Suppl 1: 63-73.

29. Bushberg JT, A.J. S, Leidholdt Jr EM, Boone J. Computed Tomography. In: Bushberg JT (ed): *The essential physics of medical imaging*. Philadelphia: Lippincott, Williams & Wilkins, 2012;312-374.

30. Saunders J, Ohlerth S. CT Physics and Instrumentation - Mechanical Design. In: Schwarz T, Saunders J (eds): *Veterinary Computed Tomography*. Chichester: Wiley-Blackwell, 2011;1-8.

31. Cody DD, Mahesh M. AAPM/RSNA physics tutorial for residents: Technologic advances in multidetector CT with a focus on cardiac imaging. *Radiographics : a review publication of the Radiological Society of North America, Inc*. 2007;27: 1829-1837.

32. Rendano Jr V. Purchase Considerations. In: Schwarz T, Saunders J (eds): *Veterinary Computed Tomography*. Chichester: Wiley-Blackwell, 2011;89-92.

33. Schwarz T, O'Brien R. CT Acquisition Parameters. In: Schwarz T, Saunders J (eds): *Veterinary Computed Tomography*. Chicheser: Wiley-Blackwell, 2011;9-28.

34. Kopp AF, Schroeder S, Kuettner A, Baumbach A, Georg C, Kuzo R, et al. Non-invasive coronary angiography with high resolution multidetector-row computed tomography. Results in 102 patients. *Eur Heart J*. 2002;23: 1714-1725.

35. Ohnesorge B, Flohr T, Becker C, Kopp AF, Schoepf UJ, Baum U, et al. Cardiac imaging by means of electrocardiographically gated multisection spiral CT: initial experience. *Radiology*. 2000;217: 564-571.

36. Halliburton S, Arbab-Zadeh A, Dey D, Einstein AJ, Gentry R, George RT, et al. State-of-the-art in CT hardware and scan modes for cardiovascular CT. *J Cardiovasc Comput Tomogr*. 2012;6: 154-163.

37. Achenbach S. Computed tomography coronary angiography. *Journal of the American College of Cardiology*. 2006;48: 1919-1928.

38. Salavati A, Radmanesh F, Heidari K, Dwamena BA, Kelly AM, Cronin P. Dual-source computed tomography angiography for diagnosis and assessment of coronary artery disease: systematic review and meta-analysis. *J Cardiovasc Comput Tomogr*. 2012;6: 78-90.

39. Miller JC, Abbara S, Mamuya WS, Thrall JH, Uppot RN. Dual-source CT for cardiac imaging. *J Am Coll Radiol*. 2009;6: 65-68.

40. Petersilka M, Bruder H, Krauss B, Stierstorfer K, Flohr TG. Technical principles of dual source CT. *Eur J Radiol*. 2008;68: 362-368.

41. Hou DJ, Tso DK, Davison C, Inacio J, Louis LJ, Nicolaou S, et al. Clinical utility of ultra high pitch dual source thoracic CT imaging of acute pulmonary embolism in the emergency department: Are we one step closer towards a non-gated triple rule out? *Eur J Radiol*. 2013;82: 1793-1798.

42. Kang JW, Do KH, Chung JY, Cho HJ, Seo JB, Lim TH. Concept of minimal heart rate for each pitch value to avoid interpolation artifact when using dual-source CT: a phantom study. *Int J Cardiovasc Imaging*. 2010;26 Suppl 1: 103-109.

43. Sieslack AK, Dziallas P, Nolte I, Wefstaedt P. Comparative assessment of left ventricular function variables determined via cardiac computed tomography and cardiac magnetic resonance imaging in dogs. *American journal of veterinary research*. 2013;74: 990-998.

44. Menke J, Unterberg-Buchwald C, Staab W, Sohns JM, Seif Amir Hosseini A, Schwarz A. Head-to-head comparison of prospectively triggered vs retrospectively gated coronary computed tomography angiography: Meta-analysis of diagnostic accuracy, image quality, and radiation dose. *Am Heart J*. 2013;165: 154-163 e153.

45. Pauwels EK, Bourguignon MH. Radiation dose features and solid cancer induction in pediatric computed tomography. *Med Princ Pract*. 2012;21: 508-515.

46. Schwarz T. Artefacts. In: Schwarz T, Saunders J (eds): *Veterinary computed tomography*. Chichester: Wiley-Blackwell, 2011;35-56.

47. Takx RA, Schoepf UJ, Moscariello A, Das M, Rowe G, Schoenberg SO, et al. Coronary CT angiography: comparison of a novel iterative reconstruction with filtered back projection for reconstruction of low-dose CT-Initial experience. *Eur J Radiol*. 2013;82: 275-280.

48. Marten K, Funke M, Rummeny EJ, Engelke C. Electrocardiographic assistance in multidetector CT of thoracic disorders. *Clin Radiol*. 2005;60: 8-21.

49. Rosset A, Spadola L, Ratib O. OsiriX: an open-source software for navigating in multidimensional DICOM images. *J Digit Imaging*. 2004;17: 205-216.

50. Alkadhi H, Leschka S. Radiation dose of cardiac computed tomography - what has been achieved and what needs to be done. *Eur Radiol*. 2011;21: 505-509.

51. Bae KT, Heiken JP. Scan and contrast administration principles of MDCT. *Eur Radiol*. 2005;15 Suppl 5: E46-59.

52. Maffei E, Martini C, Arcadi T, Clemente A, Seitun S, Zuccarelli A, et al. Plaque imaging with CT coronary angiography: Effect of intra-vascular attenuation on plaque type classification. *World J Radiol*. 2012;4: 265-272.

53. Ko JP, Brandman S, Stember J, Naidich DP. Dual-energy computed tomography: concepts, performance, and thoracic applications. *J Thorac Imaging*. 2012;27: 7-22.

54. Karcaaltincaba M, Aktas A. Dual-energy CT revisited with multidetector CT: review of principles and clinical applications. *Diagn Interv Radiol*. 2011;17: 181-194.

55. Pollard R PS. CT Contrast media and applications. In: SChwarz T SJ (ed): *Veterinary Computed Tomography*. Chichester: Wiley-Blackwell, 2011;57-66.

56. Madder RD, Raff GL, Hickman L, Foster NJ, McMurray MD, Carlyle LM, et al. Comparative diagnostic yield and 3-month outcomes of "triple rule-out" and standard protocol coronary CT angiography in the evaluation of acute chest pain. *J Cardiovasc Comput Tomogr*. 2011;5: 165-171.

57. Halpern EJ. Triple-rule-out CT angiography for evaluation of acute chest pain and possible acute coronary syndrome. *Radiology*. 2009;252: 332-345.

58. Demirpolat G, Yuksel M, Kavukcu G, Tuncel D. Carotid CT angiography: comparison of image quality for left versus right arm injections. *Diagn Interv Radiol*. 2011;17: 195-198.

59. Bae KT. Peak contrast enhancement in CT and MR angiography: when does it occur and why? Pharmacokinetic study in a porcine model. *Radiology*. 2003;227: 809-816.

60. Bae KT, Seeck BA, Hildebolt CF, Tao C, Zhu F, Kanematsu M, et al. Contrast enhancement in cardiovascular MDCT: effect of body weight, height, body surface area, body mass index, and obesity. *AJR American journal of roentgenology*. 2008;190: 777-784.

61. Bae KT, Tran HQ, Heiken JP. Multiphasic injection method for uniform prolonged vascular enhancement at CT angiography: pharmacokinetic analysis and experimental porcine model. *Radiology*. 2000;216: 872-880.

62. Kondo H, Kanematsu M, Goshima S, Watanabe H, Onozuka M, Moriyama N, et al. Aortic and hepatic enhancement at multidetector CT: evaluation of optimal iodine dose determined by lean body weight. *Eur J Radiol*. 2011;80: e273-277.

63. Lee CH, Goo JM, Lee HJ, Kim KG, Im JG, Bae KT. Determination of optimal timing window for pulmonary artery MDCT angiography. *AJR American journal of roentgenology*. 2007;188: 313-317.

64. Bae KT. Test-bolus versus bolus-tracking techniques for CT angiographic timing. *Radiology*. 2005;236: 369-370; author reply 370.

65. Bae KT, Tran HQ, Heiken JP. Uniform vascular contrast enhancement and reduced contrast medium volume achieved by using exponentially decelerated contrast material injection method. *Radiology*. 2004;231: 732-736.

66. Dennis R, Herrtage, ME. Low osmolar contrast media. *Veterinary Radiology*. 1989;30: 2-12.

67. Pollard RE, Pascoe PJ. Severe reaction to intravenous administration of an ionic iodinated contrast agent in two anesthetized dogs. *Journal of the American Veterinary Medical Association*. 2008;233: 274-278.

68. Pollard RE, Puchalski SM, Pascoe PJ. Hemodynamic and serum biochemical alterations associated with intravenous administration of three types of contrast media in anesthetized cats. *American journal of veterinary research*. 2008;69: 1274-1278.

69. Pollard RE, Puchalski SM, Pascoe PJ. Hemodynamic and serum biochemical alterations associated with intravenous administration of

three types of contrast media in anesthetized dogs. *American journal of veterinary research*. 2008;69: 1268-1273.

70. Healthcare GE. [cited; Available from: http://dailymed.nlm.nih.gov/dailymed/archives/fdaDrugInfo.cfm?archiveid=11692

71. Cademartiri F, Nieman K, van der Lugt A, Raaijmakers RH, Mollet N, Pattynama PM, et al. Intravenous contrast material administration at 16-detector row helical CT coronary angiography: test bolus versus bolus-tracking technique. *Radiology*. 2004;233: 817-823.

72. Pech M WG, Lopez-Hänninen E, Röttgen R, Bittner R, Engert U, Ricke J. The diagnostic value of radial multiplanar reformatting (MPR) in the CT-diagnosis of pulmonary embolism. *Rofo*. 2004;176: 1576-1581.

73. Wang C SO. Integrating automatic and interactive methods for coronary artery segmentation: let the PACS workstation think ahead. *Int J Comput Assist Radiol Surg*. 2010;5: 275-285.

74. Sen A LL, Doi K, Hoffmann KR. Quantitative evaluation of vessel tracking techniques on coronary angiograms. *Medical physics*. 1999;26: 698-706.

75. Kang MH, Kim DY, Park HM. Ectopic thyroid carcinoma infiltrating the right atrium of the heart in a dog. *The Canadian veterinary journal La revue veterinaire canadienne*. 2012;53: 177-181.

76. Ajithdoss DK, Trainor KE, Snyder KD, Bridges CH, Langohr IM, Kiupel M, et al. Coccidioidomycosis presenting as a heart base mass in two dogs. *J Comp Pathol*. 2011;145: 132-137.

77. Baron Toaldo M, Diana A, Morini M, Cipone M. Imaging diagnosis--intrapericardial right auricle aneurysm in a dog. *Veterinary radiology & ultrasound : the official journal of the American College of Veterinary Radiology and the International Veterinary Radiology Association*. 2010;51: 512-515.

78. Kuettner A, Beck T, Drosch T, Kettering K, Heuschmid M, Burgstahler C, et al. Image quality and diagnostic accuracy of non-invasive coronary imaging with 16 detector slice spiral computed tomography with 188 ms temporal resolution. *Heart*. 2005;91: 938-941.

79. Dewey M, Vavere AL, Arbab-Zadeh A, Miller JM, Sara L, Cox C, et al. Patient characteristics as predictors of image quality and diagnostic accuracy of MDCT compared with conventional coronary angiography for detecting coronary artery stenoses: CORE-64 Multicenter International Trial. *AJR American journal of roentgenology*. 2010;194: 93-102.

80. Shim SS, Kim Y, Lim SM. Improvement of image quality with beta-blocker premedication on ECG-gated 16-MDCT coronary angiography. *AJR American journal of roentgenology*. 2005;184: 649-654.

81. Giesler T, Baum U, Ropers D, Ulzheimer S, Wenkel E, Mennicke M, et al. Noninvasive visualization of coronary arteries using contrast-enhanced multidetector CT: influence of heart rate on image quality and stenosis detection. *AJR American journal of roentgenology*. 2002;179: 911-916.

82. Khan M, Cummings KW, Gutierrez FR, Bhalla S, Woodard PK, Saeed IM. Contraindications and side effects of commonly used medications in coronary CT angiography. *Int J Cardiovasc Imaging*. 2011;27: 441-449.

83. Khan R, Rawal S, Eisenberg MJ. Transitioning from 16-slice to 64-slice multidetector computed tomography for the assessment of coronary artery disease: are we really making progress? *Can J Cardiol*. 2009;25: 533-542.

84. Buttan AK, Yang EH, Budoff MJ, Vorobiof G. Evaluation of valvular disease by cardiac computed tomography assessment. *J Cardiovasc Comput Tomogr*. 2012;6: 381-392.

85. de Heer LM, Habets J, Chamuleau SA, Mali WP, van Herwerden LA, Kluin J, et al. Multidetector row computed tomography assessment of the native aortic and mitral valve: a call for routine assessment of left-sided heart valves during coronary computed tomography. *Cardiol Rev*. 2012;20: 222-229.

CHAPTER 2

Scientific aims

Standard computed tomography (CT) exams are well integrated into current companion animal care. Computed tomographic angiographic (CTA) exams of the vascular system of the abdomen have also been well established for the workup of mainly portosystemic shunts in companion animals.

For the evaluation of the thoracic cardiovascular system veterinarians remain to rely on the combination of traditional modalities such as radiography, contrast radiographic or fluoroscopic studies and echocardiography. Thoracic CTA has found limited implementation in the diagnostic workup of companion animals to date but will likely create opportunities to define and understand disease processes and anatomical variations, enable advanced treatment options and allow for translational research. The challenges faced are that especially the heart is constantly moving and the structures of interest such as the coronary arteries are very small in companion animal patients; in addition, veterinary patients will need to undergo sedation or anesthesia for these exams. Advanced CT equipment allowing image acquisition at high speed and resolution and gated to the cardiac cycle is becoming available in veterinary institutions and evaluation of the feasibility and capability of thoracic CTA in companion animals is needed.

The general aim of this work is to evaluate the feasibility of pulmonary and coronary CTA as well as functional cardiac CTA in dogs and to define the limitations and opportunities with regards to achievable

image quality, also in light of anesthetic protocols and comparable diagnostic modalities used for diagnosis of cardiac disorders.

The specific aims of this research project were:

- to depict the anatomy of the pulmonary and coronary arteries using CTA
- to evaluate the effect of anesthetic protocols on MDCT-CTA of the coronary arteries
- to evaluate the effect of anesthetic protocols on the measurement of cardiac parameters using MDCT-CTA
- to compare MDCT-CTA with 3T MRI and echocardiography for evaluation of cardiac parameters

CHAPTER 3

Pulmonary angiography with 64 Multidetector Row Computed Tomography in Normal Dogs

Randi Drees[1], Alex P Frydrychowicz[2], Nicholas S Keuler[2], Scott B Reeder[2], Rebecca Johnson[1]

[1] From the Department of Surgical Sciences, School of Veterinary Medicine, University of Wisconsin-Madison, Linden Drive 2015, Madison, WI 53706, USA (Drees, Johnson);
[2] Department of Radiology (Frydrychowicz, Reeder), Medical Physics (Reeder), Biomedical Engineering and Medicine (Reeder), School of Medicine and Public Health, University of Wisconsin-Madison, 600 Highland Avenue, Madison, WI 53792, USA and Department of Statistics (Keuler), University of Wisconsin-Madison, 1300 University Avenue, Madison, WI 53706, USA.

Adapted from: *Veterinary Radiology Ultrasound* 2011;52:362-367.

Summary

Pulmonary angiography using 64-multidetector-row computed tomography (MDCT) was used to evaluate pulmonary artery anatomy, and determine the sensitivity of pulmonary artery segment visualization in four Beagle dogs using images reconstructed to 0.625mm and retro-reconstructed to 1.25, and 2.5mm slice thickness. Morphologically, characteristic features included a focal narrowing in the right cranial pulmonary artery in all dogs, which should not be mistaken as stenosis. While the right cranial pulmonary artery divided into two equally sized branches that were tracked into the periphery of the lung lobe in all dogs, only a single left cranial (cranial portion) lobar artery was present. Compared to 1.25 and 2.5mm retro-reconstructions, 0.625mm reconstructions allowed for detection of significantly ($P \leq 0.05$) more pulmonary artery segments and sharper depiction of vessel margins. Clinical applications such as prevalence and significance of diameter changes, and detection of pulmonary arterial thrombembolism on lobar and sublobar level, using pulmonary angiography with 64-MDCT applying 0.625mm reconstruction slice thickness remain to be established.

Introduction

Diagnostic imaging evaluation of the pulmonary arteries in dogs is based mainly on thoracic radiographs, though in some patients more specific procedures such as angiography or scintigraphy are conducted.[1, 2] All of these methods are limited by morphological accuracy, and some also by invasiveness. Multidetector-row computed tomography (MDCT) pulmonary angiography is the standard of care for diagnosing pulmonary embolism in humans.[3-6] There is only limited information on MDCT pulmonary angiography in dogs.[7-11] Therefore, our goal was to evaluate normal canine pulmonary arteries using 64-MDCT.

Material and methods:

General anesthesia was induced in four 1-year-old beagle dogs (mean body weight 11 ± 0.5kg) with propofol (PropoFlo™, Abbott Laboratories, North Chicago, IL, USA) and maintained with isoflurane in 100% oxygen administered via an orotracheal tube. End-tidal carbon dioxide levels were kept between 35-45mmHg using a mechanical ventilator (SAV 2500, Smiths Medical, Waukesha, WI, USA). Intravenous crystalloid solution (Plasma-lyte A, Baxter Healthcare Corporation, Deerfield, IL, USA) was administered though a 22G catheter in the left cephalic vein at 10ml/kg/hr with fluid boluses of 5ml/kg as necessary to maintain blood pressure > 60mmHg. Esmolol (50-300micrograms/kg/min) was also administered through this catheter as part of a separate study of coronary angiography.

Dogs were in dorsal recumbency using a V-trough on a clinical 64-multidetector-row computed tomography scanner (VCT, GE Healthcare, Waukesha, WI, USA). A 20G catheter was placed in the right cephalic vein for contrast medium injection. The arrival time of contrast medium was determined using a test bolus approach: A bolus of 5ml iodinated contrast medium (Isovue 370, Bracco Diagnostics Inc., Princeton, NJ, USA) followed by a 20ml saline chaser was injected at 2ml/sec within maximum pressure limits of 300lb/in^2 with a dual barrel power injector (Stellant, MedRad, Indianola, PA, USA). After injection, repetitive transverse plane cine scans (80kV, 40mA, 5mm slice thickness, axial scanning mode, 1s tube rotation time, one image acquired per rotation) were acquired over the mediastinum transecting the base of the main

pulmonary artery and aorta. Time to peak enhancement in the main pulmonary artery and aorta was analyzed on the scanner by placement of a region of interest (ROI) in the center of the respective vessel.

The study bolus time was set to allow for simultaneous pulmonary arterial and aortic opacification for a related project. A triphasic injection protocol was used with an initial bolus consisting of 100% contrast medium, followed by dilute contrast medium (40% contrast medium and 60% physiologic saline solution), and a terminal saline chaser. In total, 2.4 to 3.9ml contrast medium/kg bodyweight were administered using an identical injection speed as that used for the test bolus.

Following a 4s delay from peak enhancement at the aortic root, the thorax was scanned in caudocranial direction, with the scan field of view (FOV) adapted to each dog's individual anatomy including both pulmonary apices and all costophrenic recesses. The described triphasic bolus with a prolonged injection duration was chosen to allow opacification of the pulmonary arteries as well as all chambers and great vessels for a related project. Imaging settings were: helical scan mode at 120kV tube voltage, ECG-modulated tube current (200-750mA), 0.35s tube rotation time (effective temporal resolution 250msec using SnapShot Segment feature, proprietary GE Healthcare, Waukesha, WI, USA), prospective ECG-gating with heart-rate adapted pitch, 64 x 0.625mm collimation (i.e., using 64 detector rows of 0.625mm width) was applied for all studies. Images were reconstructed to isotropic 0.625mm and retro-reconstructed to non-isotropic 1.25

and 2.5mm slice thickness using a soft tissue kernel. All dogs underwent euthanasia following a related coronary angiography study and underwent necropsy examination.

Image evaluation was performed by a board certified veterinary radiologist on a dedicated viewing station (OsiriX Medical Image software, version 3.7.1, http://www.osirix-viewer.com/). The studies were randomized and anonymized so that the reviewer was not aware of the specific reconstruction algorithm. For evaluation of images, window width and level were adjusted individually to optimize visualization of the pulmonary arteries. Enhancement levels of the main (MPA), main right (RPA), main left pulmonary (LPA) artery, and aorta were measured on 0.625mm reconstructed images by manually placing regions of interest (ROIs) in comparable regions of the respective vessels; the thinnest slice thickness allowing for the most accurate anatomical placement of the ROI.

The pulmonary arterial vessels (MPA, RPA, LPA, right cranial, middle, caudal and accessory, left cranial (cranial portion), cranial (caudal portion), and caudal pulmonary arterial lobar branches) were evaluated further using all three reconstruction thicknesses for the following criteria: 1) anatomy: relationship to major vessels, cardiac, and visible bronchial structures were qualitatively recorded; and 2) detectable lobar arterial segments: starting with the most proximal segment of the individual lobar artery, the vessel was followed distally, each point of subdivision into smaller branches marking the beginning of a new segment.

The effect of the reconstruction interval on the number of detectable segments was analyzed for each lobe separately using repeated measures ANOVA with an autoregressive correlation structure within dogs. If the overall F-test was significant, pair-wise comparisons of different reconstruction thicknesses were done using the Tukey multiple comparisons adjustment separately for each lobe. All analyses were done in Proc Mixed using SAS 9.2 for Windows.[12] The significance level was set at $p \leq 0.05$.

Results

Pulmonary angiography was performed successfully in all animals. The field of view was adjusted to the individual anatomy and extended 19.2, 22.5, 19.3, and 20.2cm in craniocaudal direction in each of the four dogs. On subsequent necropsy examination, the pulmonary arteries were within normal limits and no thrombi were found.

Results for time to peak enhancement after test bolus, individualized study bolus volumes, and enhancement after injection of study bolus are summarized in Table 1.

Table 1: Time to Peak Enhancement, Study Bolus, and Enhancement Evaluation of the Pulmonary CTA in Four Dogs.

	Time to peak enhancement after test bolus (s)		Study bolus (ml) *	Enhancement after study bolus (HU (SD))	
	MPA	AO		MPA	AO
Dog 1	4	8	22/22/16	385.4 (15.9)	406.9 (19.3)
Dog 2	4	9	24/24/20	301.0 (16.9)	359.1 (20.0)
Dog 3	4	6	18/18/16	321.1 (20.6)	327.7 (18.4)
Dog 4	6	11	30/30/19	486.7 (18.7)	502.8 (18.3)

* 100% iodinated contrast medium/ 40%/60% iodinated contrast medium/physiologic saline solution)/ 100% physiologic saline solution

Adjusting scan delay for the inter-individual temporal variability determined from test bolus arrival produced good enhancement of > 300HU in the pulmonary arteries and aorta in all dogs.

Figure 1 shows volume rendered images allowing for a morphologic overview of the anatomic relationship of the major cardiovascular structures.

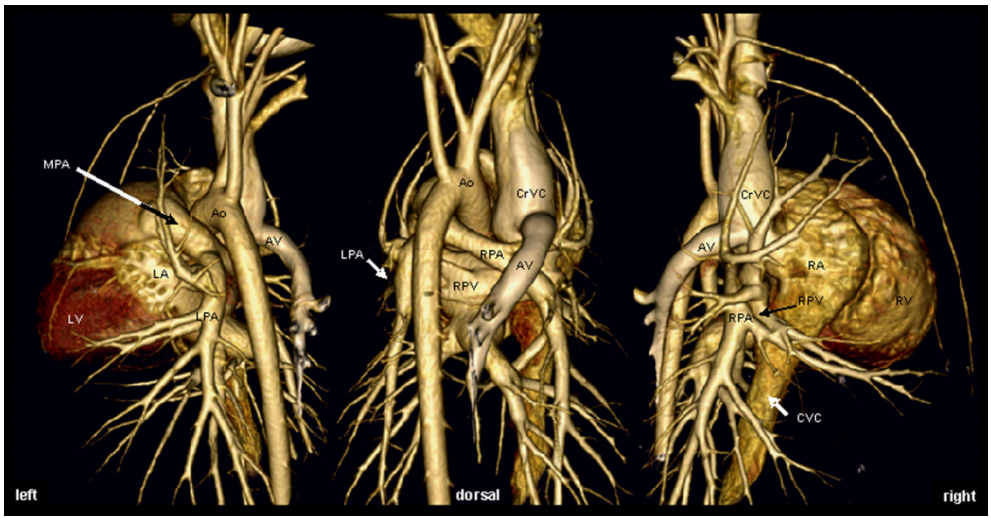

Figure 1: Volume Rendered Display of a Representative Dataset with 0.625mm collimation. Although volume rendered displays were not part of the analysis, the ability to depict the anatomy was exploited for a morphologic overview over anatomic relationships of the major cardiovascular structures that have not been reported systematically and only presented sparsely in the literature. Note the straight lateral branching of the right cranial lobar artery and the continuation as two equally sized separate branches into the right cranial lung lobe on dorsal and right oblique image.

MPA = main pulmonary artery; LPA, RPA = left and right main pulmonary artery, respectively; RPV = right pulmonary vein; CrVC = cranial vena cava; CVC = caudal vena cava; LV, RV = left and right ventricle, respectively; LA, RA = left and right atrium, respectively; AV = right azygos vein.

On transverse and multiplanar reconstructions the pulmonic cusps

were outlined faintly and the pulmonic bulb was seen distinctly on 0.625mm reconstructed images, whereas on 1.25 and 2.5mm retro-reconstructions, the cusps are indistinct or not visible and the outline of the pulmonic bulb was mild to very indistinct, respectively (Figure 2).

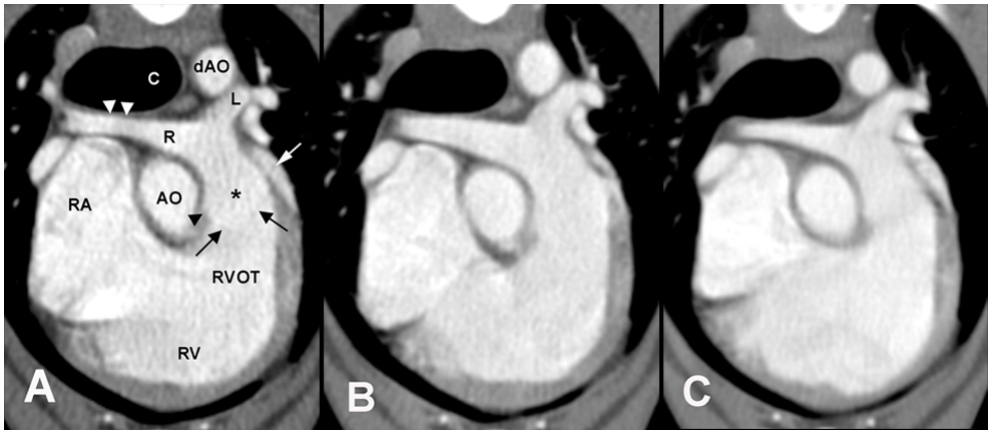

Figure 2: Transverse View of Right Ventricular Outflow Tract, Main Pulmonary Artery and its Left and Right Branches and Comparison of Three Collimation Settings. Transverse plane reconstruction of 0.625mm (A) and retro-reconstruction of 1.25mm (B), and 2.5mm (C) slice thickness. The main pulmonary artery (MPA, *) arises from the right ventricular outflow tract (RVOT) left of midline in a craniodorsal direction flanked by the tip of the left atrial appendage (white arrow) laterally and the ascending aorta (AO) medially. Only on 0.625mm reconstruction the fine outline of the cusp (black arrows) can be seen, also on the larger retro-reconstructions, the pulmonic bulb (black arrow head) is less distinct. The right cranial lobar artery has a smooth dorsoventral focal narrowing (white arrowheads) as it passes ventral to the trachea dorsally to the right atrium. LPA, RPA = left and right pulmonary artery, respectively; C = carina; dAO = descending aorta; RA = right atrium; RV = right ventricle; CrVC = cranial vena cava; Br = brachiocephalic trunk; CVC = caudal vena cava; LA = left atrium.

The MPA arose from the RVOT left of midline in a craniodorsal direction flanked by the tip of the left atrial (LA) appendage laterally and the ascending aorta (Ao) medially. The bifurcation of the MPA into

the LPA and RPA occurred dorsal to the aortic root and left ventrally to the carina (see also Figure 1).

The RPA proceeded in the dorsal plane laterally towards the right, the right cranial lobar artery branched straight laterally from its cranial aspect. A smooth dorsoventral focal narrowing of the right cranial lobar artery was observed in all dogs, which can be attributed to the passage between trachea and right atrium. On 1.25mm and 2.5mm retro-reconstructions, a decrease in diameter could be seen on one side of the right cranial lobar artery but not a focal narrowing. The right cranial lobar artery then continued cranioventrally, pivoting over the right cranial lobar bronchus, undergoing bifurcation as it crossed caudally to the right azygos vein and cranially to the right cranial lobar bronchus. Both branches ran in the cranial direction, one in a more dorsal plane extending into the craniodorsal portion of the right cranial lung lobe without crossing the midline. The second branch extended in a more ventral plane into the cranioventral tip of the right cranial lobe, crossing the midline to the left.

The RPA ran in the caudolateral direction, crossing dorsally to the right caudal pulmonary vein and ventral to the right main stem bronchus. It continued along the ventrolateral aspect of the right bronchus. At the respective lobar bronchial divisions, the right middle lobar artery originated ventrolaterally; immediately caudally the accessory lobar artery branched ventromedially. The right caudal lobar artery continued in the caudodorsal direction.

The LPA traversed dorsal to the left atrial appendage and left cranial pulmonary vein and ventrally to the descending aorta describing a caudodorsal curve. The left cranial lobar artery (cranial portion) exited ventrolaterally, curving over the cranial lobar bronchus (cranial portion). The LPA then passed dorsally to the main left lobar bronchus, which had a mild indentation at that level. The PA branch to the caudal portion of the left cranial lung lobe exited in ventrolateral direction at the level of its lobar bronchus. The left caudal pulmonary artery continued in the caudodorsal direction. All lobar pulmonary arteries followed laterally adjacent to their respective bronchi into the periphery, medium sized to very small sublobar artery branches arose in a dichotomous or trichotomous fashion, most commonly at the level of lobar bronchial divisions.

The MPA, RPA, LPA, and all lobar pulmonary arteries were visible on images of all three collimations. Mild to moderate blur of the vessel margins was seen on images retro-reconstructed to 1.25 and 2.5mm, whereas vessel margins were sharp on images reconstructed to 0.625mm slice thickness (Figure 3).

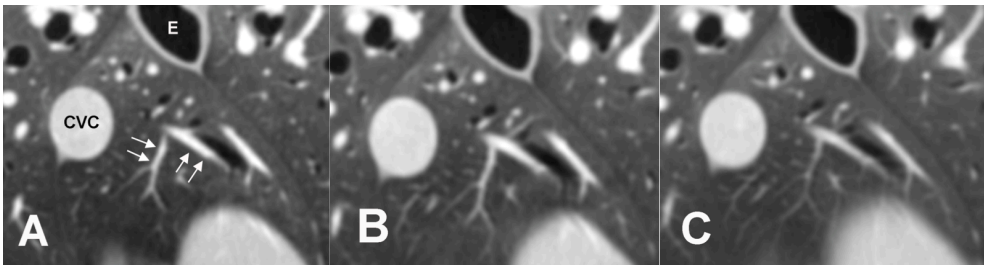

Figure 3: Visualization of Pulmonary Artery Branches and Segments using Three Different Reconstruction Slice Thicknesses. Pulmonary artery branches (white arrows) in the accessory lung lobe on 0.625mm reconstruction (A), 1.25mm (B), and 2.5mm (C) retro-reconstruction slice thickness. At 0.625mm the vessel margins are sharp whereas at the larger retro-reconstruction slice thicknesses vessel margins are mild to moderately blurred and the image is smoother and flatter due to partial volume artifact. CVC = caudal vena cava; E = esophagus.

The range of detected segments in the lobar arteries was 12-19 segments on 0.625mm reconstructions, 8-14 segments on 1.25mm, 7-11 on 2.5mm retro-reconstructions. Detailed results of recorded segments of the individual lobar arteries are given in Figure 4.

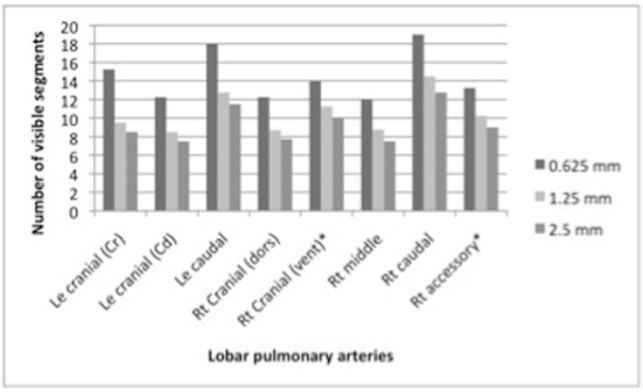

Figure 4:
Averages of visible segments of the lobar pulmonary arteries based on reconstruction slice thickness. Significant differences* in the number of visible pulmonary arterial segments were found between all reconstruction thicknesses for the right cranial (vent) and accessory lobar arteries ($P \leq 0.05$). In all other lobar arteries significant differences in the number of visible pulmonary arterial segments were found on 0.625mm reconstruction compared to both larger retro-reconstruction slice thicknesses ($P \leq 0.05$), and no significant difference was present

between 1.25 and 2.5mm retro-reconstructions ($P \geq 0.05$). Standard error for the estimated averages of visible segments of the lobar pulmonary arteries for all reconstruction thicknesses was 0.89 for the right cranial (dors), 0.58 for the right cranial (vent), 0.57 for the right middle, 0.98 for the right caudal, 0.92 for the right accessory, 0.74 for the left cranial (Cr), 1.52 for the left cranial (Cd), and 1.23 for the left caudal lobar artery

There were significant differences ($P \leq 0.05$) of visible segments between all reconstruction thicknesses in the right cranial (vent) and right accessory lobar arteries. In the right cranial (dors), right middle, and right caudal lobar artery significantly ($P \leq 0.05$) more segments could be seen on 0.625mm reconstructed images compared to both larger retro-reconstruction thicknesses. For all three left lobar arteries, there were significant differences ($P \leq 0.05$) between 0.625mm and both larger retro-reconstruction thicknesses.

Discussion

Pulmonary angiography with 64-MDCT depicted the anatomy of the canine pulmonary arterial tree *in-vivo* as described in the literature.[13-15] Understanding the pulmonary arterial anatomy and knowledge of normal variants is essential for clinical evaluation in a variety of diseases.

Even though pulmonic stenoses are observed most commonly at valvular, supravalvular, or subvalvular levels,[16] peripheral pulmonary artery stenosis has been described.[17] A focal narrowing in diameter of the right cranial lobar artery was detected in all dogs and this should not be mistaken for a stenosis. The right cranial lobar artery is the first branch of the right pulmonary artery, exiting straight laterally. When viewing in the transverse plane only, care must be applied to evaluate the right cranial lobar artery separately from the continuation of the right pulmonary artery that can be seen just caudally. The left pulmonary artery causes a focal indentation in the bronchial lumen as it passes dorsal to the left main stem bronchus, considered a normal variant. Compression of the left main stem bronchus is described on lateral radiographs in dogs with an enlarged left atrium.[18] In contrast, the right pulmonary artery passes ventral to the respective bronchus and does not cause a narrowing. Interestingly, two similar sized lobar vessels were seen in all right cranial lung lobes, whereas a single right cranial lobar vessel is usually described.[13, 14]

As only a small number of dogs of the same breed were used in this study, what has been described as anatomic variations, has to be considered with care and may not be transferred to other breeds.

Mild and mild-moderate blurring of vascular margins was observed using 1.25 and 2.5mm retro-reconstructed slice thickness, attributable to partial volume effects.[19] However, decreased image noise in reconstructed slice thickness greater than 0.625mm gives the images a more smooth and flat appearance.[20] Another trade-off between appearance and spatial resolution is that fewer generations of sublobar branches were detected on 1.25 and 2.5mm retro-reconstruction thicknesses; these were branches in the < 1mm range. Also note that non-isotropic slice-thickness can lead to decreased image analysis capabilities using multiplanar reformats.

A meta-analysis on pulmonary single detector CTA (SD-CTA) with suboptimal 5mm sections[21] led the American College of Chest Physicians and the American Thoracic Society to conclude that pulmonary SD-CTA was an insufficient clinical test to exclude pulmonary embolism in people. Reducing the collimation in pulmonary SD-CTA from 3mm to 2mm, however, increases the percentage of visualized subsegmental arteries.[22,23] Also, significant improvement of sensitivity regarding subsegmental pulmonary embolism was reported comparing 3mm pulmonary SD-CTA to 2.5 and 1.25mm multidetector row pulmonary CTA in people, the latter increasing the sensitivity.[24] Clinical relevance of subsegmental emboli is uncertain in both people and animals.[25, 26] On the other hand, diseases such as pulmonary

hypertension can affect the appearance of the small sublobar arteries in pulmonary CTA. While this is established in people,[27] this has not been investigated in animals.

Scan timing in relation to contrast medium injection is crucial for successful opacification of the pulmonary arteries or other vascular structures. To achieve this goal, various techniques can be applied. Fixed delay/best guess approaches, test bolus, and bolus tracking methods have been used previously in people[28-30] and dogs.[8, 10, 11,31] Bolus tracking methods are efficient and practical as the bolus for the diagnostic study is used to trigger the scan. Our test bolus method requires two injections (test and diagnostic bolus), thereby increasing the dose of contrast medium and fluid volume. However, it provides additional testing of the integrity of the venous access system and was used in our study as it is the preferred method in our institution. Potential hemodynamic effects, which were not considered during our study, could be overcome by the use of smaller, potentially weight- or body surface area-adapted injection volumes.

Similarly, the alternative of a fixed scan delay on the order of 15-25 seconds have given adequate results in pulmonary CTA in humans because the contrast enhancement rises rapidly with fast injections in the pulmonary arteries. However, patient dependent factors such as cardiac output and the related contrast medium transit time may delay enhancement significantly and lead to suboptimal timing. Subsequent insufficient contrast enhancement might cause the need for repeated studies.

Individualized scan delays using test bolus or bolus tracking approaches are designed to overcome such potential sources of error.[29, 32] The test bolus technique is applied routinely in clinical practice and was used in our study.[31,32,33] Time of contrast medium arrival in the pulmonary artery in our study was similar to previous work.[8,10] The prolonged injection duration and correlating high contrast medium volumes were chosen to allow for pulmonary arterial, systemic arterial, as well as all cardiac chamber opacification for a related project. Hence, described injection bolus volume is larger than necessary for only canine pulmonary CTA.

Reports on minimum or maximum enhancement levels needed for diagnostic CT angiography are sparse. Estimated values of the minimal enhancement range from 250 to 350HU (i.e. attenuation of 300 – 400HU).[29,33] We obtained higher enhancement values that can therefore be considered diagnostic.

First reports of pulmonary CTA in canine patients with clinical application are now available in the veterinary literature. A model of silicone endocasts was used to identify variations in the number of peripheral pulmonary veins in 19 dogs. Despite the variation in the periphery three consistent left atrial end points of the pulmonary arteries where seen and compared to CT and echocardiography exams in two dogs allowing for identification of these ostia; this may allow for clinical evaluation of pulmonary vein size and abnormal flow pattern in future patients.[34] Another report documents pulmonary artery dissection in eight dogs with one dog being assessed by CT.[35] Goggs et

al[36] have evaluated CTA and point-of-care tests for pulmonary thromboembolism diagnosis in 12 dogs. Out of the 12 dogs pulmonary thromboembolism was classified as positive in 4/12, suspected in 3/12 and 5/12 dogs as negative using CTA, while none of the contemporaneous tests was able to differentiate the same from pulmonary thromboembolism diagnoses. [GOGGS]. With the foundation for the procedure and anatomy of pulmonary CTA laid in the current literature, the use of this diagnostic test is expected to increase in clinical practice and diagnostic utility will likely be further evaluated in larger patient groups and disease entities in the future.

In summary, pulmonary angiography using 64-MDCT enables visualization of the canine pulmonary arterial anatomy *in-vivo*. Using slice thickness greater than 0.625mm decreases the number of visible lobar artery segments and induces blurring of vascular margins. The right cranial pulmonary artery has a focal indentation that should not be mistaken for a stenosis.

References

1. Myer C. Radiographic review: the vascular and bronchial patterns of pulmonary disease. *Veterinary Radiology*. 1980;21: 156-160.

2. Koblik PD HW, Harnagel SH, Fisher PE. A comparison of pulmonary angiography, digital subtraction angiography, and 99mTc-DTPA/MAA Ventilation-Perfusion Scintigraphy for detection of experimental pulmonary emboli in the dog. *Veterinary Radiology*. 1989;30: 159-168.

3. Remy-Jardin M, Remy J. Vascular disease in chronic obstructive pulmonary disease. *Proc Am Thorac Soc*. 2008;5: 891-899.

4. Lee KS, Bae WK, Lee BH, Kim IY, Choi EW. Bronchovascular anatomy of the upper lobes: evaluation with thin-section CT. *Radiology*. 1991;181: 765-772.

5. Cummings K, Bhalla S. Multidetector computed tomographic pulmonary angiography: beyond acute pulmonary embolism. *Radiol Clin North Am*. 2010;48: 51-65.

6. Jardin M, Remy J. Segmental bronchovascular anatomy of the lower lobes: CT analysis. *AJR Am J Roentgenol*. 1986;147: 457-468.

7. Lee CH, Goo JM, Bae KT, Lee HJ, Kim KG, Chun EJ, et al. CTA contrast enhancement of the aorta and pulmonary artery: the effect of saline chase injected at two different rates in a canine experimental model. *Invest Radiol*. 2007;42: 486-490.

8. Makara M, Glaus, T., Dennler, M., Bektas, R., Kutter, A., Dip, R., Schnyder, M., Deplazes, P., Oehlert, S. Multi-Row Computed

Tomography Angiography Technique of the Canine Pulmonary Vasculature. *Veterinary Radiology & Ultrasound*. 2010;51: 232.

9. Takahashi A, Yamada K, Kishimoto M, Shimizu J, Maeda R. Computed tomography (CT) observation of pulmonary emboli caused by long-term administration of ivermectin in dogs experimentally infected with heartworms. *Vet Parasitol*. 2008;155: 242-248.

10. Habig A, Beal, M., Brown, A., Nelwon, N., Coehlo, J., Kinns, J. Pulmonary Angiography Using 16 Slice Multidetector Computed Tomography In Clinically Normal Dogs. *Veterinary Radiology & Ultrasound*. 2010;51: 232.

11. Seiler GS, Nolan TJ, Withnall E, Reynolds C, Lok JB, Sleeper MM. Computed tomographic changes associated with the prepatent and early patent phase of dirofilariasis in an experimentally infected dog. *Vet Radiol Ultrasound*. 2010;51: 136-140.

12. SAS/STAT software, Version 9.2 of the SAS System for Windows. Copyright © 2009 SAS Institute Inc. SAS and all other SAS Institute Inc. product or service names are registered trademarks or trademarks of SAS Institute Inc., Cary, NC, USA.

13. Evans HE. The pulmonary arteries and veins. In: Evans HE(ed): *Miller's anatomy of the dog*. Philadelphia: Saunders, 1993;601-602.

14. Koch T, Berg, R. Arterien des kleinen oder Lungenkreislaufs. In: Berg R(ed): *Lehrbuch der Veterinaer-Anatomie* Stuttgart: Gustav Fischer Verlag, 1993;44-45.

15. Koenig H, Liebich, HG. Der Atmungsapparat (Apparatus respiratorius). *Anatomie der Haussaeugetiere*. Stuttgart: Schattauer GmbH, 2005;388.

16. Oyama MA DS, WP Thomas, JD Bonagura. Congenital heart disease. In: Ettinger SJ F, EC(ed): *Textbook of veterinary internal medicine*. St. Louis: Elsevier, 2005;972-1021.

17. MacGregor JM, Winter MD, Keating J, Tidwell AS, Brown DJ. Peripheral pulmonary artery stenosis in a four-month-old West Highland White Terrier. *Vet Radiol Ultrasound*. 2006;47: 345-350.

18. Bahr RJ. Heart and Pulmonary Vessels. In: Thrall DE(ed): *Textbook of Veterinary Diagnostic Radiology*. St. Louis: Saunders Elsevier, 2007;570-571.

19. Bushberg JT, Seibert, J.A. , Lediholdt Jr, E.M. , Boone, J.M. Computed tomography. In: Bushberg JT(ed): *The essential physics of medical imaging*. Philadelphia: Lippincott Williams & Wilkins, 2002;371-372.

20. Bushberg JT, Seibert, J.A. , Lediholdt Jr, E.M. , Boone, J.M. Computed tomography. In: Bushberg JT(ed): *The essentials of physics of medical imaging*. Philadelphia: Lippincott Williams & Wilkins, 2002;367-369.

21. Rathbun SW, Raskob GE, Whitsett TL. Sensitivity and specificity of helical computed tomography in the diagnosis of pulmonary embolism: a systematic review. *Ann Intern Med*. 2000;132: 227-232.

22. Remy-Jardin M, Remy J, Artaud D, Deschildre F, Duhamel A. Peripheral pulmonary arteries: optimization of the spiral CT acquisition protocol. *Radiology*. 1997;204: 157-163.

23. Remy-Jardin M, Baghaie F, Bonnel F, Masson P, Duhamel A, Remy J. Thoracic helical CT: influence of subsecond scan time and thin collimation on evaluation of peripheral pulmonary arteries. *Eur Radiol*. 2000;10: 1297-1303.

24. Patel S, Kazerooni EA, Cascade PN. Pulmonary embolism: optimization of small pulmonary artery visualization at multi-detector row CT. *Radiology*. 2003;227: 455-460.

25. Le Gal G, Righini M, Parent F, van Strijen M, Couturaud F. Diagnosis and management of subsegmental pulmonary embolism. *J Thromb Haemost*. 2006;4: 724-731.

26. MacDonald KA J, LR. *Pulmonary Hypertension and Pulmonary thrombembolism*. St. Louis: Elsevier, 2005.

27. Cummings KW, Bhalla S. Multidetector computed tomographic pulmonary angiography: beyond acute pulmonary embolism. *Radiol Clin North Am*.48: 51-65.

28. Bae KT. Optimization of contrast enhancement in thoracic MDCT. *Radiol Clin North Am*.48: 9-29.

29. Bae KT, Heiken JP. Scan and contrast administration principles of MDCT. *Eur Radiol*. 2005;15 Suppl 5: E46-59.

30. Cademartiri F, Nieman K, van der Lugt A, Raaijmakers RH, Mollet N, Pattynama PM, et al. Intravenous contrast material administration at

16-detector row helical CT coronary angiography: test bolus versus bolus-tracking technique. *Radiology*. 2004;233: 817-823.

31. Jung J, Chang J, Oh S, Yoon J, Choi M. Computed tomography angiography for evaluation of pulmonary embolism in an experimental model and heartworm infested dogs. *Vet Radiol Ultrasound*. 2010;51: 288-293.

32. Kuriakose J, Patel S. Acute pulmonary embolism. *Radiol Clin North Am*. 2009;48: 31-50.

33. Wittram C. How I do it: CT pulmonary angiography. *Ajr*. 2007;188: 1255-1261.

34. Brewer FC, Moïse NS, Kornreich BG, Bezuidenhoiut AJ. Use of computed tomography and silicone endocasts to identify pulmonary veins with echocardiography. *J Vet Cardiol.*2012;14: 293-300.

35. Scansen BA, Simpson EM, López-Alvarez J, Thomas WP, Bright JM, Eason BD, Rush JE, Dukes-McEwan J, Green HW III, Cunningham SM, Visser LC, Kent AM, Schober KE. Pulmonary artery dissection in eight dogs with patend ductus arteriosus. *J Vet Cardiol*. 2015;17: 107-119.

36. Goggs R, Chan DL, Bengini L, Hirst C, Kellett-Gregory L, Fuentes VL. Comparison of computed tompgraphy pulmonary angiography and point–of-care tests for pulmonary thrombembolism diagnosis in dogs. *J Small Anim Pract*. 2014;55:190-197.

CHAPTER 4

64-Multi-Detector Computed Tomographic Angiography of the Canine Coronary Arteries

Randi Drees[1], Alex P Frydrychowicz[2], Scott B Reeder[2], Marie E Pinkerton[2], Rebecca Johnson[1]

[1] From the Department of Surgical Sciences, School of Veterinary Medicine, University of Wisconsin-Madison, Linden Drive 2015, Madison, WI 53706, USA.,
[2] Department of Radiology, Medical Physic, Biomedical Engineering and Medicine, School of Medicine and Public Health, University of Wisconsin-Madison, 600 Highland Avenue, Madison, WI 53792, USA and Department of Pathobiological Sciences, School of Veterinary Medicine, University of Wisconsin-Madison, Linden Drive 2015, Madison, WI 53706, USA (Pinkerton).

Adapted from: *Veterinary Radiology Ultrasound* 2011;52:507-515.

Summary

Canine coronary artery angiography was performed in four anesthetized healthy dogs using 64-multidetector computed tomography (MDCT). Esmolol, a β-1 adrenergic receptor antagonist, and sodium nitroprusside, an arteriolar and venous dilator, were administered to enhance visualization of the coronary arteries by reducing heart rate and creating vasodilation. The left main coronary artery with its three main branches and the right coronary artery were visualized and subdivided in 13 segments for evaluation. Optimal reconstruction interval, expressed as percentage of the R-to-R interval, was determined at 5% in 2.9%, 35% in 1%, 75% in 21.2%, 85% in 43.3%, and 95% in 31.7% of the segments. Overall image quality was good in 41.3% of the segments and excellent in 14.4%. There was blur in 98.1%, motion in 17.3%, and stair step in 6.7% of the evaluated segments, but these artifacts did not interfere with anatomic depiction of the arteries. Cross sectional anatomy of the coronary arteries as evaluated from the coronary CTA agreed well with gross anatomic evaluation and published information. The use of esmolol did not lead to the target heart rate of 60 to 65 beats per minute (bpm). Nitroprusside had no significant effect on visualized length or diameter of the coronary artery branches. Coronary CTA is useful for the anatomic depiction of coronary artery branches in the dog.

Introduction

Multidetector computed tomography (MDCT) coronary artery angiography (coronary CTA) has been endorsed for non-invasive evaluation of the coronary arteries in symptomatic human patients.[1] Coronary CTA has been largely facilitated by the introduction of ECG-gated MDCT[2] and enables visualization of the entire coronary artery tree.[3, 4] The use of 64-MDCT has improved image quality and visibility of small coronary artery branches compared to 16-MDCT.[5] Also, coronary CTA has been used for the identification and characterization of anomalous coronary arteries which, in humans, may exhibit malignant variants potentially prone to limited exercise capability and/or sudden death.[6]

Although obstructive coronary artery disease as seen in human patients is not observed commonly in dogs, variations in individual anatomy, such as anomalous coronary arteries in Bulldogs, are important.[7-9] Such variants must be identified prior pulmonic valve balloon dilation as diminished coronary blood flow or avulsion of the coronary artery can result in death.[10]

Currently, selective catheter angiography is the gold standard for canine coronary angiography. This is invasive and has the potential of unwanted side effects. It remains used in settings where knowledge of the course of the vessels is vital.[10]

Although there are data on canine coronary CTA in basic translational research,[11] there is paucity on the anatomic description,

diagnostic performance and quality standards, as well as the influence of vasodilating drugs in canine coronary CTA. Therefore, our aim was to test the feasibility of 64-MDCT for visualization of canine coronary arteries. To account for the limited evidence that visualization of the coronary arteries is enhanced in human patients that are pretreated with nitroglycerin derivates for vasodilation,[12] an anesthetic protocol without and with injectable sodium nitroprusside, a coronary and pulmonary vasodilator, was compared for this purpose.

Material and methods

General anesthesia was induced in four 1-year old beagle dogs (mean body weight = 11 ± 0.5 kg) with propofol (PropoFlo™, Abbott Laboratories, North Chicago, IL) and maintained with isoflurane in 100% oxygen administered via orotracheal tube. End-tidal carbon dioxide levels were kept between 35-45mmHg using a mechanical ventilator (SAV 2500, Smiths Medical, Waukesha, WI, USA). For individual scans apnea was induced by hyperventilation immediately prior to the scan. Intravenous crystalloid solution (Plasma-lyte A, Baxter Healthcare Corporation, Deerfield, IL, USA) was administered through a 22G catheter in the left cephalic vein at 10ml/kg/hr with fluid boluses of 5ml/kg as necessary to maintain blood pressure level > 60mmHg (average fluid volume per dog: 110ml plus 50 +/- 5ml bolus). Esmolol (Esmolol, Bedford Laboratories, Bedford, OH, USA) was also administered through this catheter in an attempt to reduce heart rate through β-1 adrenergic receptor antagonism. In each dog, a 100μg/kg bolus was given followed by an infusion of 50μg/kg/min. However, since heart rate did not decrease, the infusion was increased every 5min to a maximum of 300μg/kg/min.

Scans were started within 15min following the onset of esmolol infusion. Short (10-15min) infusions of 10 μg/kg/min sodium nitroprusside (Nitroprusside, Hospira Inc, Lake Forrest, IL, USA) were also administered through this catheter to provide further arteriolar and venous dilation, although no target blood pressure was set. The

second study bolus was performed within 10-15min of initiating nitroprusside.

Mean blood pressure and heart rate measurements of the examinations without and with nitroprusside were compared using two-tailed paired Student's t-test using commercially available software (Sigma Stat® 3.5, Chicago, IL). Significance level was set at $p \leq 0.05$.

For image acquisition the dogs were placed in dorsal recumbency in a V-trough on a clinical 64-MDCT scanner (VCT, GE Healthcare, Waukesha, WI). A 20G catheter was placed in the right cephalic vein for injection of contrast medium to avoid streak artifacts arising from dense undiluted contrast medium in the vena cava.[13-15] A test bolus, also called a timing bolus, of 5ml iodinated contrast medium (ISOVUE 370, Iopamidol 370 mg iodine/mg, Bracco Diagnostics inc., Princeton, NJ, USA) followed by 20ml physiologic saline chaser, was injected at 2ml/sec at maximum pressure limits of 300lb/in^2 with a dual barrel power injector (Stellant, MedRad, Indianola, PA, USA). To monitor contrast medium arrival and to determine time to peak of contrast enhancement repetitive transverse scans were acquired in 1s time intervals (bolus track setting: 120kV, 40mA, axial scanning mode, 5mm slice thickness) at the level of the heart including the aortic root. Time to peak opacification in the ascending aorta (AO) was recorded.

The study contrast medium bolus was designed to maximize coronary artery opacification throughout the scan. The contrast medium bolus volume was adjusted to the requirement to cover the entire scan length with sufficient arterial opacification. Therefore, the

duration of the planned scan, as a function of scan length divided by pitch, was multiplied by the injection speed to provide the bolus volume. A 30ml physiologic saline chaser was used to advance the contrast medium through the system while washing contrast medium out of the CrVC and right ventricle to avoid streak artifacts.[13] This resulted in an average bolus volume of 2.1ml/kg (1.5 - 2.6ml/kg) contrast medium per dog for each of the two diagnostic studies. Following the individualized delay to peak enhancement calculated from the test bolus series, the scan of the heart was initiated using helical scan mode at 120kV, ECG modulated mA (200-750mA), 350ms gantry rotation time (average temporal resolution 175ms using SnapShot Segment feature, proprietary GE Healthcare, Waukesha, WI, USA), 40mm detector collimation (0.625mm x 64 detectors), heart-rate adapted variable pitch. Images were reconstructed to 0.625mm isotropic resolution using a soft tissue reconstruction kernel. The duration of the complete procedure including patient setup, test bolus and coronary scan was approximately 10-15min per dog, the scan time for coronary angiography itself was dependent on the cranial to caudal FOV, but was approximately 10s.

After a short break allowing for washout of the contrast medium from the first study bolus, nitroprusside was injected and the study bolus and scan protocol and bolus injection as described above was repeated for each dog. Following the successful termination of the experiment, all dogs underwent euthanasia and underwent necropsy examination.

As part of the post-processing of data, multiple data sets with the temporal reconstruction window increasing in 10% increments within the cardiac cycle were reconstructed, centered over the 5% through 95% interval (Figure 1).

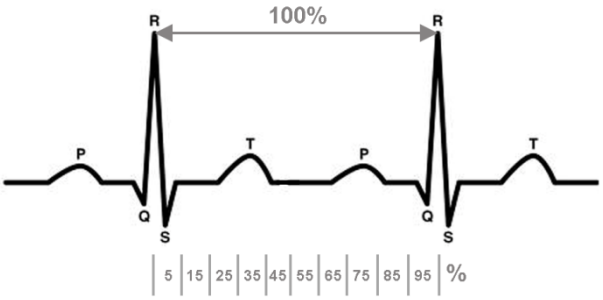

Figure 1: For Retrospective ECG Gating the reconstruction Interval, also called reconstruction window, is expressed as the percentage of the R-to-R interval. Tube current was modulated based on the ECG during the R-R interval (200-750mA).

Image evaluation was performed as a consensus review by one board certified veterinary radiologist and one board certified physician radiologist who were unaware of the acquisition parameters at the time of evaluation. Window width and level were adjusted individually. Multiplanar and curved reconstructions were applied as needed to optimize visualization of the coronary arteries. Images were reviewed on a dedicated viewing station using specialized software (VITREA®2 Version 4.0, Vital images, Minnetonka, MN, USA). First, injection and vital parameters were assessed. Time-to-contrast medium arrival (time-to-peak enhancement) of the test bolus in the ascending aorta and intensity of enhancement in the ascending aorta resulting from the

two study boluses was measured. Heart rate and blood pressure at all three injection times was recorded for each dog. Secondly, evaluation of diagnostic quality of the individual scans was performed by assessment of the left and right coronary arteries and their respective branches. For this, the coronary artery branches were subdivided in segments analogous to branching in people.[14] Then, the reconstruction interval allowing for optimal visualization of each segment was determined. Using the optimal R-to-R reconstruction interval for each segment the overall diagnostic quality of the study was evaluated for visualization of each individual segment (0 = poor, 1 = moderate, 2 = good, 3 = excellent) and presence of artifacts: stair-step, motion or blur (yes/no). Third, the maximal visualized length of the main right and left coronary artery branches was measured using a semi-automated vessel track function, and the diameter of those vessels was measured 2mm distal to their origin. A paired Student's t-test was used to determine the effect of nitroprusside on length and diameter. Significance level was set at $P \leq 0.05$. Lastly, the relation of the visualized coronary arteries and their branches to other cardiac structures was described. The results were compared to the necropsy findings and available references.[16-18]

Results

64-MDCT coronary artery angiography was performed successfully in all dogs. Detailed results for vital and injection parameters, measurement of time to contrast medium arrival from the test bolus, and intensity of enhancement from the two study bolus in the ascending aorta are given in Table 1.

Table 1:

Results for Injection and Vital parameters: Heart Rate, Blood Pressure, Time of Test Bolus Arrival in the Ascending Aorta, Study Bolus Design and Intensity of Enhancement in the Ascending Aorta from the Two Study Bolus for the Four Dogs.

	Test bolus			Study bolus 1				Study bolus 2			
	HR (bpm)	mBP (mmHG)	TTP aAO (s)	HR (bpm)	mBP (mmHg)	Bolus (ml 100% iodinated contrast medium/ ml saline)	Enhancement aAO (HU (SD))	HR (bpm)	mBP (mmHg)	Bolus (ml 100% iodinated contrast medium/ ml saline)	Enhancement aAO (HU (SD))
Dog 1	105	40	6	112	49	18/30	407 (17)	117	29	18/30	301 (18)
Dog 2	122	50	6	126	50	20/30	347 (19)	124	50	20/30	347 (19)
Dog 3	100	44	4	98	51	18/30	523 (18)	108	38	18/30	396 (21)
Dog 4	105	35	9	113	35	30/30	597 (21)	110	41	30/30	431 (19)

HR = heart rate, TTP = time to peak enhancement in ascending aorta after test bolus injection, aAO = ascending aorta, mBP = mean blood pressure. Before injection of study bolus two a vasodilator was injected intravenously.

Heart rate, recorded at the time of the scan, was not significantly different between the scans and averaged 111 (range 98 – 126) beats per minute. No arrhythmias or rapid changes in heart rate were noted at any time. Similarly, the combination of inhalant anesthesia, esmolol, and nitroprusside produced hypotension in all dogs, and mean blood pressure recorded at scan time was not significantly different between scans, averaging 42.7 ± 7.4mmHg (all $P > 0.05$). Mean time-to-peak

enhancement in the ascending aorta from the test bolus injection was 6.7s (range 4-9s). Adjusting for this inter-individual temporal variability from the test bolus arrival, the study bolus produced good enhancement of > 300 Hounsfield units (HU) in the ascending aorta in all dogs.

All eight scans were of diagnostic quality. Thirteen coronary artery segments were identified (LCA, LIVP 1-3, LS 1-2, LCX 1-4, RCA 1-3, see anatomic definition below). A total of 104 coronary artery segments were evaluated in all eight studies. The optimal reconstruction interval for the individual segments, given as the percentage of the R-to-R interval, was determined as 35% in 1%, 5% in 2.9%, 75% in 21.2%, 95% in 31.7% and 85% in 43.3% of the segments (Table 2).

Table 2: Optimal Reconstruction Interval Displayed as Percentage of the R-to-R Interval for the Individual Coronary Artery Segments Observed on Exams Without and With Injection of Vasodilator in the total of 104 Segments Evaluated.

	% Reconstruction interval (number of segments)				
	5%	35%	75%	85%	95%
LCA 0			2	3	3
LIVP 1			1	6	1
LIVP 2			2	5	1
LIVP 3			1	4	3
LS 1			2	3	3
LS 2			2	3	3
LCX 1			1	1	6
LCX 2			1	5	2
LCX 3	1		2	3	2
LCX 4		1	1	4	2
RCA 1			2	3	3
RCA 2	1		2	3	2
RCA 3	1		3	2	2
Overall	3	1	22	45	33

LCA = left main coronary artery, LIVP = interventricular paraconalis branch of left coronary artery, LS = septal branch of left coronary artery, LCX = circumflex branch of left coronary artery, RCA = right coronary artery

Overall diagnostic quality was rated on a per segment basis, as poor in 8/104 (7.7%), moderate in 38/104 (36.5%), good in 43/104 (41.3%) and excellent in 15/104 (14.4%). Out of the segments rated as poor, 1/8 was the second most proximal segment, all others were third most proximal or further distal segments; for the segments rated with image quality as moderate, 10/38 were the second most proximal segment, all others were third most proximal or further distal segments. Out of the segments rated with overall diagnostic image quality good, 30/43 were within the segment 0-2. For the rating excellent, 13/15 were within segment 0-1 and two were the second most proximal segment.

No artifacts were seen in the main left coronary artery segment in two scans (2/104, 1.9%,). Out of the three evaluated artifacts (stair-step, motion, blur) one was observed in 79/104 (76%), two were observed in 21/104 (20.2%), and three artifacts were observed in 2/104 (1.9%) of the coronary artery segments; in summary one or more artifacts were seen in 98.1% of the segments. Blur was the most common artifact and was present in 102/104 (98.1%) of the evaluated segments; motion was present in 18/104 (17.3%), and stair step artifact was seen in 7/104 (6.7%) of segments. Motion was most commonly present in segments in perpendicular orientation to the scan plane.

Results for length and diameter of the coronary arteries are given in Table 3

Table 3: Averages of Maximally Visualized Length of the Main Coronary Artery Branches using Semi-Automated Vessel Track Function and Maximal Diameter Measured 2mm Distal to Origin of the Individual Segment Observed Without and With Injection of Vasodilator.

	Length (mm)		Diameter (mm)	
	w/o nitro	w nitro	w/o nitro	w nitro
LCA	4.8*	4.3*	2.9	3.2
LIVP	68.6	62.5	3.1	2.9
LS	34.1	33.0	1.8	1.8
LCX	73.2	71.3	3.2	3.1
RCA	41.2	37.5	2.1	2.3

RCA = right coronary artery, LCA = main left coronary artery, LIVP = interventricular paraconalis branch of left coronary artery, LS = septal branch of left coronary artery, LCX = circumflex branch of left coronary artery, w/o nitro = without injection of vasodilator nitroprusside, w nitro = with injection of vasodilator nitroprusside, * n =2.

In two dogs the exact length of the LCA segment could not be determined in the study without and with injectable vasodilator as the LIVP and LCX branches followed a close parallel path before diverging. In those dogs the diameter of the artery was measured as in all other studies.

No significant impact of nitroprusside on length or diameter was found. Although mean blood pressure was lower in the dogs following

nitroprusside administration (46.3 +/- 7.5 versus 39.5 +/- 8.7mmHg) these differences were not statistically significant.

The main left coronary artery (LCA) arose from the left sinus of the aortic bulb in dorsal-left-lateral orientation, just caudal to the level of the main pulmonary artery and medially to the left auricle.

The short LCA was seen as a distinct segment in two dogs without and with vasodilator. In two dogs the segment was very short and the two main branches (LVIP and LCX) followed a close parallel path before diverging, arising in the same location directly from the aorta. On gross pathology exam, a short main LCA was present in all dogs, with a length of 3-5mm and diameter at the opening of 3-4mm, as described.[16-18]

The paraconal interventricular branch of the LCA (LIVP) (Figure 2) was seen as a separate branch in all studies, in one dog arising directly from the aorta, in the other three dogs as branch of the terminal LCA.

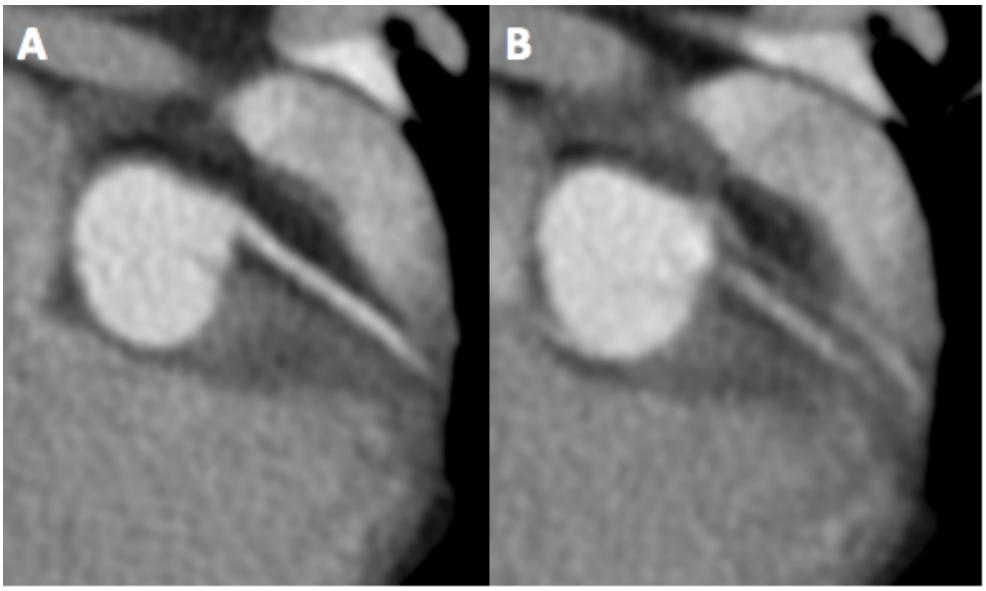

Figure 2: Transverse images of the paraconal interventricular branch of the left coronary artery (LPIV), reconstructed at 95% (A) and 5% (B) of the R to R interval. At 5% reconstruction interval, motion artifact causes the false display of two vessels and blur, whereas only mild blur is evident using the 95% reconstruction interval.

In all dogs it ran in left ventrolateral and slight caudal orientation almost parallel to the scan plane just caudal to the main pulmonary artery and ventromedially to the left auricle (LIVP 1), to continue very superficially in the paraconal interventricular groove in caudoventral direction almost perpendicular to the scan plane (LIVP 2), turning slightly more parallel to the scan plane towards the apex of the heart (LIVP 3). On gross examination this branch arose as a direct extension of the terminal LCA, and followed the paraconal interventricular groove as described above, with multiple smaller branches. This is in accordance with published information.[16-18]

The septal branch was seen in all dogs and ran in obliquely horizontal orientation in the interventricular septum (LS 1) and then turned perpendicular to the scan plane to continue as the descending segment (LS 2). In three of the four dogs it arose from the most proximal paraconal interventricular branch of the LCA in both studies; in one of these dogs a separation into two branches was seen at the mid level of the interventricular septum in both studies. In one dog, two septal branches arose from the medial aspect of the paraconal interventricular branch, one small branch from the proximal LIVP, and one larger one approximately 1cm distal to its origin, both traveling ventromedially just caudal to the main pulmonary artery into the interventricular septum (Figure 3).

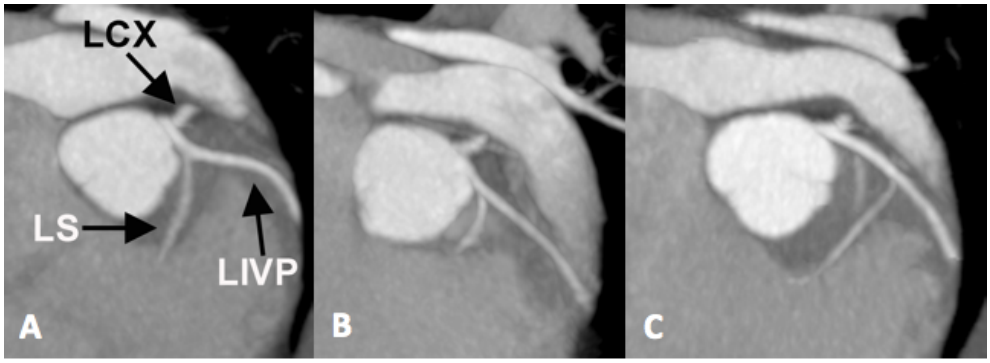

Figure 3: Variation of the branching pattern of the left coronary artery in three dogs displayed as thick slice reconstruction (6.48mm): The left circumflex (LCX), left interventricular paraconalis (LIVP) and left septal (LS) branch arise from the short coronary artery as separate branches (A), but when the main left coronary artery is very short, this may appear as direct branching off the LCX and LIVP off the aorta (B). Variation of the branching pattern with two separate branches was seen in one dog (C).

Grossly, the origin of the septal branch was not dissected. A variable origin of the septal branch is reported: 48% from the paraconal interventricular branch, 27% as terminal branch of the LCA, 19% from the LCA, 5% from the aorta, and 1% from the circumflex branch.[16-18]

The circumflex branch of the LCA (LCX) was seen as a separate artery in all dogs in both studies (Figure 4).

Figure 4: Circumflex Branch of the Left Coronary Artery (LCX): Curved Multiplanar Reconstruction (A, B) and Transverse Images (C, D) Reconstructed at 85% (A, C) and 65 % (B, D) of the R-to-R Interval. Reconstruction at the Suboptimal Reconstruction Interval Leads to Stair-Step Artifact in the Plane of the Artery (B) and Motion (D). Mild blur is evident even at optimal reconstruction interval due to limits in resolution, but this does not impact the anatomic localization of the coronary artery branch.

In all dogs the LCX (LCX1) traveled caudally perpendicular to the scan plane, initially laterodorsally adjacent to the aortic root and ventrally adjacent to the left atrial appendage, then continuing caudally in the coronary groove, slightly dorsolaterally adjacent to the left atrioventricular junction, ventrally to the vena cordis magna (left circumflex vein). It continued caudally around the left atrium to the right side almost perpendicular to the scan plane, where it turned very superficially caudoventrally in the subsinuosal interventricular groove (ramus interventricularis subsinuosus, LCX 2) to continue ventrally along the caudolateral wall of the left ventricle almost parallel to the scan plane (LCX 3) to turn perpendicular to the scan plane towards the apex of the heart (LCX 4). The anatomic location of this left coronary branch corresponded to the description in the literature.[15-20] On gross examination, the position of LCX1 was confirmed but further branches were not examined.

In each scan the right coronary artery (RCA, Figure 5 and 6) arose in cranioventral direction on midline from the right sinus at the bulb of the aorta at the level of the main pulmonary artery.

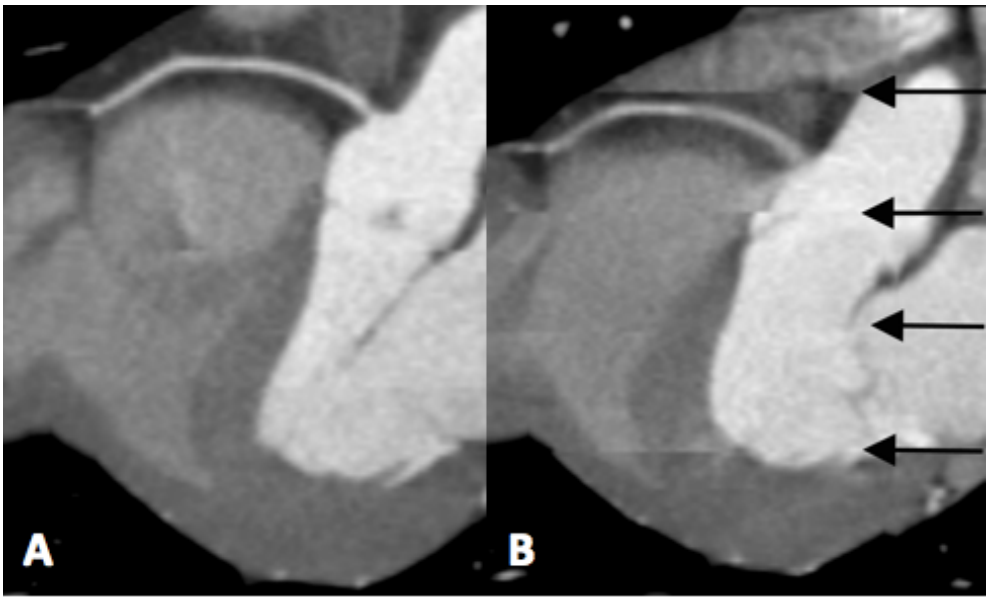

Figure 5: Curved multiplanar reconstruction at the level of the right coronary artery (RCA) reconstructed at 75% (A) and 25% (B) of the R-to-R interval. Reconstruction at the suboptimal interval at 25% causes increased blur and introduces stair step artifact. Stair-step artifact however is not in the image plane of the right coronary artery and does not interfere with anatomic depiction of this vessel.

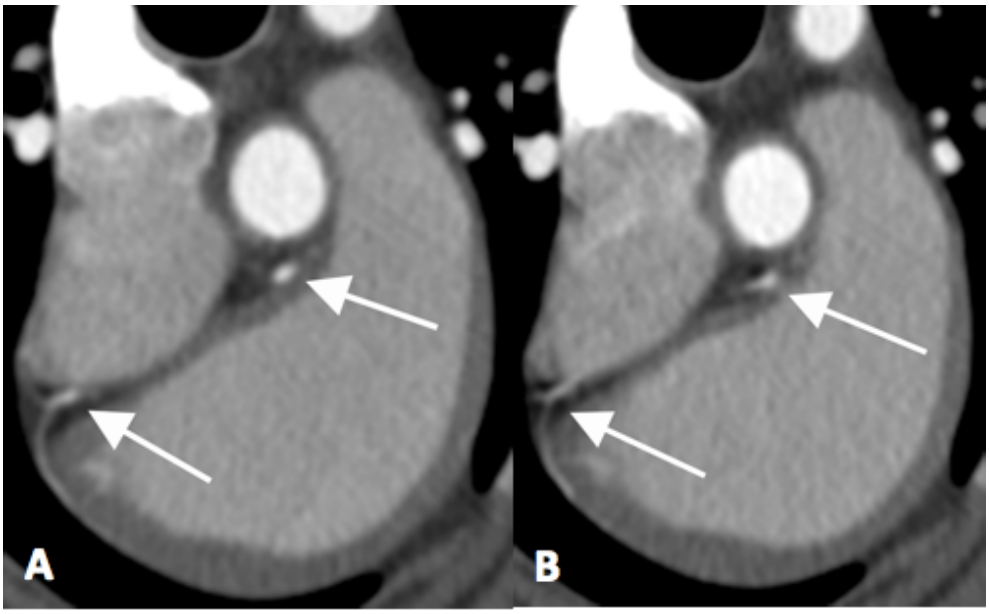

Figure 6: Motion artifact in the right coronary artery on transverse plane reconstruction is increased from 75% (A) to 95% (B) Reconstruction interval of the R-to-R interval. Motion artifact can be observed when the vessel runs perpendicular to the imaging plane.

In one dog a widening of the most proximal portion of the RCA was seen. Grossly, an accessory RCA was found and could be followed with a probe for 5mm. The RCA curved in right ventral orientation along the cranioventral aspect of the right atrium and medially to the right ventricle in the coronary grove, initially almost parallel to the transverse plane (RCA 1), then perpendicular to the scan plane as it approached the right lateral of the heart (RCA 2). It continued as right marginal branch (ramus marginalis dextra, RCA 3) caudoventrally along the lateral wall of the right ventricle towards the apex of the heart. The anatomic location of the RCA was in accordance with the literature.[16-18]

Discussion

Coronary artery angiography using 64-MDCT enables excellent depiction of the right and left coronary artery and the three main branches of the left coronary artery in the dog.

Heart rate has a major impact on the diagnostic quality of coronary CTA studies. In human patients the target heart rate is below 60 to 65bpm and is achieved routinely with the use of β-adrenergic receptor antagonism.[16] In an attempt to maintain a heart rate of 60-65bpm, esmolol was administered to dogs in our study. Esmolol decreases the heart rate and mean arterial blood pressure and prolongs the PR interval in healthy human subjects,[21-22] and is a safe drug to control heart rate for 64-MDCT coronary CTA in children.[23] In addition, esmolol has been reported to decrease isovolumetric relaxation and myocardial acceleration during isovolumetric relaxation in healthy dogs.[24] However, we were unable to reach the target heart rate with esmolol administration. Heart rate remained above the targeted 60-65bpm, well within the range for normal heart rates of the dog (70-120bpm). It is possible that heart rate was maintained in a baroreflexive attempt to maintain blood pressure, although general anesthesia blunts this response to an extent.[25] Alternatively, esmolol reduces heart rate by blocking the action of endogenous catecholamines (epinephrine and norepinephrine) at the β-1 adrenergic receptor.[21,22,25] Because the sympathetic nervous system is significantly attenuated during inhalant anesthesia, activation of adrenergic receptors may have been attenuated, reducing the effects of β-1 adrenergic receptor

antagonism by esmolol. Although we did not investigate the lack of bradycardia further, alternative techniques, such as calcium channel blockers, to lower heart rate could be assessed.

Hypotension (mean blood pressure < 60mmHg) was severe. Although many factors contribute to hypotension during general anesthesia, the concurrent use of systemic vasodilators (e.g. isoflurane, nitroprusside) and β-1 adrenergic blockade (e.g. esmolol) most likely all played part in the profound hypotension through a reduction in systemic vascular resistance, cardiac output and/or contractility. Thus, these protocols are not recommended for use in clinical patients. Although nitroprusside increases myocardial blood flow and is a potent, short acting coronary artery vasodilator in humans and dogs, an alternate choice may be the use of nitroglycerin which similarly dilates the coronary vasculature but may be associated with less systemic hypotension.[26,27]

The bolus design was optimized successfully for visualization of the coronary arteries while avoiding artifacts from right heart or cranial vena cava opacification. Based on previous work an optimum bolus profile for this is best achieved using a saline chaser and this was adapted for our study.[13,19] Bolus volumes were determined arbitrarily focusing on maximal opacification of the coronary arteries and not on weight adaption. The total bolus volume exceeded the commonly used dose of 2ml/kg in canine vascular CTA and may therefore have to be adapted for translation to the use in clinical patients.

The anatomic visualization of the coronary arteries using

coronary CTA was in good agreement with the gross anatomic observation and anatomy reported in the literature, although only the proximal portion of the coronary arteries was dissected.[16-18] Due to the small size of the vessels in the periphery and absence of the blood pressure distending vessels on the post mortem samples exact comparison of the length of the vessels may prove difficult also in future studies. The ability to visualize the normal canine coronary arteries using coronary CTA can serve as a baseline for visualizing anatomic variants in future studies and in patients. A standard segmental classification system developed by the American Heart Association for reporting of coronary angiography in 1975 is still in use, although a modified version has been proposed.[20,28] This system was adapted successfully for the canine coronary artery tree and allowed for reproducible description of the canine coronary artery segments. While coronary CTA allows for noninvasive visualization of the coronary arteries in multiple planes, potential drawbacks such as the exposure to increased doses to radiation may have to be considered.

Spiral/helical CT scanners acquire data continuously over the heart cycle and the ECG can be recorded during the scan. The retrospective reconstruction interval (also called window, expressed as R-to-R interval, Figure 1) can be placed anywhere in the R-to-R interval and images specific for that phase of the cardiac cycle can be displayed using specialized software. Motion of the coronary arteries is continuous during the cardiac cycle, but modest during the mid- to end-diastolic phase just before atrial contraction and at the end of

ventricular contraction in human subjects, allowing for motion-poor reconstruction. The optimal visualization has been determined using 4-MDCT for the left anterior descending artery (LAD) at 60-70%, for the left circumflex artery at 50%, and the right coronary artery at 40% of the R-to-R interval, indicating the need for separate reconstructions for each coronary artery.[29] Using 64-MDCT the best image quality was found at 60% and 65% of the R-to-R interval with heart rates < and ≥ 65bpm.[30,31] In our study the majority of the segments were best displayed at 75-95% of the R-to-R interval. This indicates that there may be a slightly different motion and rotation pattern in the canine heart compared to the human heart. Also, this interval corresponds to diastolic phase of the cardiac cycle, in which coronary blood flow is maximal.

Despite the small size of the canine coronary arteries, and low impact of bradycardic medication in this study, good to excellent overall image quality was achieved in greater than half of the evaluated segments, particularly the proximal to mid segments, allowing for accurate anatomic depiction. Whether canine coronary artery CTA using 64-MDCT is sufficient to detect possible occlusive disease canine patients remains to be determined.

Blur was the most commonly observed artifact, indicating slightly blurred vessel margin depiction. Partial volume effect and motion are the two major underlying reasons for blur. Two strategies to overcome this degradation would be to use a smaller reconstruction interval and reducing motion by improving bradycardic heart rate

control or using technology allowing for faster image acquisition. Motion artifact as evaluated in this study occurs due to the motion of arterial vessels that are perpendicular to the scan plane. It is not to be confused with blooming artifact described in human patients from high density calcium deposition in coronary plaques that can have a similar appearance, causing apparent enlargement of the plaque due to partial volume averaging effects.[32] It was found, as expected, in segments that are perpendicular to the scanning plane. It is likely to interfere with luminal measurements but did not affect anatomic localization of the segments. Occurrence of stair step artifact relates to speed of image acquisition and heart rate.[33] Despite the relatively poor efficacy of the bradycardic medication used in this study, stair step artifact was observed only in 6.7% of the segments. It was, however, present more commonly in the specific image plane but did not affect the coronary artery segment visualization in these instances.

Canine coronary artery length has been reported to be 0.5cm for the left main coronary artery, 8cm for the left circumflex branch, 7cm for the left paraconal interventricular branch, 5cm for the right coronary artery, with no length being reported for the left septal branch.[16-18] Length measurements achieved using 64-MDCT coronary CTA were comparable but slightly shorter, indicating that visualization of the most distal portion of the coronary arteries may have been insufficient. Alternatively differences in breed, body weight or age of the dogs as well as a different definition for the end of the arteries between anatomic specimens and coronary CTA samples may be

considered for this discrepancy. The diameter of coronary arteries has been reported as 5mm for the left main coronary artery, 1.5mm for the left circumflex and paraconal interventricular branch, and 1.5mm for the right coronary artery. No measurement was given for the left septal branch.[16-18] Using coronary CTA the semi-automated measurement of the diameter of all previously described segments was slightly larger, ranging from 2.1 to 3.2mm; the left septal branch was the smallest measuring 1.8mm.

Nitroglycerin results in a 20% increase in coronary artery diameter in human subjects and is of critical importance for assessment of the distal coronary artery.[26] Due to the relatively smaller size of the coronary arteries in dogs compared to humans the effect of nitroglycerin would be desirable in canine patients undergoing coronary CTA. However, no significant effect on maximally visualized length and maximal diameter was observed using nitroprusside. This may relate to small sample size.

In summary, canine coronary CTA using 64-MDCT was performed successfully and the description can serve as a cross-sectional anatomic reference. Esmolol did not have the desired bradycardic effect and nitroprusside did not enhance visualization of coronary artery branches. Optimal anesthetic protocol and bolus volume need to be determined

References:

1. Budoff MJ, Achenbach S, Blumenthal RS, Carr JJ, Goldin JG, Greenland P, et al. Assessment of coronary artery disease by cardiac computed tomography: a scientific statement from the American Heart Association Committee on Cardiovascular Imaging and Intervention, Council on Cardiovascular Radiology and Intervention, and Committee on Cardiac Imaging, Council on Clinical Cardiology. Circulation. 2006;114: 1761-1791.

2. Kalender WA, Seissler W, Klotz E, Vock P. Spiral volumetric CT with single-breath-hold technique, continuous transport, and continuous scanner rotation. Radiology. 1990;176: 181-183.

3. Hacioglu Y, Gupta M, Budoff MJ. Noninvasive anatomical coronary artery imaging versus myocardial perfusion imaging: which confers superior diagnostic and prognostic information? J Comput Assist Tomogr. 2010;34: 637-644.

4. de Graaf FR, Schuijf JD, Delgado V, van Velzen JE, Kroft LJ, de Roos A, et al. Clinical application of CT coronary angiography: state of the art. Heart Lung Circ. 2010;19: 107-116.

5. Wang YN, Jin ZY, Kong LY, Zhang ZH, Song L, Zhang SY, et al. Comparison of coronary angiography between 64-slice and 16-slice spiral CT. Zhongguo Yi Xue Ke Xue Yuan Xue Bao. 2006;28: 26-31.

6. Datta J, White CS, Gilkeson RC, Meyer CA, Kansal S, Jani ML, et al. Anomalous Coronary Arteries in Adults: Depiction at Multi-Detector Row CT Angiography. Radiology. 2005.

7. Liu SK TL, Tappe JP, Fox PR. Clinical and pathologic findings in dogs with atherosclerosis: 21 cases (1970-1983). J Am Vet Med Assoc. 1986: 227-232.

8. Buchanan JW. Pulmonic stenosis caused by single coronary artery in dogs: four cases (1965-1984). J Am Vet Med Assoc. 1990;196: 115-120.

9. Buchanan JW. Pathogenesis of single right coronary artery and pulmonic stenosis in English Bulldogs. J Vet Intern Med. 2001;15: 101-104.

10. Fonfara S, Martinez Pereira Y, Swift S, Copeland H, Lopez-Alvarez J, Summerfield N, et al. Balloon valvuloplasty for treatment of pulmonic stenosis in English Bulldogs with an aberrant coronary artery. J Vet Intern Med. 2010;24: 354-359.

11. George RT, Ichihara T, Lima JA, Lardo AC. A method for reconstructing the arterial input function during helical CT: implications for myocardial perfusion distribution imaging. Radiology. 2010;255: 396-404.

12. Chun EJ, Lee W, Choi YH, Koo BK, Choi SI, Jae HJ, et al. Effects of nitroglycerin on the diagnostic accuracy of electrocardiogram-gated coronary computed tomography angiography. J Comput Assist Tomogr. 2008;32: 86-92.

13. Utsunomiya D, Awai K, Sakamoto T, Nishiharu T, Urata J, Taniguchi A, et al. Cardiac 16-MDCT for anatomic and functional analysis: assessment of a biphasic contrast injection protocol. AJR Am J Roentgenol. 2006;187: 638-644.

14. Kerl JM RJ, Nguyen SA, Suranyi P, Thilo C, Costello P, Bautz W, Schoepf UJ. Right heart: split-bolus injection of diluted contrast medium for visualization at coronary CT angiography. . Radiology. 2008 356-364.

15. Cao L, Du X, Li P, Liu Y, Li K. Multiphase contrast-saline mixture injection with dual-flow in 64-row MDCT coronary CTA. Eur J Radiol. 2009;69: 496-499.

16. Evans HE. The heart and the arteries. In: Evans HE(ed): Miller's Anatomy of the dog. Philadelphia: Saunders, 1993;598-601.

17. Koch T, Berg, R. Blutgefäß- und Lymphsystem, Angiologia. In: Koch T, Berg, R.(ed): Lehrbuch der Veterinär-Anatomie: Die grossen Versorgungs- und Steuerungssysteme. Stuttgart: Gustav FIscher Verlag Jena, 1993;45-62.

18. König H, Liebich HG. Organe des Herz-Kreislauf-Systems. In: Koenig H LH(ed): Anatomie der Haussäugetiere. Stuttgart: Schattauer GmbH, 2005;445-448.

19. Bae KT. Intravenous contrast medium administration and scan timing in CT: considerations and approaches. Radiology 2010, 256:32-61.

20. Austen WG, Edwards JE, Frye RL, et al. A reporting system on patients for coronary artery disease. A report of the Ad Hoc Committee for Grading of Coronary Artery Disease, Council on Cardiovascular Surgery, American Heart Association. Circulation 1975;51:5-40.

21. Alexander R, Binns J, Hetreed M. A controlled trial of the effects of esmolol on cardiac function. Br J Anaesth. 1994;72: 594-595.

22. Ellenbogen KA, McCarthy EA, Pritchett EL. Effects of bolus injection of esmolol in healthy, exercising subjects. Clin Pharmacol Ther. 1987;41: 455-459.

23. Rigsby CK, Defreitas RA, Nicholas AC, Leidecker C, Johanek AJ, Anley P, et al. Safety and efficacy of a drug regimen to control heart rate during 64-slice ECG-gated coronary CTA in children. Pediatr Radiol. 2010.

24. Hori Y, Kunihiro, S., Kanai, K., Hoshi, F., Itoh, N., Higuchi, S. . The relationship between invasive hemodynamic measurements and tissue-doppler-derived myocardial velocity and acceleration during isovolumic relaxation in healthy dogs. J Vet Med Sci. 2009;71: 1419-1425.

25. Stoelting RK HS. Pharmacology & Physology in Anesthetic Practice. In: Stoelting RK HS(ed): Anesthetics in Pharmacology & Physology in Anesthetic Practice. Philadelphia: Lippincott Williams & Wilkins, 2006;42-86.

26. Capurro NL, Kent KM, Epstein SE. Comparison of nitroglycerin-, nitroprusside-, and phentolamine-induced changes in coronary collateral function in dogs. J Clin Invest. 1977;60: 295-301.

27. Pagani M, Vatner SF, Braunwald E. Hemodynamic effects of intravenous sodium nitroprusside in the conscious dog. Circulation. 1978;57: 144-151.

28. Konuralp C, Idiz M, Ates M. A novel reporting approach to coronary angiography: "segmental coding system". Int J Cardiol. 2005;98: 113-121.

29. Kopp AF, Schroeder S, Kuettner A, Heuschmid M, Georg C, Ohnesorge B, et al. Coronary arteries: retrospectively ECG-gated multi-detector row CT angiography with selective optimization of the image reconstruction window. Radiology. 2001;221: 683-688.

30. Leschka S, Husmann L, Desbiolles LM, Gaemperli O, Schepis T, Koepfli P, et al. Optimal image reconstruction intervals for non-invasive coronary angiography with 64-slice CT. Eur Radiol. 2006;16: 1964-1972.

31. Rahmani N, Jeudy J, White CS. Triple rule-out and dedicated coronary artery CTA: comparison of coronary artery image quality. Acad Radiol. 2009;16: 604-609.

32. Zhang S, Levin DC, Halpern EJ, Fischman D, Savage M, Walinsky P. Accuracy of MDCT in assessing the degree of stenosis caused by calcified coronary artery plaques. AJR Am J Roentgenol. 2008;191: 1676-1683.

33. Kimura F, Umezawa T, Asano T, Chihara R, Nishi N, Nishimura S, et al. Coronary computed tomography angiography using prospective electrocardiography-gated axial scans with 64-detector computed tomography: evaluation of stair-step artifacts and padding time. Jpn J Radiol. 2010;28: 437-445.

CHAPTER 5

Effect of two different anesthetic protocols on 64-MDCT coronary angiography in dogs

Randi Drees[1], Rebecca A Johnson[1], Marie Pinkerton[2], Alejandro Munoz Del Rio[3,5], Jimmy H Saunders[4], Christopher J François[5]

UW-Madison VMTH [1]DSS and [2]PBS, 2015 Linden Drive, Madison, WI 53706, USA;
[3]UW-Madison Department of Medical Physics, 600 Highland Avenue, Madison, WI 53792, USA;
[4]UGent, Faculty of Veterinary Medicine, Salisburylaan 133, 9820 Merelbeke, Belgium; [5]UW-Madison, School of Medicine and Public Health, Department of Radiology, 600 Highland Avenue, Madison, WI 53792, USA

Adapted from: *Veterinary Radiology Ultrasound* 2015;56:46-54.

Summary

Heart rate is a major factor influencing diagnostic image quality in computed tomographic coronary artery angiography (MDCT-CA) with an ideal heart rate of 60-65 beats/min in humans. The purpose of this prospective study was to compare the effects of two different clinically applicable anesthetic protocols on cardiovascular parameters and 64-MDCT-CA quality in 10 healthy dogs. The anesthetic protocols used consisted of premedication with (protocol A) IV fentanyl (5µg/kg; Fentanyl citrate, West-Ward, Eatontown, NJ, USA) and midazolam (0.2mg/kg; Midazolam, Hospira, Inc., Lake Forest, IL, USA) bolus followed by continuous rate infusion (0.2mg/kg/h midazolam and fentanyl 10µg/kg/hr and (protocol B IV premedication with dexmedetomidine (1µg/kg; Dexdomitor, Pfizer Animal Health, New York, NY, USA) followed by continuous rate infusion (dexmedetomidine 1µg/kg/h). For either protocol propofol bolus to effect (2-6 mg/kg IV) and isoflurane (1-2% vaporizer setting) in 100% oxygen administered via orotracheal tube was used for anesthetic maintenance. Scan protocols and contrast medium bolus volumes were standardized. Image evaluations were preformed in random order by a board-certified veterinary radiologist who was unaware of the anesthetic protocols used. Heart rate during image acquisition did not differ between protocols ($P = 1$), with 80.6 ± 7.5bpm for protocol A and 79.2 ± 14.2bpm for protocol B. Mean blood pressure was significantly higher ($P > 0.05$) using protocol B (protocol A 62.8 ± 9.1 vs protocol B 72.4 ± 15.9 mmHg). R-R intervals allowing for the best depiction of the

individual coronary artery segments were found in the end diastolic period and varied between the 70-95% interval. Diagnostic quality was rated excellent, good and moderate in the majority of the segments evaluated, with higher scores given for more proximal segments and lower for more distal segments, respectively. Blur was the most commonly observed artifact and most affected the distal segments. No significant differences were identified between the two protocols for optimal reconstruction interval, diagnostic quality and measured length of individual segments or proximal diameter of the coronary arteries (P = 1). Findings indicated that, when used with a standardized bolus volume, both of these anesthetic protocols yielded diagnostic quality coronary 64-MDCTA-CA exams in healthy dogs.

Introduction

Individual variations of the anatomy of the coronary arteries, such as aberrant coronary arteries, can significantly alter treatment decisions for related congenital abnormalities in dogs[1-3]. Multidetector computed tomography coronary artery angiography (MDCT-CA) has recently been introduced as a non-invasive method to depict the coronary arteries in normal dogs[4]. 64-MDCT-CA exam was able to show the left main coronary artery and its three main branches (paraconal interventricular, septal and circumflex branch) as well as the right coronary artery. The anesthetic protocol used in that canine study did not result in the desired target heart rate of 60-65 beats/minute, which has been shown to result in optimal image quality in humans undergoing coronary MDCT-CA[5]. Furthermore, the use of nitroprusside as a vasodilator showed no significant effect on the visualized length or diameter of the coronary arteries in the canine study[4], but caused significant hypotension so that the clinical applicability of this protocol is questionable. The use of nitroprusside improves the diagnostic accuracy of MDCT-CA in human due to improved vessel visibility and therefore optimized detection of anatomic variations or obstructive disease[6]. Canine coronary artery angiography with a clinically applicable anesthetic protocol that allows for adequate reduction of heart rate and therefore adequate diagnostic image quality for depiction of the coronary arteries has not been established.

In veterinary medicine, pre-anesthetic medications including fentanyl, midazolam and dexmedetomidine are commonly administered for

many reasons including patient sedation, facilitation of intravenous (IV) catheter placement, and as induction agent and for their inhalant sparing effects. Since bradycardia is associated with the use of opioids (i.e. fentanyl) and alpha-2 adrenergic agonists (i.e. dexmedetomidine), these drugs should reduce heart rate following their administration, an effect necessary for high-quality images during MDCT-CA exams. In addition, the sedative (and cardiovascular) effects of these agents are reversible with pharmacologic antagonists readily available to the practitioner, a technique commonly employed following short diagnostic procedures[7-12].

Thus, the aim of this study was to test two different, clinically applicable, anesthetic protocols for their effect on lowering heart rate and achieving diagnostic imaging quality for depicting coronary artery anatomy, diameter and length. We hypothesized that application of protocols using midazolam and fentanyl would decrease the canine heart rate to target values necessary to achieve adequate image quality for canine coronary artery angiographic studies using MDCT while having low impact on blood pressure. In contrast, dexmedetomidine would decrease heart rate to the target range (resulting in excellent image quality) while possibly producing undesirable effects on the blood pressure.

Material and methods

Animal preparation: The University of Wisconsin's Institutional Animal Care and Use Committee approved all procedures of this prospective trial. Ten beagle dogs (mean ± 1 SD age 12.4 ± 3.3 months, body weight 10.7 ± 1.2 kg) underwent 64-MDCT-CA (Discovery CT750 HD, General Electrics Medical Systems, Waukesha, WI, USA) on two different days using one of two anesthetic protocols for each occasion in a randomized fashion. Randomizing was performed by withdrawing one of 10 slips of paper from a jar. Five papers were labeled with number 1 (midazolam/fentanyl = 1) and five were labeled with number 2 (dexmedetomidine = 2). The first chosen number was used on study day 1 and the other on study day 2. One 20G intravenous catheter was placed in the right and left cephalic vein each in all dogs; the left was used for anesthesia purposes and the right for contrast administration, connected to a dual barrel power injector line. Electrocardiogram leads were placed on the food pads and elecrocardiogram signal was recorded through the imaging software and used for determination of heart rate during image acquisition and number of cardiac cycles needed for image acquisition. Pulse-oximetry was used to monitor heart rate, rhythm and hemoglobin saturation. Non-invasive systolic, diastolic and mean arterial pressure was monitored using the oscillometric method with a Cardell® Veterinary Monitor (Model 9401, CAS Medical Systems, Branford, CT, USA). Baseline heart rate was manually recorded just prior to anesthetic induction by auscultating the thorax. Heart rate, blood pressure and end-tidal CO_2 were recorded

once every 5 minutes immediately following anesthetic induction and instrumentation and for the duration of the anesthetic episode. Additionally, the CT software recorded the heart rate during the short period of angiographic image acquisition.

Anesthesia protocols: Anesthetic protocol A consisted of premedication with IV fentanyl (5µg/kg; Fentanyl citrate, West-Ward, Eatontown, NJ, USA) and midazolam (0.2mg/kg; Midazolam, Hospira, Inc., Lake Forest, IL, USA) bolus followed by continuous rate infusion (0.2mg/kg/h midazolam and fentanyl 10µg/kg/hr. Anesthetic protocol B consisted of IV premedication with dexmedetomidine (1µg/kg; Dexdomitor, Pfizer Animal Health, New York, NY, USA) and followed by continuous rate infusion (dexmedetomidine 1µg/kg/h). For both protocols, dogs were induced using a propofol bolus to effect (2-6 mg/kg IV) and maintained with isoflurane (1-2% vaporizer setting) in 100% oxygen administered via orotracheal tube in addition to the respective continuous rate infusion. Intravenous crystalloid Lactated Ringer's Solution Solution (5-10 ml/kg/hr; Abbott Laboratories, North Chicago, IL, USA) was also administered though the left cephalic catheter. End-tidal carbon dioxide levels were maintained at 35-45mmHg using a mechanical ventilator (SAV 2550 Small Animal Ventilator, Smiths Medical, Dublin, OH, USA). Short-term apnea was induced for the exams using mechanical hyperventilation and stopping ventilator activity immediately before initiation of the scan.

Coronary CTA: The CT exam was initiated 15 min after reaching a stable anesthetic plane with the dog positioned on the patient couch of the 64-

MDCT unit in a custom made V-trough in dorsal recumbency. First, a non-contrast exam of the whole thorax was performed to aid localizer placement for the following semi-automated bolus tracking (SmartPrep®). CTA was performed following the IV administration of 15ml iodinated contrast medium (Omnipaque 300, NovaPlus GE Healthcare, Princeton, NJ, USA; 420mgI/kg) and 5ml physiologic saline flush injected at 2ml/s and 325PSI. Using semi-automated bolus tracking, the angiographic CT scan was triggered when the contrast bolus reached the right ventricular outflow tract, as a 5 second scan delay was inherent to the machine software before initiating the retrospectively gated scan. Helical scan parameters were as follows: 80kVp, 200mA, 0.35s gantry rotation time, 40mm detector collimation (0.625mm x 64 detectors), 1.25mm slice thickness and spiral pitch factor 0.24. Images were reconstructed at 0.625mm isotropic resolution using a standard convolution kernel and 16cm display field of view.

After the imaging procedure, the dogs were humanely euthanized according to institutional protocol requirements and underwent gross necropsy for evaluation of the hearts and macroscopic coronary artery anatomy.

Image analysis: The images were post-processed to generate multiple data sets in 5% intervals within the cardiac cycle (4-94% R-R interval) as described previously[4]. Image evaluation was performed by a board certified veterinary radiologist (RD) in a randomized fashion, blinded to the individual anesthetic protocol used for the scans. Images were reviewed using dedicated viewing software[13], window width and level

were adjusted individually and three-plane as well as curved multiplanar reconstructions were applied as needed to optimize depiction of the coronary arteries.

For each scan contrast medium arrival time and the intensity of contrast enhancement at the base of the ascending aorta was recorded.

The diagnostic quality of the retrospectively gated exams was also recorded and the left and right coronary artery branches were subdivided into segments analogous to branching in humans, similar to our previous study[4, 14]. The R-R reconstruction interval allowing for optimal visualization of each segment was recorded. Using this interval, the diagnostic quality was scored for depiction of each individual segment (3 = excellent, 2 = good, 1 = moderate, 0 = poor or not visible; Figure 1) as well as for the presence of artifacts (yes/no; if yes: blur or stair step/motion was classified).

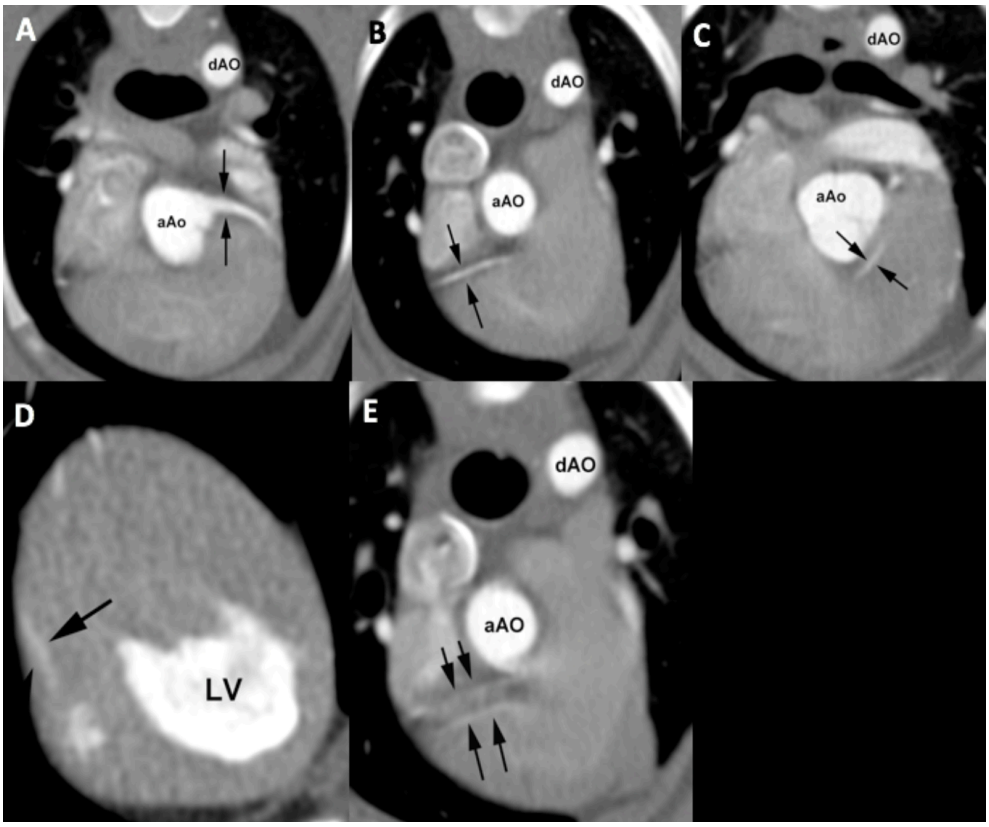

Figure 1: Evaluation of the individual coronary artery segments: Excellent depiction of the left coronary artery (LCA) and the proximal portion of the left interventricular paraconal branch (LIVP 1, arrows; A). Good depiction of the right coronary artery (RCA 2, arrows; B). Moderate depiction of the right coronary artery, blur of the vessel margins is also present (RCA 2, arrows; C). Poor depiction of the distal segment of the left circumflex coronary artery, blur of the vessel margins is also present (LCX 4, arrows; D). Due to cardiac motion the right coronary artery (RCA 2) is depicted as two vessels (arrows, E). aAO = ascending aorta, dAO = descending aorta.

The different artifacts could be simultaneously present per segment. The maximally seen length of the right (RCA) and left (LCA) coronary arteries as well as the main branches of the right coronary artery (right marginal (RM), right circumflex (RCX)) and left coronary artery (left

interventricular paraconal (LIVP), left circumflex (LCX), left septal (LS) branch) was recorded using a semiautomated vessel tracking function; additionally the diameter of the RCA, LCA, LIVP, LCX and LS was measured 2mm distal to their origin.

Statistical analysis: Statistical analysis was performed using R open source software[15]. Summary statistics were generated for all parameters evaluated. Continuous measures are summarized as mean ± 1 SD (standard deviation). For comparison of the vital parameters the Friedman rank sum test was used; then a pairwise comparison using the Wilcoxon signed rank test was performed and P-values were adjusted using the Holm-Bonferroni step down procedure[16]. Significance was set as $P \leq 0.05$. A Wilcoxon signed rank test was used to compare the measured length and proximal diameter of the coronary artery segments for protocols A and B. Significance was set at $P \leq 0.05$ and a Holm-Bonferroni step down procedure was performed[16].

Results

No anesthetic complications were encountered in any of the dogs using either anesthetic protocol. The entire CT procedure including patient setup, acquisition of localizer images, pre-contrast thorax exam, the retrospectively gated cardiac exam until the patient was moved off the patient table lasted for 9.31 ± 0.17min; while the duration of the retrospectively gated coronary angiography itself was an average of 5.0s ± 0.68s and included an average of 6.4 ± 0.95 cardiac cycles.

The heart rate immediately prior to induction was 105 ± 16bpm for all studies. For the duration of the anesthetic procedure the mean heart rate was 81.1 ± 11.6bpm using protocol A and 84.1 ± 19.2bpm using protocol B, no significant difference was determined (P=1). During image acquisition for the CTA the mean heart rate was 80.6 ± 7.5 bpm using protocol A and 79.2 ± 14.2 bpm using protocol B, also no significant difference was present (P=1) and heart rate was considered stable during image acquisition in 16/20 dogs. One dog showed a rapid increase of heart rate immediately after the contrast medium injection in both anesthetic episodes. The heart rate of this dog returned to near-normal values within 10-15 minutes of contrast injection. Mean blood pressure was significantly higher (P > 0.05) using protocol B (Protocol A 62.9 ± 9.1 vs protocol B 72.4 ± 15.9mmHg).

Differences in scan delay (18.1 ± 3.4s Protocol A, 19.4 ± 5.0 Protocol B) and aorta enhancement (441.2 ± 231.6 HU Protocol A, 519.7 ± 203.1 Protocol B) with the two anesthesia protocols were not significant (P=1).

For each dog, 14 coronary artery segments were investigated (LCA 0, LIVP 1-3, LS 1-2, LCX 1-4, RCA 1-2, RM, RCX). A total of 139 and 127 coronary artery segments using protocol A and B respectively were evaluated. One dog from protocol B had inadequate coronary artery enhancement for evaluation and was excluded from this analysis.

All optimal R-to-R reconstruction intervals were situated in the late diastolic phase, distributed between the 70-95% intervals. The optimal R-to-R reconstruction interval did not vary markedly within one dog between the two anesthetic episodes for the left or right coronary artery branches, respectively (P=1). An overview for the optimal reconstruction interval for the individual segments is given as a percentage of the R-to-R interval in Table 1.

Table 1: Optimal R-R Reconstruction interval of the individual coronary artery segments in the cardiac cycle determined using protocol A (midazolam/fentanyl) and B (dexmedetomedine). In one dog the LIVP 3 segment was not seen using protocol A; a total of 139 segments were evaluated using protocol A. Using Protocol B one dog had poor intravascular contrast enhancement and only the LCA was seen; a total of 127 segments were evaluated using protocol B. There was no statistical difference for the optimal reconstruction interval for each segment between both protocols (P=1). LCA, left main coronary artery; LIVP, left interventricular paraconalis branch of the left coronary artery; LS, left septal branch of the left coronary artery; LCX, circumflex branch of the left coronary artery; RCA, right coronary artery; RM, marginal branch of the right coronary artery; RCX, circumflex branch of the right coronary artery; #, number of.

Protocol	Reconstruction interval						# dogs
A/B	70%	75%	80%	85%	90%	95%	
LCA	1/1	3/2	1/2	2/1	2/1	1/2	10/9
LVIP 1	1/2	3/1	1/3	2/1	2/1	1/1	10/9
LVIP 2	1/2	3/1	1/3	2/1	2/1	1/1	10/9
LVIP 3	1/2	2/1	1/3	2/1	2/1	1/1	9/9
LS 1	1/2	3/1	1/4	2/-	2/1	1/1	10/9
LS 2	1/2	3/1	1/4	2/-	2/1	1/1	10/9
LCX 1	1/2	4/1	1/3	2/1	2/1	-/1	10/9
LCX 2	1/2	4/1	1/3	2/1	2/1	-/1	10/9
LCX 3	1/2	4/1	1/3	2/1	2/1	-/1	10/9
LCX 4	1/2	4/1	1/3	2/1	2/1	-/1	10/9
RCA 1	1/2	3/2	4/3	1/-	1/2	-/1	10/9
RCA 2	1/2	3/2	3/3	1/-	2/2	-/-	10/9
RM	1/2	3/2	3/3	1/-	2/2	-/1	10/9
RCX	1/2	3/2	4/3	1/-	1/2	-/-	10/9
# segments	14/27	45/19	25/44	24/8	25/18	6/11	
% segments	10.07/ 21.26	32.37/ 14.96	17.99/ 34.65	17.27/ 6.3	17.99/ 14.17	4.32/ 8.66	

The overall diagnostic quality was evaluated per segment and was rated as excellent in 23.5 and 24.4%, good in 27.1 and 28.4%, moderate in 32.1 and 40.9% and poor/not seen in 17.1 and 6.3% using protocol A and B, respectively (P=1, Table 2).

Table 2: Overall Diagnostic Quality of the Coronary Artery Segment Depiction using Protocol A and B as well as Scoring for Artifacts is given. The LVIP 3 segment was not seen in one dog using Protocol A; one dog was excluded of the evaluation (except from LCA) of Protocol B as poor contrast enhancement was present. There was no statistical difference for the given parameters for each segment between both protocols (P=1). LCA, left main coronary artery; LIVP, left interventricular paraconalis branch of the left coronary artery; LS, left septal branch of the left coronary artery; LCX: circumflex branch of the left coronary artery; RCA, right coronary artery; RM, marginal branch of the right coronary artery; RCX, circumflex branch of the right coronary artery; # dogs, number of dogs.

Protocol A/B	Overall Diagnostic Quality of Segment				Artifact			# Dogs
	Excellent	Good	Moderate	Poor/not seen	No	Yes		
						Blur	Stair step/Motion	
LCA	8/8	2/-	-/1	-/-	8/9	2/1	-/-	10/9
LVIP 1	7/8	3/1	-/-	-/-	7/8	3/1	-/-	10/9
LVIP 2	-/1	5/6	4/2	1/-	-/-	10/8	-/1	10/9
LVIP 3	-/-	1/1	4/5	4/3	-/-	10/9	-/1	10/9
LS 1	1/1	4/5	5/3	-/-	1/1	9/8	-/-	10/9
LS 2	3/-	1/2	1/4	5/3	1/-	9/9	-/-	10/9
LCX 1	7/9	3/-	-/-	-/-	7/1	3/-	-/-	10/9
LCX 2	4/1	3/6	3/2	2/-	4/-	6/9	-/1	10/9
LCX 3	-/-	3/3	4/6	5/-	-/-	10/9	-/-	10/9
LCX 4	-/-	1/-	3/7	-/2	1/-	9/9	-/-	10/9
RCA 1	3/2	7/7	-/-	-/-	3/1	7/5	1/1	10/9
RCA 2	-/-	5/5	5/4	-/-	-/-	10/9		10/9
RM	-/-	-/-	7/9	3/-	-/-	10/9		10/9
RCX	-/-	-/-	9/9	1/-	-/-	10/9		10/9
# segments	33/31	38/36	45/52	24/8	32/31	108/95	1/4	

The lower scores were predominantly given for the more distal segments whereas the higher scores were predominantly given for the more proximal segments.

No artifact was observed in 22.9 and 24.4% of the evaluated segments using protocol A and B, respectively (P=1). In the segments where artifact was observed, blur dominated with 77.1 and 74.8% over 0.7 and 3.2% stairstep/motion observed with protocol A and B, respectively (P=1). Blur was most often encountered as a non-sharp depiction of the vessel margins and was mostly seen in the more distal segments, also influencing the overall diagnostic quality as described above.

There were no significant differences in visualized length or diameter between the two anesthetic protocols (P=1; except for maximal length of RCA length P=0.52 and maximal diameter of RCA P=0.84). The individual results for the semi-automated measurement of length of the coronary artery segments and the manual measurement of the diameter of the proximal portion of the segments are given in Table 3 and 4.

Table 3: Averages of Maximally Visualized Length of the Left and Right Coronary Artery and Their Respective Branches Using Protocol A (Midazolam/Fentanyl) and B (Dexmedetomidine). No significant differences were determined between the protocols (P=1). LCA, left main coronary artery; LIVP, left interventricular paraconalis branch of the left coronary artery; LS, left septal branch of the left coronary artery; LCX: circumflex branch of the left coronary artery; RCA, right coronary artery; RM, marginal branch of the right coronary artery; RCX, circumflex branch of the right coronary artery.

	Protocol A (mean ± SD)	Protocol B (mean ± SD)	P-Value
LCA (cm)	0.48 ± 0.7	0.55 ± 0.9	1
LIVP (cm)	4.89 ± 1.9	5.87 ± 1.3	1
LS (cm)	2.89 ± 1.2	2.98 ± 0.9	1
LCX (cm)	7.45 ± 2.3	8.28 ± 2.6	1
RCA (cm)	2.47 ± 0.3	2.62 ± 0.4	0.52
RM (cm)	2.98 ± 1.9	2.37 ± 0.7	1
RCX (cm)	2.87 ± 0.6	2.64 ± 0.8	1

Table 4: Averages of maximally Visualized Diameter of the Left and Right Coronary Artery and Their Respective Branches Using Protocol A (Midazolam/Fentanyl) and B (Dexmedetomidine). No significant differences were determined between the protocols (P>0.05). LCA, left main coronary artery; LIVP, left interventricular paraconalis branch of the left coronary artery; LS, left septal branch of the left coronary artery; LCX: circumflex branch of the left coronary artery; RCA, right coronary artery.

	Protocol A (mean ± SD)	Protocol B (mean ± SD)	P-Value
LCA (cm)	0.39 ± 0.4	0.39 ± 0.1	1
LIVP (cm)	0.22 ± 0.1	0.21 ± 0.1	1
LS (cm)	0.13 ± 0.0	0.13 ± 0.0	1
LCX (cm)	0.22 ± 0.0	0.22 ± 0.0	1
RCA (cm)	0.17 ± 0.04	0.49 ± 0.6	0.84

The left coronary artery anatomy was observed and evaluated as previously described[4]. However, in this cohort the circumflex branch of the right coronary artery (RCX) was consistently seen and therefore also evaluated separate from the right marginal branch. This branch originates at the bifurcation of the RCA2 segment on the right lateral aspect of the heart. The right marginal branch (RM) runs caudoventrally along the lateral wall of the right ventricle towards the apex of the heart and the right circumflex branch continues in right caudodorsal direction in the coronary grove laterally along the right atrioseptal junction (RCX).

The gross anatomic evaluation of the hearts showed no abnormalities and the anatomy of the coronary arteries seen in the individual dogs corresponded to the description based on the CTA exams.

Discussion

Both anesthetic protocols allowed for excellent delineation of the left and right coronary arteries and their respective branches in the dog and there was no difference found for measured length and proximal diameter measured using either protocol.

The protocols used were directed at stabilizing the physiological heart rate of dogs (awake, normal rate is ~80-120bpm) as optimal diagnostic quality for coronary CTA studies is achieved in humans at a heart rate of 60-65bpm[17, 18]. A previous study in isoflurane-anesthetized dogs used esmolol and nitroprusside to attempt heart rate regulation and dilation of the coronary arteries and allowed for excellent depiction of the vessels, although with marked systemic hypotension; heart rate was also not consistently lowered[4]. Hypotension, if prolonged and/or severe, can threaten organ perfusion, causing injury and a state of "shock". When organs such as the heart, brain, kidneys, liver and lungs are affected by hypotension, significant patient morbidity and even mortality may result. Both anesthetic protocols applied in the current study consistently lowered the heart rate to a mean of approximately 80bpm. Even though this heart rate was higher than the desired heart rate of 60-65bpm, the generated image quality was overall very good and the coronary arteries and their branches were easily evaluated. It may be speculated that for evaluating the anatomy the canine heart rate may not be needed as low as in humans, where evaluation of small plaques is the prime focus of these exams. Additionally, differences in heart rate may be encountered based on age or possibly body weight of

the patient[19]. Therefore, it may be hypothesized that heart rate control may play a lesser role for image quality in MDCT-CA in large breed dogs or dogs over one year of age; however, further studies to evaluate these protocols in a more varied population of dogs would be needed to validate this. Newer technologies such as dual source CT units allow further reduction in the acquisition time. Also, recently developed advanced applications such as adaptive prospective triggering may further reduce the need of heart rate control[20].

For both anesthetic protocols an injectable drug was used for premedication and as continuous rate infusion during maintenance, reducing the minimal alveolar concentration of inhalant needed. For Protocol A, a combination of midazolam and fentanyl was used. Midazolam acts as a GABAA receptor agonist[7] and at clinical doses, midazolam has little effect on the cardiopulmonary system but exhibits cardiovascular depression when used at very high doses[8, 21]. Only clinically relevant doses of midazolam were used in the current study for achievement of anesthetic-sparing effects and to facilitate multimodal anesthesia. Fentanyl acts as an μ-opioid receptor agonist and is commonly used in dogs for analgesia[9, 10]. Administration is routinely performed as a bolus followed by a constant rate infusion due to its rapid onset of action and short duration[22]. In awake animals, fentanyl produces minimal cardiac depression[11], whereas it is associated with bradycardia in isoflurane-anesthetized dogs[23]. Together, these agents were efficacious in reducing the inhalant level

required, minimizing direct cardiovascular depression, and achieving acceptable target heart rate for MDCT-CA in this study.

For Protocol B, dexmedetomidine, a α-2 adrenergic receptor agonist, was used. Administration results in sedation and analgesia; constant rate infusions are also associated with bradycardia and profound cardiovascular depression, even at low doses[12, 24-27]. Thus, although it reduced the canine heart rate in our study to an acceptable level, its use may not be recommended in dogs with cardiovascular disease.

These investigations did not result in the same degree of hypotension as reported in our previous study using esmolol[4]. This is most likely due to the absence of beta-adrenergic receptor blockade from esmolol and vascular smooth muscle relaxation and vasodilation from nitroprusside administration. Especially protocol A, which combines midazolam and fentanyl, may be clinically applicable.

In the previous feasibility study[4], the injected fluid volume including the contrast bolus volume used up to 2.6ml/kg in addition to the 30ml/dog saline chaser was considerably larger than the current, weight-based bolus volume recommendation of 2ml/kg in companion animals[28, 29]. Here, we aimed to minimize the bolus volume to minimize fluid overloading while still preserving optimal visualization of the small cardiac vessels. A standard bolus volume of 15ml contrast medium and 5ml saline chaser was used; this equaled approximately 2ml/kg bolus volume in the study population and would be applicable in clinical patients. The saline chaser is used to advance contrast medium that would otherwise be wasted in the tubing or trailing in venous the

circulation from the injection site and mainly serves to produce an optimized tight bolus profile[30, 31] The scan delay applied here was longer than reported previously[4]. This study was performed on a different MDCT unit compared to the previous study; the current unit had a longer delay than expected from triggering the diagnostic scans to starting the diagnostic scan. This was addressed by triggering the scan with contrast arrival in the right heart to account for the circulation time of the contrast medium through the lung but could otherwise have been addressed with changing to a test bolus injection technique instead; the latter was not pursued to aim for consistency in experimental design. As a result, a larger standard deviation of the enhancement at the base of the aorta resulted, but diagnostic scan quality was achieved in all dogs except one dog using protocol B. This specific dog did show a rapid increase of heart rate to the contrast medium injection in both anesthetic episodes that might have contributed to faster advancement of the bolus through the heart and lungs, leaving insufficient contrast for defining the coronary artery branches. The heart rate of this dog returned to near-normal values within 10-15 minutes of contrast injection. The intravenous injection of non-ionic contrast media is generally well tolerated by dogs. In a study evaluating the effect of non-ionic contrast media injection in dogs undergoing cross-sectional imaging exams there was no change in heart rate, but a 2% incidence of hypertension[32]. Hypertension per se was not observed following contrast administration in our study but a slightly higher mean blood pressure was recorded when using protocol B.

The anatomic depiction of the left and right coronary artery branches was easily performed when evaluating the coronary CTA exams and agreed with the gross anatomical description of the proximal left and right coronary branches as inspected on gross necropsy. The gross anatomical description was focused on the proximal portion of the left and right coronary artery branches to detect anatomical variations and did not follow the small distal branches. We consider the depiction and correlation of the proximal portion of the coronary artery anatomy the main interest in canine patients at this time since aberrant coronary arteries may be of clinical significance. Even though coronary artherosclerosis has been reported in dogs[3], the current understanding of the canine cardiac anatomy and physiology attributes lower importance to obstructive coronary disease compared to people, as anastomoses are formed commonly in canines[1-3].

The systematic reporting of coronary segments was done in accordance with that proposed by the American Heart Association in 1975 and adapted in a previous publication describing the coronary CTA anatomy in dogs[4, 14]. In this study population, the description of the distal segments of the right coronary artery was amended from the previous description[4], as the right coronary artery split into a similarly developed circumflex and marginal branch all study subjects. This branch was not well observed in all study subjects in the previous study population and therefore not included in the evaluation at the time. As the dogs for the current and previous studies originated from a purpose breeding institution, one could speculate if the different breeding lines

between the current and previous study contributed to this discrepancy.

The R-R intervals for optimal depiction of the left and right coronary artery and their respective branches were found in the late diastolic phase, as expected from the previous canine study, yet differed from humans, where the 60-65% interval is recommended for heart rates around 65bpm using 64-MDCT[4, 33, 34]. There was little within-subject variation during a study and in the left or right coronary artery and their branches, but there was moderate inter-subject variation. Reconstructions were performed in 5% intervals and the distribution of the results throughout the 70-95% interval confirms the need for segmenting the data in 5% and not larger increments to optimize the visualization.

In this and the previous study, blur was the most commonly observed artifact[4]. The indistinct vessel margins relate to the limits of spatial resolution for these small structures. Motion or stair step artifact was found in only a few study subjects. Motion artifact commonly relates to the heart rate during the scan. Neither anesthetic protocol produced the optimal 60-65bpm heart rate[35] and therefore motion artifact was expected. Neither of the artifacts affected the detection of the respective vessel.

There were no differences in the length of the canine coronary arteries between anesthetic protocols. The LCA and the LIVP were shorter compared to the previous reported length using coronary CTA, whereas the LS and LCX were comparable[4]. Additionally, the RCA was measured

differently in the present study as the distal RM and RCX were measured separately; adding the RM to the RCA measurement would give comparable or slightly longer measurements as previously reported[4]. Anatomical measurements published describe 0.5cm for the left main coronary artery, 8cm for the left circumflex branch, 7cm for the left paraconal interventricular branch and 5cm for the RCA; a length has not been described in an anatomical study for the left septal branch[36-38]. As there was low inter-subject variation and our coronary CTA measurements are similar to the anatomical reports, we speculate that these are variations in the anatomy of these dogs originating from a different breeding line as the dogs used in the previous study[4]. Alternatively, the lower contrast bolus volume used in the current study may have affected measurements, however, we would expect a more systematic drift in the results and not an effect on two segments only.

The diameter of the coronary artery branches reported in this study is similar, yet somewhat smaller for multiple comparable measures reported in the previous study[4]. This might relate to the lower volume contrast bolus used or the difference in anesthetic protocols applied. As obstructive disease is not the primary focus for evaluation of the coronary arteries in dogs[3] we accept this finding as a possible limitation that is outweighed by the clinically applicable anesthetic protocols and contrast bolus volume used which allow for very good depiction of the anatomy.

The main limitation of our study was the small sample size, which limits statistical power; consequently, caution should be applied in concluding

that these protocols are equivalent when no significant differences are reported. Offsetting this is that each animal received both anesthetic protocols, which increase precision and limits intersubject variation. Still, ideally a larger cohort of dogs of different weights and breeds would be investigated, in addition to clinical patients. Also the variation in contrast enhancement achieved at the base of the aorta could possibly be remedied with applying the test bolus technique in future studies.

We conclude that both anesthetic protocols allowed similar and adequate reduction of the canine heart rate to achieve diagnostic quality canine coronary artery angiographic studies using 64-MDCT. Even though the target heart rate of <65bpm was not reached with either protocol, good image quality was achieved, allowing for depiction of the left and right coronary artery and their respective branches as well as measurement of their diameter and length. No significant difference was found for these parameters comparing both anesthetic protocols. Both protocols were well tolerated by the study subjects, but protocol B resulted in higher systemic blood pressures. Therefore, clinically used anesthetic protocols need to be chosen on an individual patient basis, taking into consideration patient signalment and disease processes as the tested protocols may not be suitable for all patients. Evaluating this technique in clinical patients with suspected aberrant coronary arteries or obstructive disease is desirable.

References

1. Buchanan JW. Pulmonic stenosis caused by single coronary artery in dogs: four cases (1965-1984). *Journal of the American Veterinary Medical Association*. 1990;196: 115-120.

2. Buchanan JW. Pathogenesis of single right coronary artery and pulmonic stenosis in English Bulldogs. *J Vet Int Med*. 2001;15: 101-104.

3. Liu S, Tappe JP, Fox PR. Clinical and pathological findings in dogs with atheroclerosis: 21 cases. *J Am Vet Med Assoc*. 1986: 227-232.

4. Drees R, Frydrychowicz A, Reeder SB, Pinkerton ME, Johnson R. 64-multidetector computed tomographic angiography of the canine coronary arteries. *J Vet Radiol & Ultrasound*. 2011;52: 507-515.

5. Menke J, Unterberg-Buchwald C, Staab W, Sohns JM, Seif Amir Hosseini A, Schwarz A. Head-to-head comparison of prospectively triggered vs retrospectively gated coronary computed tomography angiography: Meta-analysis of diagnostic accuracy, image quality, and radiation dose. *Am Heart J*. 2013;165: 154-163 e153.

6. Chun EJ, Lee W, Choi YH, Koo BK, Choi SI, Jae HJ, et al. Effects of nitroglycerin on the diagnostic accuracy of electrocardiogram-gated coronary computed tomography angiography. *J Comput Assist Tomogr*. 2008;32: 86-92.

7. Seddighi R, Egger CM, Rohrbach BW, Cox SK, Doherty TJ. The effect of midazolam on the end-tidal concentration of isoflurane necessary to prevent movement in dogs. *Vet Anaesth Analg*. 2011;38: 195-202.

8. Jones DJ, Stehling LC, Zauder HL. Cardiovascular responses to diazepam and midazolam maleate in the dog. *Anesthesiology*. 1979;51: 430-434.

9. Steagall PV, Teixeira Neto FJ, Minto BW, Campagnol D, Correa MA. Evaluation of the isoflurane-sparing effects of lidocaine and fentanyl during surgery in dogs. *J Am Vet Medical Assoc*. 2006;229: 522-527.

10. Aguado D, Benito J, Gomez de Segura IA. Reduction of the minimum alveolar concentration of isoflurane in dogs using a constant rate of infusion of lidocaine-ketamine in combination with either morphine or fentanyl. *Vet J*. 2011;189: 63-66.

11. Grimm KA, Tranquilli WJ, Gross DR, Sisson DD, Bulmer BJ, Benson GJ, et al. Cardiopulmonary effects of fentanyl in conscious dogs and dogs sedated with a continuous rate infusion of medetomidine. *Am J Vet Res*. 2005;66: 1222-1226.

12. Uilenreef JJ, Murrell JC, McKusick BC, Hellebrekers LJ. Dexmedetomidine continuous rate infusion during isoflurane anaesthesia in canine surgical patients. *Vet Anaesth Analg*. 2008;35: 1-12.

13. Rosset A, Spadola L, Ratib O. OsiriX: an open-source software for navigating in multidimensional DICOM images. *J Digit Imaging*. 2004;17: 205-216.

14. Austen WG, Edwards JE, Frye RL, Gensini GG, Gott VL, Griffith LS, et al. A reporting system on patients evaluated for coronary artery disease. Report of the Ad Hoc Committee for Grading of Coronary

Artery Disease, Council on Cardiovascular Surgery, American Heart Association. *Circulation*. 1975;51: 5-40.

15. R Development Core Team. *R: A language and environment for statistical computing.* Vienna: R Foundation for Statistical Computing, 2012.

16. Holm S. A simple sequentially rejective multiple test procedure. *Scandinavian Journal of Statistics*. 1979;17: 571-582.

17. de Graaf FR, Schuijf JD, van Velzen JE, Kroft LJ, de Roos A, Sieders A, et al. Evaluation of contraindications and efficacy of oral Beta blockade before computed tomographic coronary angiography. *Am J Cardiol*. 2010;105: 767-772.

18. de Graaf FR, Schuijf JD, Delgado V, van Velzen JE, Kroft LJ, de Roos A, et al. Clinical application of CT coronary angiography: state of the art. *Heart Lung Circ*. 2010;19: 107-116.

19. Ferasin L, Ferasin H, Little CJ. Lack of correlation between canine heart rate and body size in veterinary clinical practice. *J Small An Pract*. 2010;51: 412-418.

20. Pan CJ, Qian N, Wang T, Tang XQ, Xue YJ. Adaptive prospective ECG-triggered sequence coronary angiography in dual-source CT without heart rate control: Image quality and diagnostic performance. *Exp Ther Med*. 2013;5: 636-642.

21. Heniff MS, Moore GP, Trout A, Cordell WH, Nelson DR. Comparison of routes of flumazenil administration to reverse midazolam-induced respiratory depression in a canine model. *Acad Emerg Med*. 1997;4: 1115-1118.

22. Sano T, Nishimura R, Kanazawa H, Igarashi E, Nagata Y, Mochizuki M, et al. Pharmacokinetics of fentanyl after single intravenous injection and constant rate infusion in dogs. *Vet Anaesth Analg*. 2006;33: 266-273.

23. Keating SC, Kerr CL, Valverde A, Johnson RJ, McDonell WN. Cardiopulmonary effects of intravenous fentanyl infusion in dogs during isoflurane anesthesia and with concurrent acepromazine or dexmedetomidine administration during anesthetic recovery. *Am J Vet Res*. 2013;74: 672-682.

24. Pascoe PJ, Raekallio M, Kuusela E, McKusick B, Granholm M. Changes in the minimum alveolar concentration of isoflurane and some cardiopulmonary measurements during three continuous infusion rates of dexmedetomidine in dogs. *Vet Anaesth Analg*. 2006;33: 97-103.

25. Braz LG, Braz JR, Castiglia YM, Vianna PT, Vane LA, Modolo NS, et al. Dexmedetomidine alters the cardiovascular response during infra-renal aortic cross-clamping in sevoflurane-anesthetized dogs. *J Invest Surg*. 2008;21: 360-368.

26. Lin GY, Robben JH, Murrell JC, Aspegren J, McKusick BC, Hellebrekers LJ. Dexmedetomidine constant rate infusion for 24 hours during and after propofol or isoflurane anaesthesia in dogs. *Vet Anaesth Analg*. 2008;35: 141-153.

27. Ebner LS, Lerche P, Bednarski RM, Hubbell JA. Effect of dexmedetomidine, morphine-lidocaine-ketamine, and dexmedetomidine-morphine-lidocaine-ketamine constant rate

infusions on the minimum alveolar concentration of isoflurane and bispectral index in dogs. *Am J Vet Res*. 2013;74: 963-970.

28. Sieslack AK, Dziallas P, Nolte I, Wefstaedt P. Comparative assessment of left ventricular function variables determined via cardiac computed tomography and cardiac magnetic resonance imaging in dogs. *Am J Vet Res*. 2013;74: 990-998.

29. Pollard R PS. CT Contrast media and applications. In: SChwarz T SJ (ed): *Veterinary Computed Tomography*. Chichester: Wiley-Blackwell, 2011;57-66.

30. Utsunomiya D, Awai K, Sakamoto T, Nishiharu T, Urata J, Taniguchi A, et al. Cardiac 16-MDCT for anatomic and functional analysis: assessment of a biphasic contrast injection protocol. *AmJ Roent*. 2006;187: 638-644.

31. Kerl JM, Ravenel JG, Nguyen SA, Suranyi P, Thilo C, Costello P, et al. Right heart: split-bolus injection of diluted contrast medium for visualization at coronary CT angiography. *Radiology*. 2008;247: 356-364.

32. Pollard RE, Puchalski SM, Pascoe PJ. Hemodynamic and serum biochemical alterations associated with intravenous administration of three types of contrast media in anesthetized dogs. *Am J Vet Res*. 2008;69: 1268-1273.

33. Leschka S, Husmann L, Desbiolles LM, Gaemperli O, Schepis T, Koepfli P, et al. Optimal image reconstruction intervals for non-invasive coronary angiography with 64-slice CT. *Eur Radiol*. 2006;16: 1964-1972.

34. Rahmani N, Jeudy J, White CS. Triple rule-out and dedicated coronary artery CTA: comparison of coronary artery image quality. *Acad Radiol*. 2009;16: 604-609.

35. Kimura F, Umezawa T, Asano T, Chihara R, Nishi N, Nishimura S, et al. Coronary computed tomography angiography using prospective electrocardiography-gated axial scans with 64-detector computed tomography: evaluation of stair-step artifacts and padding time. *Jpn J Radiol*. 2010;28: 437-445.

36. Evans H. The heart and the arteries. In: HE E (ed): *Miller's anatomy of the dog*. Philadelphia: Saunders, 1993;598-601.

37. Koch T, Berg R. Blutgefäß- und Lymphsystem, Angiologia. In: Koch T BR (ed): *Lehrbuch der Veterinär-Anatomie: Die grossen Versorgungs- und Steuerungssyteme*. Stuttgart: Gustav Fischer Verlag Jena, 1993;45-62.

38. König H, Liebich HG. Organe des Herz-Kreislauf-Systems. In: König H LH (ed): *Anatomie der Haussäugetiere*. Stuttgart: Schattauer GmbH, 2005;445-448.

CHAPTER 6

Quantitative planar and volumetric cardiac measurements using 64 MDCT and 3T MRI versus standard 2D and M-mode echocardiography: Does anesthetic protocol matter?

Randi Drees[1], Rebecca A Johnson[1], Rebecca L Stepien[2], Alejandro Munoz Del Rio[3,5], Jimmy H Saunders[4], Christopher J François[5]

UW-Madison VMTH [1]DSS and [2]DMS, 2015 Linden Drive, Madison, WI 53706, USA;
[3]UW-Madison Department of Medical Physics, 600 Highland Avenue, Madison, WI 53792, USA;
[4]UGent, Faculty of Veterinary Medicine, Salisburylaan 133, 9820 Merelbeke, Belgium;
[5]UW-Madison, School of Medicine and Public Health, Department of Radiology, 600 Highland Avenue, Madison, WI 53792, USA

Adapted from: *Veterinary Radiology Ultrasound* 2015 doi: 10.1111/vru.12269.

Summary

Cross-sectional imaging of the heart utilizing computed tomography (CT) and magnetic resonance imaging (MRI) has been shown to be superior for the evaluation of cardiac morphology and systolic function in humans compared to echocardiography. The purpose of this prospective study was to test the effects of two different anesthetic protocols on cardiac measurements in 10 healthy beagle dogs using 64-multidetector row computed tomographic angiography (64-MDCTA), 3T magnetic resonance (MRI) and standard awake echocardiography. Both anesthetic protocols used propofol for induction and isoflurane for anesthetic maintenance. In addition, protocol A used midazolam/fentanyl and protocol B used dexmedetomedine as premedication and constant rate infusion during the procedure. Significant elevations in systolic and mean blood pressure were present when using protocol B. There was overall good agreement between the variables of cardiac size and systolic function generated from the MDCTA and MRI exams and no significant difference was found when comparing the variables acquired using either anesthetic protocol within each modality. Systolic function variables generated using 64-MDCTA and 3T MRI were only able to predict the left ventricular end diastolic volume as measured during awake echocardiogram when using protocol B and 64-MDCTA. For all other systolic function variables, prediction of awake echocardiographic results was not possible (P = 1). Planar variables acquired using MDCTA or MRI did not allow prediction of the

corresponding measurements generated using echocardiography in the awake patients (P=1). Future studies are needed to validate this approach in a more varied population and clinically affected dogs.

Introduction

In companion animals the evaluation of cardiac morphology and systolic function has mainly been based on echocardiographic evaluation and cardiac catheterization.[1-6] The potential role of MRI in the future of veterinary clinical cardiology has been reviewed critically[7] and recent publications have utilized MRI and/or MDCT for functional and morphological cardiac evaluations[8-14]. Cross-sectional imaging of the heart utilizing computed tomography (CT) and magnetic resonance imaging (MRI) has shown to be superior for the evaluation of cardiac morphology and systolic function in humans compared to echocardiography[15-22]; providing for assessment of global pulmonary and cardiac anatomy for workup and treatment planning or follow up further to the regional two or three dimensional image provided using echocardiography. Specifically the MRI has shown higher accuracy for assessment of the aortic annulus and right systolic ventricular function, MDCTA for the left atrial volume. Apart from case reports describing congenital or neoplastic morphological abnormalities involving the heart or great vessels in companion animals[8,23-29] these modalities have rarely been compared for their use in evaluation of cardiac function[7,9-14]. While these cross-sectional exams are generally performed in the awake human patient[30] companion animal patients require anesthesia or heavy sedation at a minimum to undergo these studies. Although different anesthetic protocols have been used[9-10,12-14,31], the effects of specific anesthetic protocols on image quality, systolic function and cardiac morphologic variables as determined by cross-sectional

imaging have not been systematically evaluated. Furthermore, to optimize image quality, a target heart rate of <65bpm is recommended for multidetector computed tomographic angiography (MDCTA) in people[32]. The canine heart rate varies with many factors, including choice of anesthetic/sedative agents as well as body weight; however, rates between 80-150 are commonly seen in awake patients[33].

The primary goal of this study was to analyze variables of cardiac morphology and systolic function using 64-MDCTA and magnetic resonance imaging (MRI) at 3 Tesla by comparing two anesthetic protocols for heart rate control and impact on cardiac function in 10 healthy dogs. The secondary goal was to compare the variables of cardiac size and systolic function generated by MDCTA to MRI and to relate those to the current clinical practice of echocardiography in the awake dog. The results were intended to provide baseline recommendations for further cardiac investigations using MDCTA and MRI in dogs. The hypothesis for this study was that parameters acquired using CT and MRI with either anesthetic protocol would be comparable but differ from parameters acquired using echocardiography on the awake dogs.

Material and Methods

Animal preparation: The University of Wisconsin's Institutional Animal Care and Use Committee approved all procedures. Ten purpose-bred healthy beagle dogs with a mean age of 10.4 (range 7-20) months and mean body weight of 10.7 (range 8.9-12.7) kg were used in this study and underwent awake echocardiography once and then retrospectively ECG-gated MDCTA and MRI under anesthesia on two different days, using a different anesthetic protocol for each of the two anesthetic episodes. The order of MDCTA and MRI was randomized as well as the order of the anesthetic protocols for heart rate regulation for each dog.

A 20G intravenous catheter was placed in both the right and left cephalic veins; the left was used for anesthesia purposes and the right for contrast administration in all dogs. Anesthetic monitoring included modality specific recording of electrocardiography (using the footpads for the CT exam and the chest for the MRI exam for electrode placement) as well as pulse-oximetry to monitor heart rate, rhythm and hemoglobin saturation; systolic, diastolic and mean blood pressure was non-invasively monitored with a cardiac monitor (Cardell® Veterinary Monitor, Model 9401, CAS Medical Systems, Branford, CT, 06405). Short periods of apnea were induced by mild hyperventilation and halting the mechanical ventilator when needed during image acquisition.

Echocardiography: standard awake auscultation and echocardiographic exam (Vivid 7, GE Health Care, Waukashea, WI, USA, 8 and 5MHz transducers) was performed by a board certified veterinary cardiologist

(RLS) once, prior to the anesthetic episodes for cross-sectional imaging. The following variables were recorded using M-mode: diastolic and systolic interventricular septal thickness (IVSd, IVSs), left ventricular internal diameter (LVIDd, LIVDs) and left ventricular posterior wall thickness (LVPWd, LVPWs). Additionally, standard single plane 2D B-mode images were used to acquire measurements of the aortic, left atrial and main pulmonary arterial diameter; left atrium to aorta ratio (LA/Ao ratio) and aorta to pulmonary artery (Ao/PA ratio) were calculated from those measurements. Fractional shortening (FS %) was calculated using the following formula: FS = (LVIDd – LVIDs)/LVIDd x 100. End diastolic volume (EDV), end systolic volume (ESV), ejection fraction (EF) and stroke volume (SV) were calculated using the Simpson method.[34] Left ventricular mass was calculated from M-mode measurements using the following formula: LVM = 1.04 x [(LVIDd + LVWd + IVSd)^3 – (LVIDd)^3] – 13.6g^2.

Anesthesia protocols: All dogs were induced using a propofol bolus to effect (2-6 mg/kg) for each of the two cross-sectional imaging events. The animals were orally intubated, placed in dorsal recumbency in a custom made trough for positioning in CT and MRI and maintained on isoflurane (Vaporizer set at 1-2%) and 100% oxygen using mechanical ventilation to an end-tidal CO2 level between 35-40mmHg. The dogs also received maintenance intravenous Lactated Ringer's Solution (5-10 ml/kg/h; Abbott Laboratories, North Chicago, IL, USA) through the left cephalic catheter. Protocol A used fentanyl (Fentanyl Citrate, West-ward, Eatontown, NJ, USA) 5µg/kg bolus for premedication followed by

10µg/kg/h continuous rate infusion (CRI) and midazolam (Midazolam, Hospira, Inc., Lake Forest, IL, USA) 0.2mg/kg bolus followed by 0.2mg/kg/h CRI. Protocol B used dexmedetomedine (Dexdomitor, Pfizer Animal Health, New York, New York, USA) 1-2µg/kg bolus for premedication and 1-2µg/kg/h CRI.

Cardiac MDCTA: Cardiac exams were performed using a 64-MDCT unit (Discovery CT750 HD, General Electrics Medical Systems, Waukesha, WI, USA). A transverse plane helical exam of the thorax was performed using 1.25mm slice thickness and reconstruction interval, medium frequency reconstruction kernel, 80kVp, 200mA, 0.35s tube rotation time and a pitch of 0.51, followed by acquisition of a localizer image over the right ventricular outflow tract and the aortic root. Using the semi-automated bolus tracking function a retrospectively ECG-gated cardiac MDCTA was performed using 15ml iodinated contrast medium (Omnipaque 300, NovaPlus GE Healthcare, Princeton, NJ, USA) followed by a 5ml saline flush administered from a dual barrel injector at 2ml/s and 325PSI. Contrast injection was timed to mainly opacify the left atrium, left ventricle, coronary arteries and thoracic aorta. Scan parameters used for the retrospectively gated scan were set to 1.25mm slice thickness, 0.625mm spacing between slices, medium frequency reconstruction algorithm, DFOV 12cm centered over the heart, 80kVp, 200mA, 0.35s tube rotation time and helical pitch of 0.24.

Cardiac MRI: The exams were performed using a 3 Tesla MRI unit (Discovery MR750, GE Healthcare, Waukesha, WI, USA) using a 32-channel upper torso coil. Insulated ECG leads were placed on the chest

wall, as placement of ECG leads on the footpads using non-insulated cables did not produce an ECG trace when the dogs were advanced into the magnet. Localizer scans were acquired in three planes. Then the following sequences were acquired: ECG-gated cine transverse plane, approximate three chamber, approximate four chamber, short axis cine balanced steady-state free precession (SSFP; TR 3.3-4.1ms, TE 45ms, 45 degree flip angle, 224x224 matrix, FOV 230-310x184-207mm, pPOV 0.6-0.8, VPS 12-18, ETL 1, NEX 1, BW 125, 6mm slice thickness).
After the last cross-sectional imaging modality per day was completed the animals were recovered; after the last episode the dogs were humanely euthanized according to institutional protocol requirements.

Image analysis: Evaluation of the MDCTA and MRI studies was performed using semi-automated software (OsiriX 5.6 64-bit[35] and ReportCARD™ 4.4.6, GE Healthcare, Waukesha, WI, USA, respectively) by a board certified veterinary radiologist (RD) under guidance of a human radiologist specialized in cardiovascular imaging (CJF). The exams were randomized for evaluation and the reviewer was blinded to the anesthetic protocol used for each study. Short axis, approximate three- and four-chamber views of the MDCTA images were generated at 1.25mm slice thickness using open source software[35] to mirror the plane alignment generated in the MRI exams. All studies were inspected for diagnostic image quality to apply measurements by evaluating for adequate contrast, border definition and presence or absence of artifacts.

Using the short axis planes, regions of interest were semi-automatically drawn along the endocardial and epicardial border on all images including the left ventricle from the apex to the level of the annulus; where slices with greater than 25% of annulus in the imaging plane marked the basal border of the ventricle included in the evaluation. The papillary muscles were included in the ventricular volume for consistency (Figure 1).

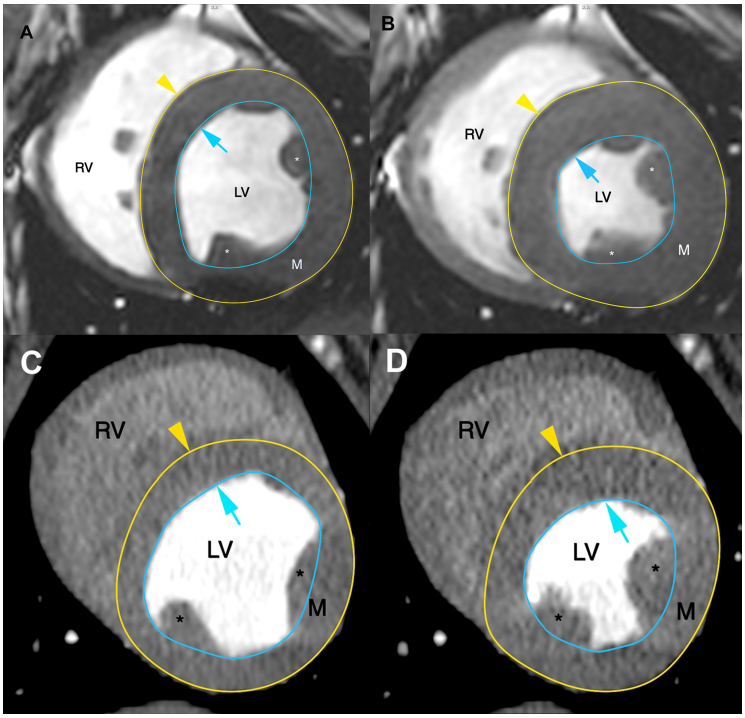

Figure1: Using the short axis plane the epicardial (yellow line, arrow head) and endocardial (turquoise line, arrow) surface of the left ventricle (LV) were outlined on all images including the left ventricle to calculate the volumetric variables; each at the end diastolic (A, C) and end systolic (B, D) phase for MDCTA and MRI respectively; exemplary views are given at the level of the papillary muscles. Papillary muscles (*) were included in the left ventricular volume. RV = right ventricle; M = left ventricular myocardium.

Using the transverse plane images, semi-automated regions of interest were also placed along the endocardial borders of the right ventricle, where the tricuspid and pulmonic annulus marked the borders of the ventricular volume included, also here the papillary muscles were included with the ventricular volume for consistency (Figure 2).

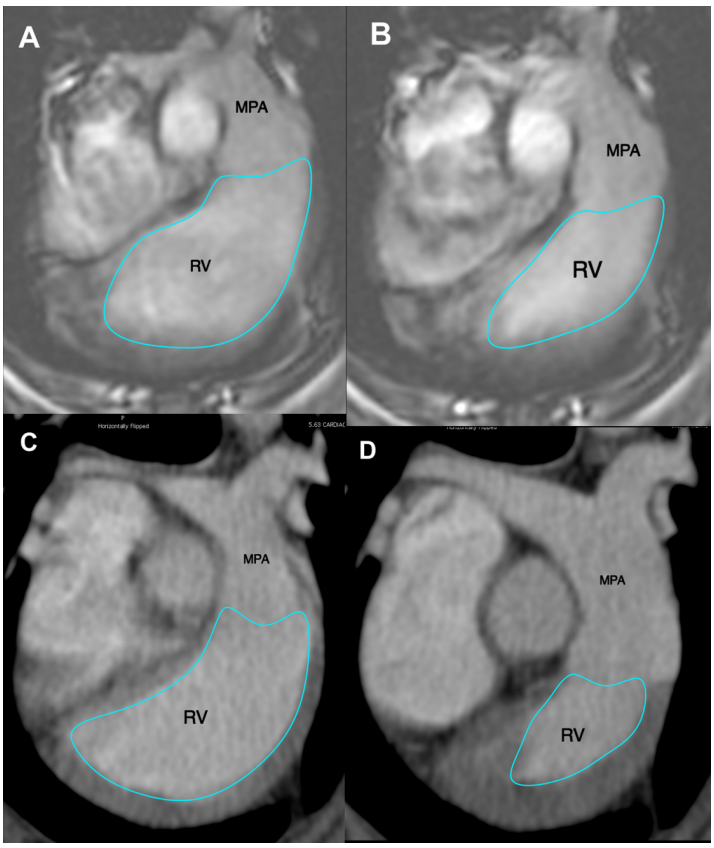

Figure 2: Using transverse plane images the endocardial surface (turquoise line) of the right ventricle (RV) was outlined on all images including the right ventricle, where the tricuspid and pulmonic annulus marked the borders of the ventricular volume included. This was performed at the end diastolic (A, C) and end systolic (B, D) phase for MDCTA and MRI respectively; exemplary views are given at the level of the right ventricular outflow tract. MPA = main pulmonary artery.

This method was used to generate the following volumetric variables from the MDCTA and MRI exams respectively using the Simpson method:[36] Left ventricular end diastolic and end systolic volume (LVEDV and LVESV); left ventricular end diastolic and end systolic epicardial volume (epiEDV and epiESV). Left ventricular stroke volume (LVSV = LVEDV - LVESV) and left ventricular ejection fraction (LVEF = LVSV / LVEDV) were calculated from these measurements. To verify alignment of the regions of interest drawn only 10% variability between the measurements for left ventricular end diastolic and end systolic myocardial mass (LVmassD and LVmassS) was allowed per dog within the same and between anesthetic episodes. Right ventricular diastolic volume (RVEDV) and right ventricular end systolic volume (RVESV) were recorded; right ventricular stroke volume (RVSV = RVEDV – RVESV) and right ventricular ejection fraction (RVEF = RVSV / RVESV) were calculated from these measurements.

The following planar measurements were obtained: systolic and diastolic interventricular septal wall thickness (IVSs, IVSd) and left ventricular posterior wall thickness (LVPWs, LVPWd) thickness; left ventricular internal diameter (LVIDs, LVIDd), mitral and aortic annulus diameter, proximal aortic, proximal pulmonary artery and left atrial diameter.

The short axis view, corresponding to the right parasternal short axis view used in echocardiography, was used to measure the systolic and

diastolic interventricular septal wall and left ventricular posterior wall thickness as well as the internal diameter of the left ventricle (Figure 3).

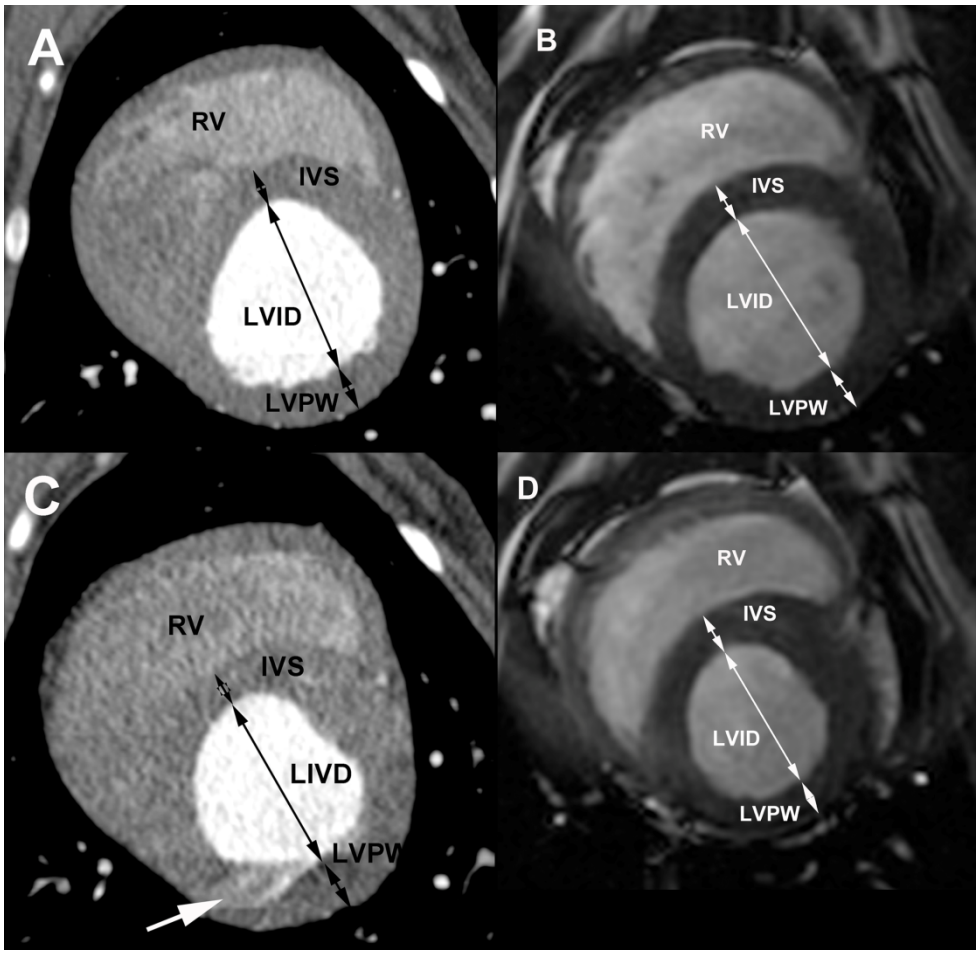

Figure 3: Short axis view of the left ventricle end diastolic (A, C) and end systolic (B, D) using MDCTA and MRI respectively, showing the measurement of IVS (interventricular septum) and LVPW (left ventricular posterior wall) thickness and LVID (left ventricular internal diameter) using double-headed arrows. Single-headed arrow showing mild motion artifact in end systole, this did not interfere with placement of measurements. RV = Right ventricle.

Fractional shortening (FS %) was calculated from these values (FS = (LVIDd – LVIDs)/LVIDd x 100).

The approximate three chamber view, corresponding to the parasternal long axis view used in echocardiography, was used to measure the end systolic left atrial diameter and aortic annulus diameter just prior to opening of the mitral valves and while the aortic valves were open as well as end diastolic mitral annulus diameter while the mitral valves were open (Figures 4 and 5).

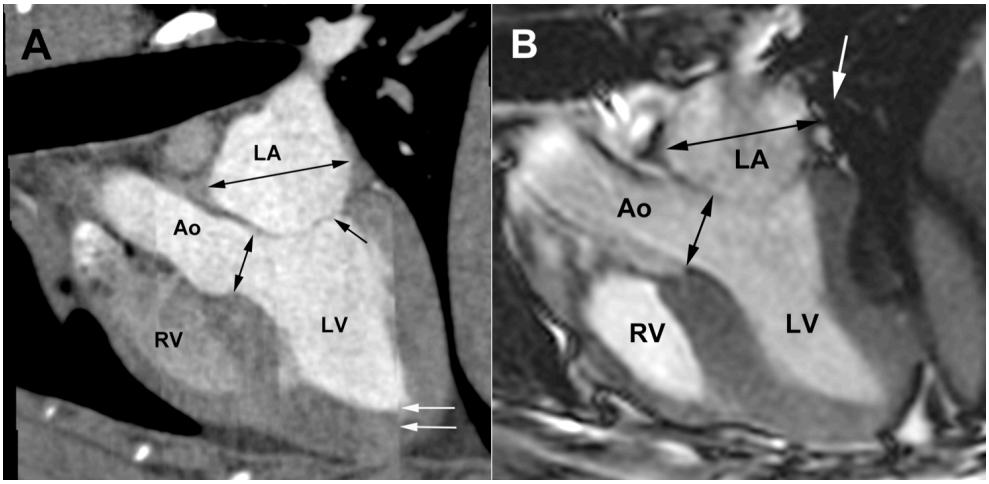

Figure 4: End systolic three-chamber view generated using MDCTA (A) and MRI (B) respectively for measurement of the left atrial (long double-headed arrow) and aortic annulus (short double-headed arrow) diameter. Mitral valves (black arrow) are closed, aortic valves are open. There is mild flow artefact on the MRI image over the caudal aspect of the left atrium (single white arrow on B) arising from inflow from the pulmonary veins and mild motion artefact over the caudal aspect of the left ventricle (white arrows on A) over the left ventricle on the MDCTA image. LA = left atrium; LV = left ventricle; RV = right ventricle; Ao = aorta.

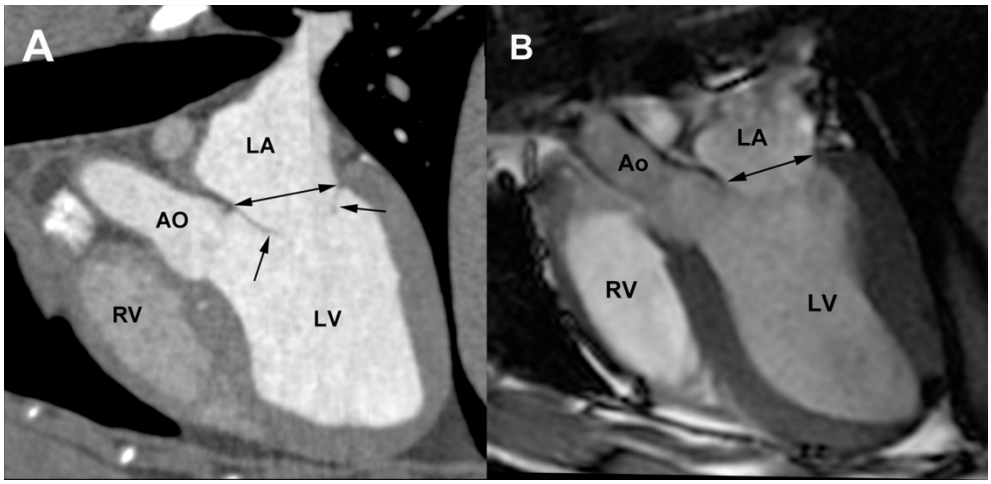

Figure 5: End diastolic three-chamber view generated using MDCTA (A) and MRI (B) respectively for measurement of the mitral annulus diameter measurement (double-headed black arrow). Mitral valves are open (black arrows). LA = left atrium; LV = left ventricle; RV = right ventricle; Ao = aorta.

The left atrium/aorta ratio (La/Ao ratio) was calculated from these values (La/Ao = left atrial diameter/aortic annulus diameter). The approximate four chamber view, corresponding to the left apical four chamber view as used in echocardiography, was used for a repeat measurement of the mitral annulus (Figure 6).

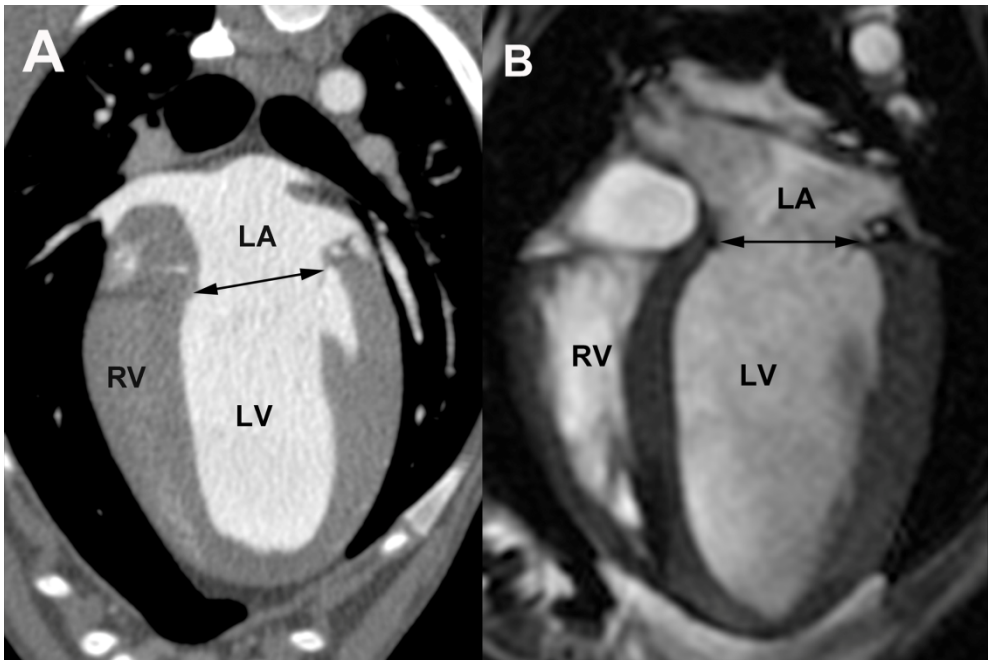

Figure 6: Approximate four-chamber view using MDCTA (A) and MRI (B) for repeat measurement of the mitral annulus diameter (double-headed arrow) at end diastole. LA = left atrium; LV = left ventricle; RV = right ventricle.

The transverse plane views, similar to the right parasternal short axis views in echocardiography, were used to measure the diameter of the proximal aorta and the main pulmonary artery (Figure 7).

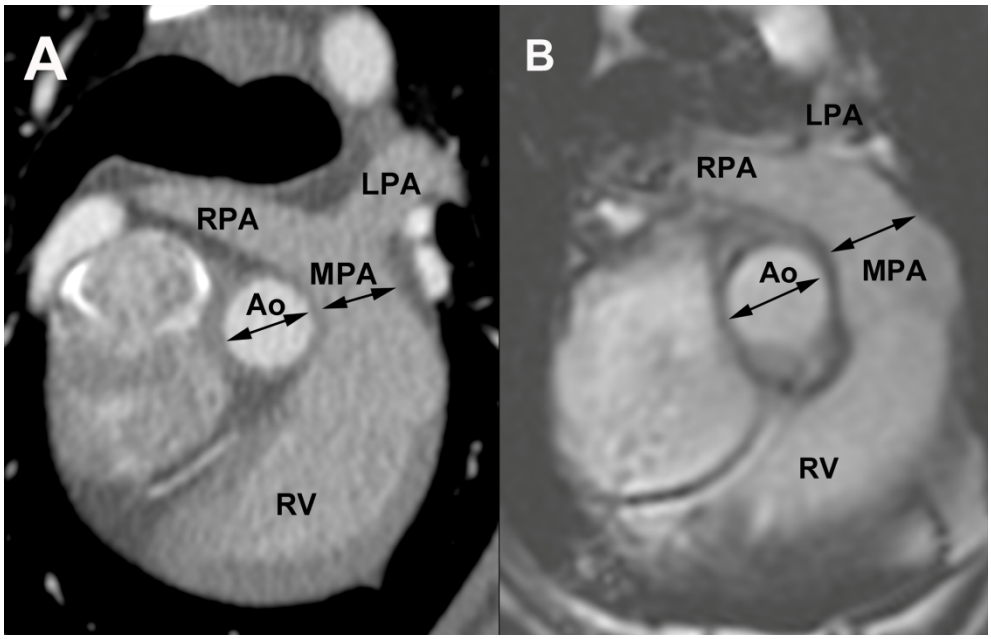

Figure 7: Transverse plane view using MDCTA (A) and MRI (B) respectively for measurement of the diameter of the proximal aorta (Ao, double-headed arrow) and the main pulmonary artery (MPA, double-headed arrow). RPA = right pulmonary artery; LPA = left pulmonary artery; RV = right ventricle.

The aorta/pulmonary artery ratio (Ao/Pa ratio) was calculated from these measurements (Ao/Pa = base of the aorta diameter/main pulmonary artery diameter).

Statistical analysis: Open source software was used for statistical evaluation[37]. For all variables evaluated summary statistics (quartiles, mean, standard deviation (SD), minimum and maximum) were computed by one observer (AMR). Medians and extremes were recorded.

To establish baseline comparison of the two anesthetic protocols within each imaging modality (i.e. MDCTA and MRI) the data was compared with a paired Wilcoxon signed rank test. Significance was set at $P \leq 0.05$. One test was done for MDCTA values and another for the MRI values. Within each type of measurement (i.e. individual variables to compare) the P-values were adjusted with a Holm-Bonferroni step-down procedure[38].

To characterize the typical discrepancy between MDCTA and MRI when measuring the same cardiac attribute, Bland-Altman 95% limits of agreement analysis was used; bias (average difference), lower (LLOA) and upper level of agreement (ULOA) are reported. As both anesthesia protocols were pooled, possible correlation arising from the repeated measures needed to be allowed for, since each dog contributed two observations[39].

Lastly, the results for the left ventricular systolic function and planar variables generated using the cross-sectional modalities with each anesthetic protocol were compared to the comparable variables acquired using echocardiography using the Friedman rank sum test, pairwise comparisons were then generated using the Wilcoxon signed rank test. A simple linear regression was used to determine whether any of the anesthesia-by-imaging modality combinations could predict the values observed with echocardiography when the dogs were awake. The Holm-Bonferroni step-down procedure was used to adjust the P-values for the significance of the slope variable[38].

Results

On awake auscultation, 2/10 dogs had an irregular cardiac rhythm and no murmurs were auscultated in any dog at an average heart rate of 115 ± 19bpm. One dog had a marked respiratory sinus arrhythmia during echocardiography; the remaining 9 dogs had a normal sinus rhythm. Echocardiographic examination showed a trivial amount of mitral regurgitation in one dog and trace tricuspid insufficiency in one dog. Two dogs showed very mild left ventricular enlargement with normal function. Overall, no hemodynamically significant abnormalities were noted in any of the 10 dogs.

Both anesthetic protocols provided adequate anesthesia of all dogs and recovery was uneventful in all cases. The median (minimum-maximum) heart rate with protocol A was 81.6 (68.6-96.0) bpm and 76.8 (66-98.6) bpm (P = 1) during the MDCTA and MRI exam respectively. Using protocol B, the median heart rate was 73.3 (62.7-102.6) bpm and 71 (64.4-118.8) bpm (P = 1) during the MDCTA and MRI exam, respectively. In one dog the target heart rate of < 65bpm was consistently achieved using protocol B. Vital variables recorded during the CT and MRI exams using protocol A and B are summarized in detail in Table 1.

Table 1: Summary of the Vital Variables Recorded during MDCTA and MRI Exams using Protocol A (Midazolam/Fentanyl) and Protocol B (Dexmedetomedine) in ten dogs. *

		Protocol A	Protocol B
		Median (min-max)	Median (min-max)
CT			
	heart rate (bpm)	81.6 (68.6-96)	73.3 (62.7-102.6)
	mean blood pressure (mmHg)	65.0 (48.8-74.0)	65.3 (57-102.8)*
	systolic arterial pressure (mmHg)	92.5 (74.3-100.4)	92.7 (81.0-129.8)
	diastolic arterial pressure (mmHg)	37.6 (28.2-47.2)	44.2 (31.8-75.8)*
	CO2 (%)	39.7 (34.7-46.7)	35.5 (34.7-45.0)
MRI			
	heart rate (bpm)	76.8 (66-98.6)	71 (64.4-118.8)
	mean blood pressure (mmHg)	60.5 (48.4-68.9)	75.3 (66.1-94.0)
	systolic arterial pressure (mmHg)	89.1 (75.3-95.6)	101.9 (91.7-117.6)
	diastolic arterial pressure (mmHg)	36.2 (29.2-43.4)	51.9 (30.9-72.5)
	CO2 (%)	37.5 (34.3-45.8).	34.1 (30.6-37.0)

*When comparing Protocol A and B there was significant difference for the mean (P = 0.012), diastolic arterial (P = 0.033) and marginal difference for the systolic arterial blood pressure (P = 0.052). For the remaining variables no difference was found (heart rate, CO2; P = 1).

Comparing protocol A and B, diastolic and mean blood pressure were significantly higher (P = 0.033 and P = 0.012) and systolic blood pressure was marginally higher (P = 0.052) using protocol B. There was no significant difference found between the remaining recorded physiological values using either protocol (systolic blood pressure P = 0.052, Co2 P = 0.075; Table 1). One dog experienced slight tachycardia immediately following CT contrast medium administration but the heart rate spontaneously returned to pre-contrast levels within 10 minutes of administration. On average the duration of the MDCTA exam including set up of the dogs, acquisition of localizer images, pre contrast exam and retrospectively gated cardiac exam was 9.31 ± 0.17min; the duration of the retrospectively gated angiography itself lasted an average of 5.0 ± 0.68s. Average duration of the MRI exam including patient positioning, setup of anesthetic and gating equipment, acquisition of localizer images and the cardiac exam lasted for 51.0 ± 3.26min. In the first study dog, delays were encountered, mainly due to difficulties in obtaining an accurate ECG signal, which was remedied by switching to a different, insulated, ECG cable. Thus, this time was not accounted for in calculation of the average duration. The acquisition of the four plane SFFP sequences only took 19.21 ± 7.58min.

The smart prep feature was used to manually trigger the angiographic exam when contrast medium was seen in the right ventricular outflow tract; the MDCT unit had an inherent additional delay of 5s to start the diagnostic scan. All MDCTA and MRI exams resulted in studies of diagnostic image quality. Mild motion artifact was seen on the MDCTA

studies during systole but did not influence the ability to apply measurements. This was mainly displayed as a mild shift between the acquisition segments during systole.

Volumetric measurements generated from the awake echocardiograms, MDCTA and cardiac MRI using anesthetic Protocol A and B are listed in Table 2. There were no significant differences for the evaluated volumetric variables between the two anesthetic protocols when comparing within the individual cross-sectional modalities (MDCTA and MRI, $P > 0.05$; Table 2 and 3).

Table 2: Volumetric Measurements Generated from the Echocardiograms Obtained in the Ten Dogs Awake as well as the cardiac 64-MDCTA and 3T MRI Exams Using Anesthetic Protocol A and Protocol B.

Modality	Echocardiography	MDCTA		MRI	
Anesthetic protocol	Awake	Protocol A	Protocol B	Protocol A	Protocol B
		Median (min-max)	Median (min-max)	Median (min-max)	Median (min-max)
LVEDV (ml)	42.5 (29.0-56.0)*	34.7 (26.9-41.1)	37.8 (26.6-43.2)†	38.1 (30.0-45.2)	36.2 (26.7-45.1)
LVESV (ml)	15.5 (8.0-21.0)*	16.9 (8.8-25.2)	17.0 (14.8-26.8)	17.8 (13.0-25.8)	18.75 (12.9-25.8)
LSV (ml)	25.5 (19.0-39.0)*	17.2 (15.2-25.1)	18.2 (11.7-22.5)	19.5 (15.4-22.1)	17.6 (9.9-26.0)
LVEF (%)	62.0 (51.0-79.0)*	52.5 (37.7-71.1)	47.3 (36.2-60.3)	52.8 (42.9-59.7)	43.9 (33.8-64.5)
LVmassD (mg)	60.2 (30.7-68.4)	39.4 (27.7-46.4)	38.6 (28.2-44.1)	39.4 (27.5-45.7)	39.4 (26.7-48.7)
LVmass (mg)	NA	39.1 (26.9-47.2)	37.0 (28.5-44.8)	39.1 (28.7-47.3)	40.1 (27.8-43.3)
RVEDV (ml)	NA	36.8 (29.2-41.1)	35.6 (27.2-44.4)	42.7 (32.2-50.9)	40.2 (30.1-50.5)
RVESV (ml)	NA	22.4 (14.6-28.7)	21.9 (14.9-32.5)	22.5 (15.5-29.1)	25.4 (15.1-30.6)
RVSV (ml)	NA	14.5 (8.2-20.3)	12.2 (7.3-21.3)	18.5 (14.6-25.3)	16.2 (8.1-22.7)
RVEF (%)	NA	40.0 (22.3-55.1)	37.4 (23.6-48.2)	45.2 (38.6-58.2)	43.3 (23.6-50.0)

*Simpson's Method, †P-value for comparison of echocardiography and MDCT for LVEDV = 0.01, all other P-values are greater than 0.05 or N/A.

LVEDV = left ventricular end diastolic volume; LVESV = left ventricular end systolic volume; LSV = left ventricular stroke volume; LVEF = left ventricular ejection fraction; LVmassD = diastolic left ventricular myocardial mass; LVmassS = systolic left ventricular myocardial mass; RVEDV = right ventricular end diastolic volume; RVESV = right ventricular end systolic volume; RVSV = right ventricular stroke volume; RVEF = right ventricular ejection fraction

Comparing the evaluated planar variables between the two anesthetic protocols within the individual cross-sectional modalities (MDCTA and MRI) using the paired Wilcoxon signed rank test, no significant differences were found for any of the variables; P = 0.292 for LVIDs using MRI and P = 1 for all other variables (Table 3).

Table 3: Planar Measurements Generated from the Echocardiographic Exam Obtained in the Ten Dogs Awake as well as Cardiac 64-MDCTA and 3T MRI Exams Using Protocol A and B.*

Modality	Echo	CTA		MRI	
Anesthetic protocol	Awake	Protocol A	Protocol B	Protocol A	Protocol B
	Median (min-max)	Median (min-max)	Median (min-max)	Median (min-max)	Median (min-max)
IVSd (cm)	0.76 (0.66-0.88)	0.73 (0.52-0.79)	0.74 (0.49-0.82)	0.79 (0.66-1.02)	0.77 (0.59-0.98)
IVSs (cm)	1.06 (0.95-1.2)	0.8 (0.58-0.95)	0.85 (0.61-0.96)	0.94 (0.66-1.47)	0.77 (0.54-1.04)
LVIDd (cm)	3.25 (2.79-3.63)	2.97 (2.69-3.31)	2.98 (2.78-3.35)	3.19 (2.97-3.45)	3.41 (2.84-3.63)
LIVDs (cm)	2.15 (1.67-2.45)	2.56 (2.23-2.76)	2.64 (2.35-3.03)	2.6 (2.04-2.96)	2.67 (2.23-3.07)
LVPWd (cm)	0.68 (0.53-0.79)	0.75 (0.6-1.0)	0.75 (0.66-0.84)	0.76 (0.52-0.94)	0.73 (0.7-0.94)
LVPWs (cm)	1.03 (0.85-1.17)	1.0 (0.72-1.23)	0.9 (0.72-1.0)	1.04 (0.46-1.25)	0.92 (0.65-1.22)
FS (%)	33.5 (26.0-41.0)	13.11 (6.88-25.22)	12.08 (3.53-20.22)	21.5 (12.11-32.44)	16.81 (11.85-29.53)
LA diam 3ch (cm)	2.21 (1.92-2.49)	2.93 (2.62-3.24)	2.99 (2.63-3.34)	2.8 (2.10-2.92)	2.72 (2.41-2.99)
Mitral annulus 3ch (mm)	NA	2.01 (1.82-2.08)	1.93 (1.5-2.2)	2.02 (1.71-2.34)	1.94 (1.83-2.20)
Ao annulus 3ch (%)	1.71 (1.55-1.97)*	1.3 (0.99-1.37)	1.3 (1.09-1.38)	1.17 (0.94-1.47)	1.18 (1.04-1.34)
LA/Ao ratio	1.27 (1.18-1.49)	2.34 (1.97-3.05)	2.34 (1.97-3.05)	2.41 (1.93-3.04)	2.35 (1.8-2.64)
Mitral annulus diam 4ch (cm)	NA	2.4 (2.12-2.58)	2.4 (2.19-2.69)	2.13 (1.69-2.23)	2.04 (1.8-2.34)
prox Ao (cm)	NA	1.27 (1.14-1.52)	1.28 (1.08-1.51)	1.28 (1.07-1.6)	1.32 (1.18-1.56)
MPA (cm)	1.6 (1.5-1.8) †	1.39 (1.21-1.56)	1.33 (0.92-1.56)	1.23 (1.11-1.24)	1.3 (1.12-1.56)
Ao/PA ratio	0.99 (0.86-1.31)	0.96 (0.82-1.04)	0.96 (0.8-1.48)	1.03 (0.96-1.22)	1.09 (0.98-1.19)

IVSd = diastolic interventricular septal thickness; IVSs = systolic interventricular septal thickness; LVIDd = diastolic left ventricular internal diameter, measured just proximal to the papillary muscles; LVIDs = systolic left ventricular internal diameter, measured just proximal to the papillary muscles; LVPWd = diastolic left ventricular posterior wall thickness; LVPWs = systolic left ventricular posterior wall thickness; FS% = percent fractional shortening; LA diam 3ch = left atrial diameter measured on three chamber view; Mitral annulus 3ch = mitral annulus measured on approximated three-chamber view; Ao annulus 3ch = aortic annulus measured on three-chamber view; LA/Ao ratio = Left atrium to aorta ratio; Mitral annulus 4ch = mitral annulus measured on four-chamber view; prox Ao = Proximal aorta measured on transverse plane; MPA = main pulmonary artery transverse plane; Ao/PA ratio = Aorta to pulmonary artery ratio. *Aortic annulus measured in right parasternal view for the left ventricular outflow tract on echocardiography; † MPA measured in right parasternal short axis view on echocardiography

‡No statistically significant differences were found between the anesthetic protocols within the cross-sectional modalities using the paired Wilcoxon rank sum test (P = 0.292 for LVIDs using MRI; P = 1 for all other variables). The cross-sectionally acquired measurements did not allow for prediction of the values generated using echocardiography in the awake dogs (P = 1 for all variables).

There was also no difference between the measurements repeated for the same variable on different imaging planes (P = 1). The anesthesia protocols were therefore combined for the following analysis. Evaluation of the difference for the volumetric variables generated from MDCTA and MRI while combining the measures for the two different anesthetic episodes per modality and individual as generated by the Bland-Altman analysis are given in Table 4.

Table 4: Results of the Bland-Altman Analysis Characterizing the Differences for the Volumetric Measurements Between the 64-MDCTA and 3T MRI Exams (MRI minus CT) When Combining the Results of the two Anesthetic Protocols per Modality and Individual.

Volumetric cardiac variable	**LLOA**	**Bias**	**ULOA**
LVEDV (ml)	-5.43	1.42	8.27
LVESV (ml)	-4.28	1.37	7.02
LSV (ml)	-6.84	0.05	6.94
LVEF (%)	-17.45	-2.11	13.24
LVmassD (mg)	-6.51	2.05	10.62
LVmassS (mg)	-5.33	1.62	8.58
RVEDV (ml)	-6.87	5.08	17.04
RVESV (ml)	-7.88	0.89	9.66
RVSV (ml)	-3.63	4.19	12.02
RVEF (%)	-9.54	5.51	20.57

LLOA = 95% lower level of agreement; ULOA = 95% upper level of agreement; LVEDV = left ventricular end diastolic volume; LVESV = left ventricular end systolic volume; LSV = left ventricular stroke volume; LVEF = left ventricular ejection fraction; LVmassD = diastolic left ventricular myocardial mass; LVmassS = systolic left ventricular myocardial mass; RVEDV = right ventricular end diastolic volume; RVESV = right ventricular end systolic volume; RVSV = right ventricular stroke volume; RVEF = right ventricular ejection fraction.

The graphical output is displayed in Figure 8 for the left ventricular variables and Figure 9 for the right ventricular variables.

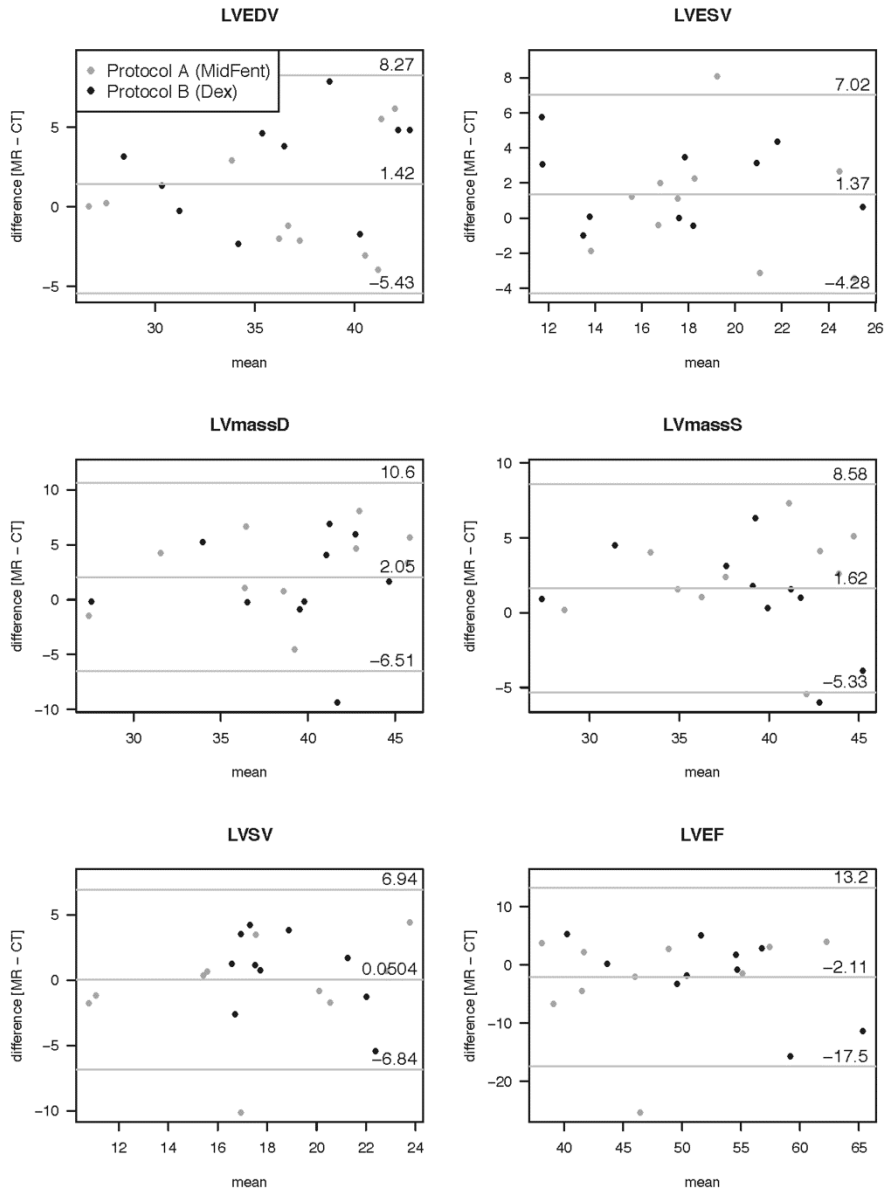

Figure 8: Graphical display of the Bland-Altman analysis comparing the left ventricular volumetric measurements generated using 64-MDCTA (CT) versus 3T-MRI (MR) while combining the measures for the two different anesthetic episodes per modality. The bias is given by the central horizontal line, the 95% lower and upper level of agreement are indicated by the above and below horizontal lines. LVEDV: Left Ventricular End Diastolic Volume (ml); Left Ventricular End Systolic Volume (ml); LVmassD: Left Ventricular Myocardial Mass at Diastole (mg); LVmassS: Left Ventricular Myocardial Mass at Systole (mg); LVSV: Left Ventricular Stroke Volume (ml); LVEF: Left Ventricular Ejection Fraction (ml). Dex = Anesthetic Protocol B; MidFent = Anesthetic Protocol A.

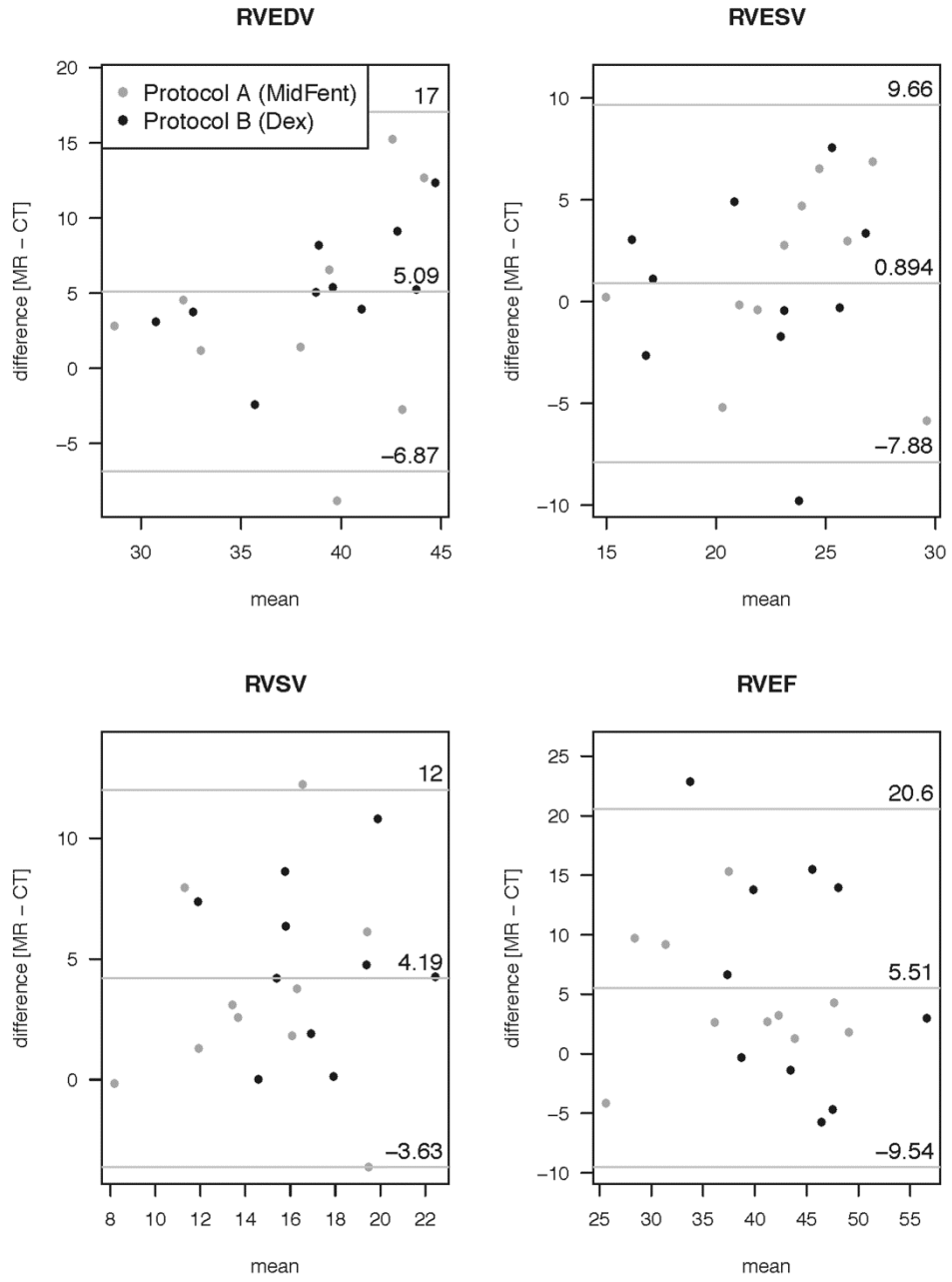
RVEDV
Protocol A (MidFent)
Protocol B (Dex)
17
5.09
−6.87
difference [MR − CT]
mean
RVESV
9.66
0.894
−7.88
difference [MR − CT]
mean
RVSV
12
4.19
−3.63
difference [MR − CT]
mean
RVEF
20.6
5.51
−9.54
difference [MR − CT]
mean

Figure 9: Graphical display of the Bland-Altman analysis comparing the right ventricular volumetric measurements generated using MDCTA versus MRI while combining the measures for the two different anesthetic episodes per modality. The bias is given by the center horizontal line, the 95% lower and upper level of agreement are indicated by the above and below horizontal lines. RVEDV: Right Ventricular End Diastolic Volume (ml); RVESV: Right Ventricular End Systolic Volume (ml); RVSV: Right Ventricular Stroke Volume (ml); RVEF: Right Ventricular Ejection Fraction (ml). Dex = Anesthetic Protocol B; MidFent = Anesthetic Protocol A.

The bias resulting from the comparison between MDCTA and MRI when accounting for both measures of each individual per modality generated in the Bland-Altman analysis is given in Table 5;

Table 5: Bias and 95% Upper (ULOA) and Lower Level of Agreement (ULOA) Generated by the Comparison of the Planar Variables Acquired using 64-MDCTA and 3T MRI (MRI minus CT) using the Bland-Altman Analysis are Reported.

Planar variable	LLOA	Bias	ULOA
IVSd (cm)	- 0.19	0.08	0.35
IVSs (cm)	- 0.29	0.09	0.46
LVIDd (cm)	- 0.15	0.21	0.56
LIVDs (cm)	- 0.49	- 0.01	0.47
LVPWd (cm)	- 0.21	- 0.01	0.18
LVPWs (cm)	- 0.42	0.0	0.42
FS (%)	- 9.29	5.94	21.18
LA diam (cm)	- 0.37	- 0.3	0.18
Mitral annulus 3ch (cm)	- 0.31	0.04	0.38
Ao annulus 3ch (cm)	- 0.37	- 0.1	0.18
LA/Ao ratio	- 0.88	- 0.01	0.86
Mitral annulus 4ch (cm)	- 0.8	- 0.35	0.09
prox Ao (cm)	- 0.16	0.02	0.21
MPA (cm)	- 0.45	- 0.09	0.27
Ao/PA ratio (cm)	- 0.19	0.08	0.65
Mitral annulus: 3ch vs 4ch (cm)	- 0.29	0.27	0.83

LLOA = lower level of agreement; ULOA = upper level of agreement; IVSd = diastolic interventricular septal thickness; IVSs = systolic interventricular septal thickness; LVIDd = diastolic left ventricular internal diameter, measured just proximal to the papillary muscles; LVIDs = systolic left ventricular internal diameter, measured just proximal to the papillary muscles; LVPWd = diastolic left ventricular posterior wall thickness; LVPWs = systolic left ventricular posterior wall thickness; FS% = percent fractional shortening; LA diam 3ch = left atrial diameter measured on three chamber view; Mitral annulus 3ch = mitral annulus measured on approximated three-chamber view; Ao annulus 3ch = aortic annulus measured on three-chamber view; LA/Ao ratio = Left atrium to aorta ratio; Mitral annulus 4ch = mitral annulus measured on four-chamber view; prox Ao = Proximal aorta measured on transverse plane; MPA = main pulmonary artery transverse plane; Ao/PA ratio = Aorta to pulmonary artery ratio

Overall good agreement was found between the modalities when combining the anesthetic protocols per modality and individual. Figures 10 and 11 show the left ventricular variables and selected further planar measurements respectively as graphical output.

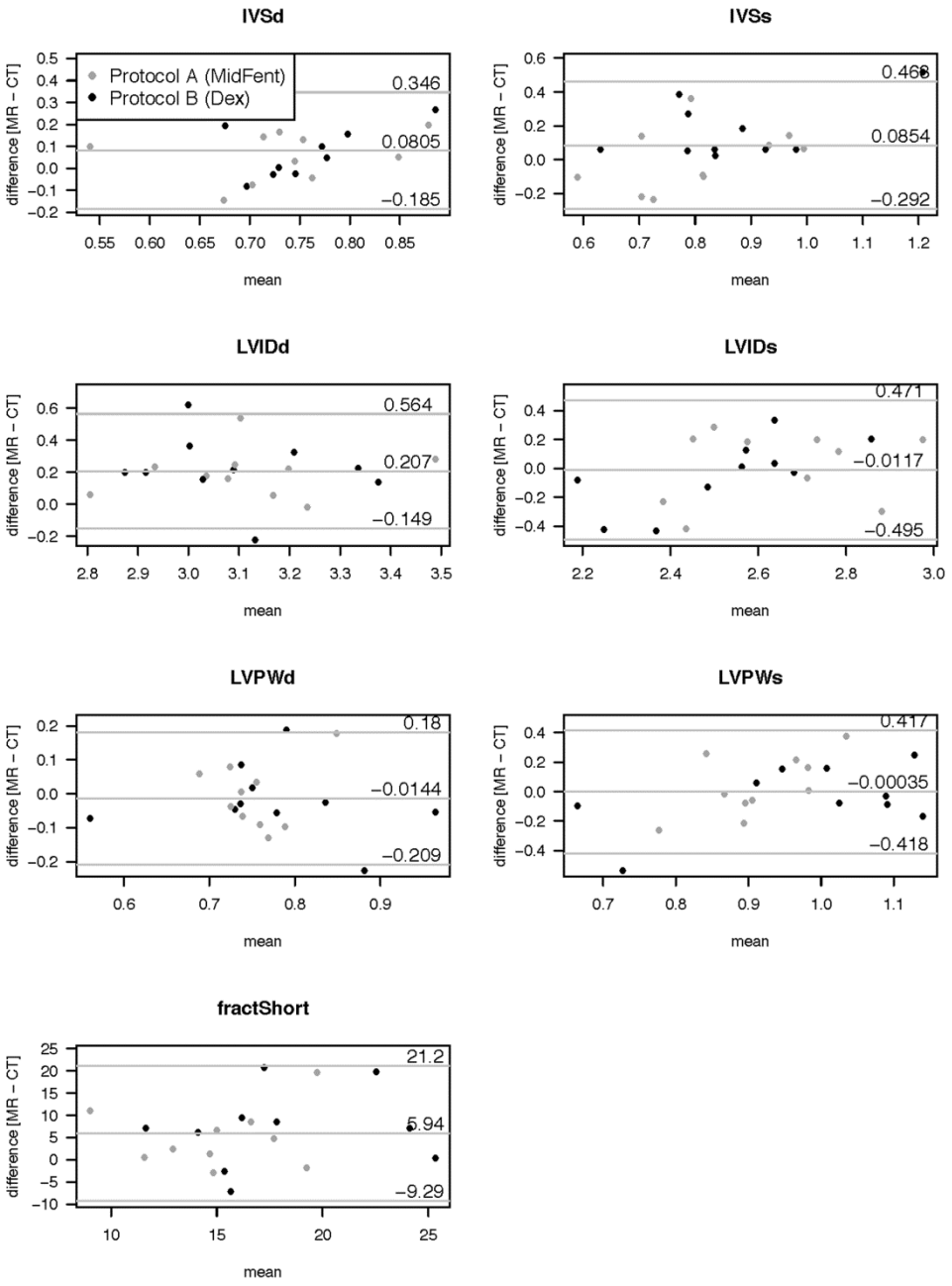
IVSd
Protocol A (MidFent)
Protocol B (Dex)
0.346
0.0805
−0.185
IVSs
0.468
0.0854
−0.292
LVIDd
0.564
0.207
−0.149
LVIDs
0.471
−0.0117
−0.495
LVPWd
0.18
−0.0144
−0.209
LVPWs
0.417
−0.00035
−0.418
fractShort
21.2
5.94
−9.29
difference [MR − CT]
mean

Figure 10: Graphical display of the Bland-Altman analysis comparing the planar left ventricular measurement generated using MDCTA (CT) versus MRI (MR) when combining the measures for the two different anesthetic episodes per modality. The bias is shown by the central horizontal line, the 95% lower and upper levels of agreement are depicted as the horizontal lines above and below.

IVSd: interventricular septum thickness at diastole (cm); IVSs: interventricular septum thickness at systole (cm); LVIDd: left ventricular internal diameter at diastole (cm); left ventricular internal diameter at systole (cm); LVPWd: left ventricular diameter at diastole (cm); LVPWs: left ventricular diameter at systole (cm); fractShort: fractional shortening (%)

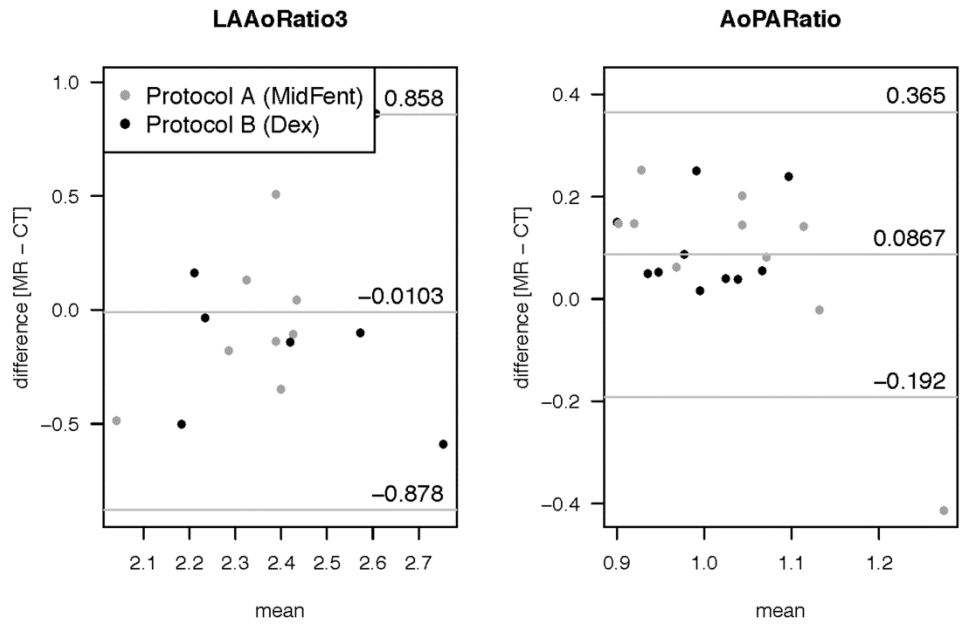

Figure 11: Graphical display of the Bland-Altman analysis comparing the LA/Ao-Ratio (left atrium (generated from three chamber view) to aorta ratio) and Ao/PA-Ratio (aorta to pulmonary artery ratio) generated from the planar measurements using MDCTA (CT) versus MRI (MR) when combining the measurements for the two different anesthetic episodes per modality. The bias is shown by the central horizontal line, the 95% lower and upper levels of agreement are depicted as the horizontal lines above and below.

Finally, when determining if the left ventricular volumetric values generated using the cross-sectional modalities with anesthetic protocol A and B would be able to predict the comparable variables generated with echocardiography on the awake dog, significant agreement was found only for LVEDV using MDCTA and anesthetic protocol B ($P = 0.01$). All other modality and anesthesia combinations for LVEDV, LVESV, LVSV, LVEF did not agree ($P > 0.05$) and would not allow for prediction of measurements generated using echocardiography in the awake animal (Table 2, Figure 12).

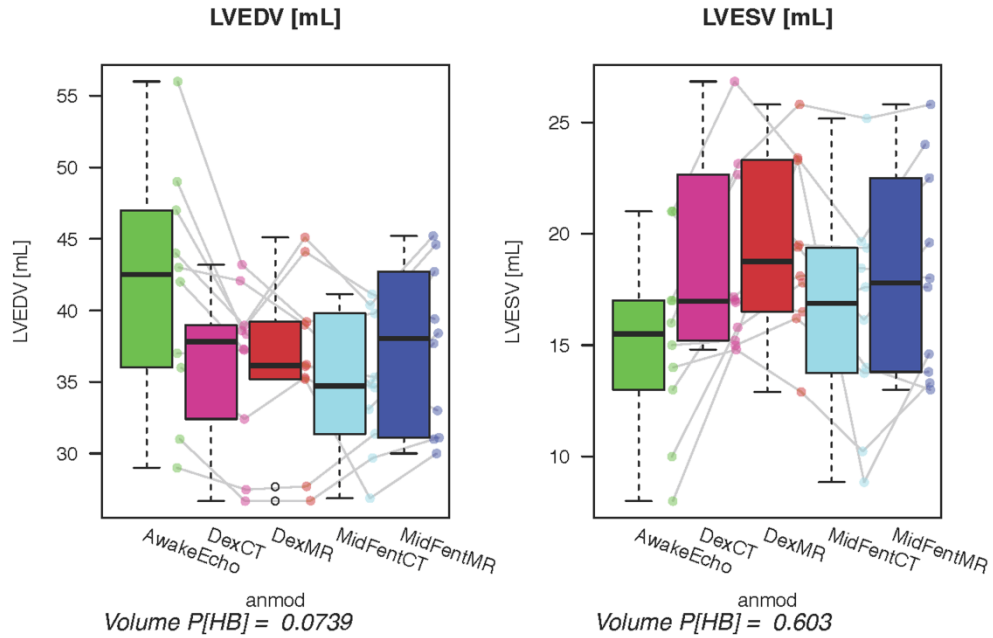
LVEDV [mL]
LVEDV [mL]
55
50
45
40
35
30
AwakeEcho
DexCT
DexMR
MidFentCT
MidFentMR
anmod
Volume P[HB] = 0.0739
LVESV [mL]
LVESV [mL]
25
20
15
10
AwakeEcho
DexCT
DexMR
MidFentCT
MidFentMR
anmod
Volume P[HB] = 0.603

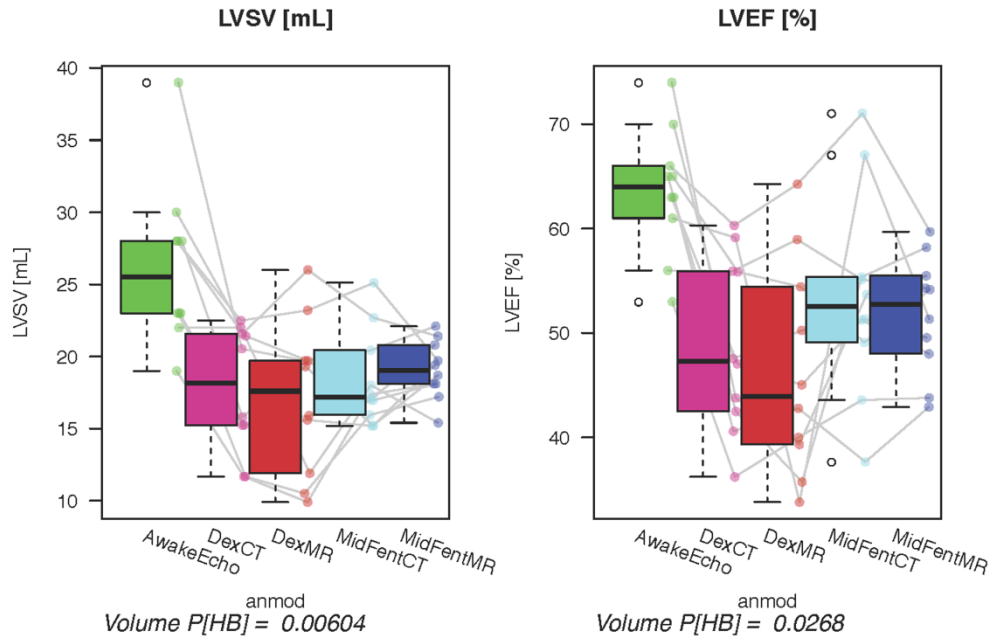
LVSV [mL]
LVSV [mL]
40
35
30
25
20
15
10
AwakeEcho
DexCT
DexMR
MidFentCT
MidFentMR
anmod
Volume P[HB] = 0.00604
LVEF [%]
LVEF [%]
70
60
50
40
AwakeEcho
DexCT
DexMR
MidFentCT
MidFentMR
anmod
Volume P[HB] = 0.0268

Figure 12: Graphical Display using Box-Pots to Compare the Volumetric Measurements acquired using the Anesthetic Protocol and Cross-sectional Modality Combinations to the Echocardiographic Results Gathered from the Awake Animals. Adjusted P-Values for all five exams (awake echocardiogram, anesthesia and MDCT, MRI using Protocol A, B) are given below the plots. Only LVEDV using MDCTA and anesthetic protocol B (P = 0.01) was able to allow for measurements generated using awake echocardiogram. LVEDV (ml): Left Ventricular End Diastolic Volume; LVESV (ml): Left Ventricular End Systolic Volume; LVSV (ml): Left Ventricular Stroke Volume; LVEF (%): Left Ventricular Ejection Fraction
AwakeEcho = Echocardiogram performed on the awake dogs; DexCT = MDCTA using Anesthetic Protocol B; DexMR = MRI using Anesthetic Protocol B; MidFentCT = MDCTA using Anesthetic Protocol A; MidFentMR = MRI using Anesthetic Protocol A. Line segments join observations obtained from the same dog as imaging and anesthesia protocols vary.

Comparison of the planar variables from the five exams (awake echocardiography and MDCTA, MRI using Protocol A, B) showed significant differences for the following variables: IVSs P=0.0006, LVIDd P=0.03, LVIDs P=0.002, FS P=0.0005, AoDiam P=0.004, LADiam P=0.003, PADiam P=0.0009, LAAoRatio P=0.0421, AoPARatio P=0.048 (Figure 13 and 14).

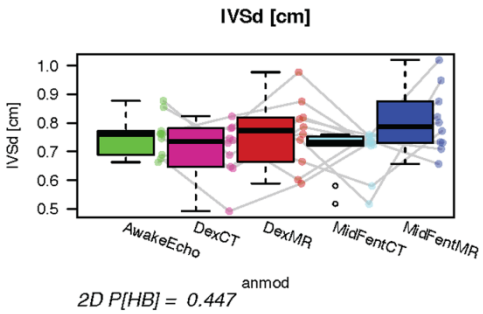

2D P[HB] = 0.447

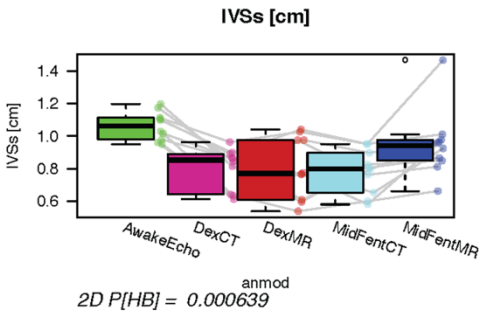

2D P[HB] = 0.000639

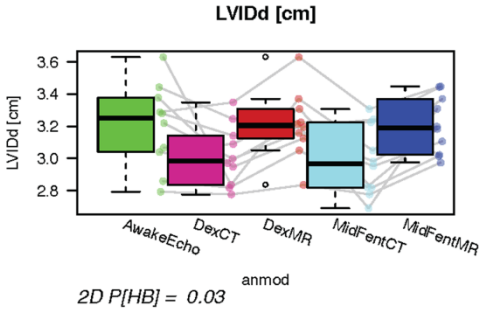

2D P[HB] = 0.03

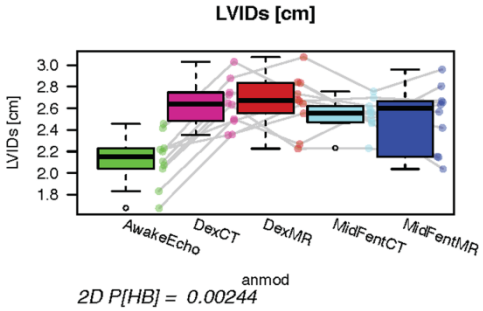

2D P[HB] = 0.00244

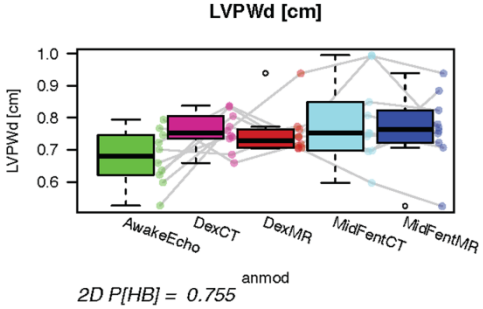

2D P[HB] = 0.755

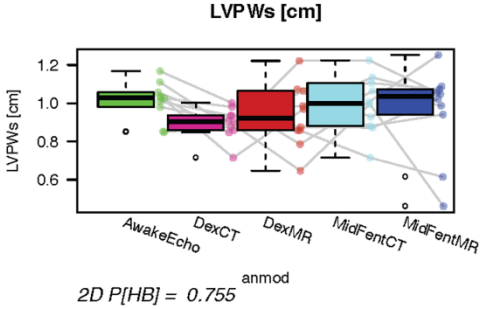

2D P[HB] = 0.755

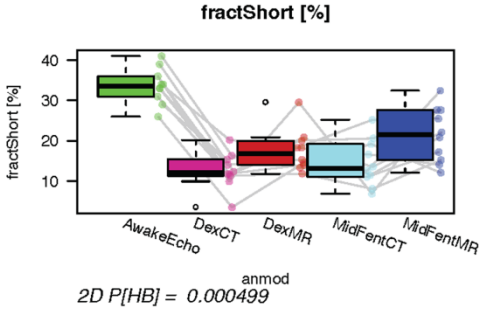

2D P[HB] = 0.000499

Figure 13: Graphical display using box-plots to compare left ventricular planar measurements generated using the four anesthetic protocol and modality combinations to the echocardiographic results gathered from the awake animals. No significant differences were found for any of the variables comparing the anesthesia protocols within each modality using paired Wilcoxon testing. Adjusted P-values comparing all five exams (awake echocardiogram, anesthesia and MDCT, MRI using Protocol A, B) are given below the plots. Prediction of echocardiographic measurements using the cross-sectional modalities was not possible (P =1).
IVSd (cm): interventricular septal thickness at diastole; IVSs (cm): interventricular septal thickness at systole; LVIDd (cm): left ventricular internal diameter at diastole. Using protocol A and 64-MDCTA this was the only variable allowing for predictions of the echocardiographic measurement in the awake dog; LIVDs (cm): left ventricular internal diameter at systole; LVPWd (cm): left ventricular posterior wall at diastole; LVPWs (cm): left ventricular posterior wall at systole; FractShort (%): fractional shortening.
AwakeEcho = echocardiogram performed on the awake dogs; DexCT = MDCTA using anesthetic protocol B; DexMR = MRI using anesthetic protocol B; MidFentCT = MDCTA using anesthetic protocol A; MidFentMR = MRI using anesthetic protocol A. Line segments join observations obtained from the same dog as imaging and anesthesia protocols vary.

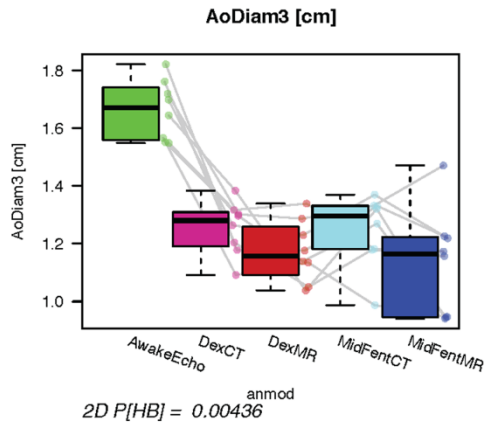

2D P[HB] = 0.00436

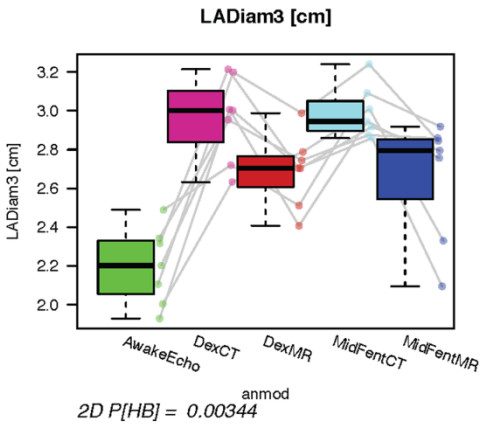

2D P[HB] = 0.00344

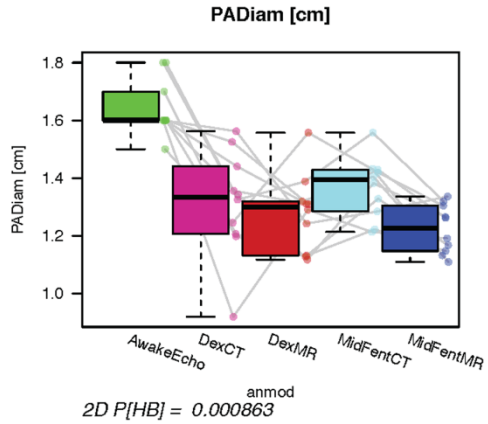

2D P[HB] = 0.000863

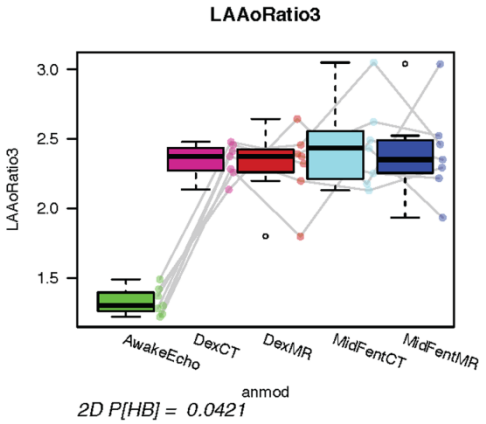

2D P[HB] = 0.0421

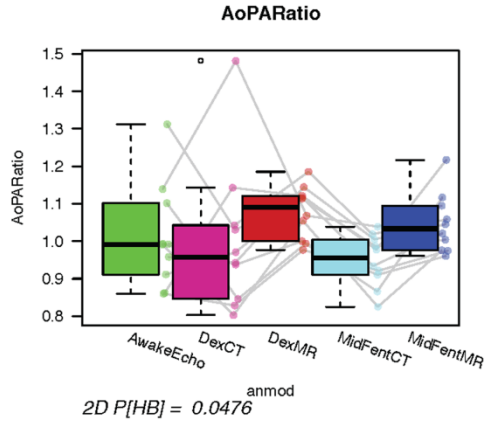

2D P[HB] = 0.0476

Figure 14: Graphical display using Box-Pots showing comparison of selected planar measurements generated using the four anesthetic protocol and modality combinations to the echocardiographic results gathered from the awake animals. There were no significant differences were found for any of the variables comparing the anesthesia protocols within each modality using paired Wilcoxon testing. Adjusted P-values comparing all five exams (awake anesthesia and MDCT, MRI using Protocol A, B) are given below the plots. Prediction of echocardiographic measurements using the cross-sectional modalities was not possible (P =1).
AoDiam3 (cm): Aortic diameter generated on the three chamber view using the cross-sectional modalities; LaDiam3 (cm): left atrial diameter measured on three chamber view using the cross-sectional modalities; PADiam (cm): pulmonary artery diameter; LaAODiam (cm): left atrium (measured on three chamber view) to aorta ratio; AoPADiam (cm): aorta to pulmonary artery ratio
AwakeEcho = echocardiogram performed on the awake dogs; DexCT = MDCTA using anesthetic protocol B; DexMR = MRI using anesthetic protocol B; MidFentCT = MDCTA using anesthetic protocol A; MidFentMR = MRI using anesthetic protocol A. Line segments join observations obtained from the same dog as imaging and anesthesia protocols vary.

When testing if the planar measurements acquired using the cross-sectional imaging modalities with the dogs anesthetized would be able to predict measurements generated by echocardiography in the awake dog, no significant agreement was found (P = 1 all variables).

Discussion

In the current study, diagnostic quality cardiac examinations were successfully acquired in a group of healthy beagle dogs using two different anesthetic protocols and both 64-MDCTA and 3T MRI. The use of different anesthetic protocols for the use in cardiac cross-sectional exams has not yet been evaluated; both anesthetic protocols used in this study were well tolerated and produced comparable results for the vital variables recorded in the healthy study population.

Heart rate control has been reported essential for image quality for MDCT acquisitions; high and irregular heart rates will cause motion artifact as the anatomy of the heart and the intravascular bolus may be depicted at different points of the cardiac cycle in the different acquisition segments[32]. The target heart rate of <65 bpm recommended in the human literature for cardiac MDCTA was not reached consistently using either protocol. Despite this, overall very good image quality was achieved at the given temporal resolution using a 64-MDCTA unit and a 0.35s tube rotation time. Mild motion artifact was seen in during systole exams that was displayed as mild shifting between the acquisition segments, yet this did not negatively influence the diagnostic quality of the studies and allowed for all measurements. Further advancement of CT technology using 320 detector row or dual source units are further increasing the speed of image acquisition and may lessen the need for lowering the heart rate for cardiac CT exams in the future[57]. A recent study used dual source MDCT for the evaluation of left ventricular volumes in dogs, and even though no specific comments

on image quality were made a mean heart rate greater than 70 bpm allowed for acquisition of the volumetric measurements[14].

The SSFP MRI sequences were acquired retrospectively ECG-gated during a breath hold. The arrhythmia rejection feature was turned off during acquisition as this commonly aborted the scan in the initial dog. The time to repetition (TR) is a function of the patients heart rate as recorded by the gating software and varied between 3.3-4.1ms in the exams and resulted in excellent image quality at the given heart rates[58].

Left ventricular systolic function variables investigated in this study were LVEDV, LVESV, LSV, LVEF and no difference between either anesthetic protocol or either of the three imaging modalities was identified. This differs from a recent study using a similar population of dogs, where the authors report higher end diastolic volume values generated on cardiac CT exams compared to MRI exams represented by a linear relationship between the modalities[13]. The reason for this disagreement is not clear but we speculate that this might relate to a systematic discrepancy in the evaluation of the measurements performed between CT or MRI versus a true alteration induced by the larger contrast bolus injected for the CT exam compared to no contrast injected for the MRI exam; alternatively the order of imaging modalities was not randomized in that study and an effect of anesthetic duration may have contributed. It is important to verify inclusion of the same portion of the heart in the analysis by comparison of the systolic to diastolic myocardial volume mass as calculated by subtraction of endocardial from the epicardial volumes; this was performed in our

study and might have aided to minimize an effect by modality compared to the report by Sieslack et al[13].

In addition, since all dogs also had a low level (~1-2%) of isoflurane added to their anesthetic protocol in our study, any potential differences in these variables associated with the two protocols may have been masked by isoflurane since administration produces dose-dependent cardiovascular depression in dogs[59].

Measurement of the myocardial mass is of interest in people in evaluating hypertrophic cardiomyopathies or the effects of hypertension and is used as an independent variable in patients with heart disease. It has also been applied in experimental animal studies for the left and right ventricle[2, 60-63]. This variable has rarely been reported generated using MRI or MDCTA in companion animals but left ventricular myocardial wall thickness is regularly included in echocardiographic reporting in companion animals and further evaluation of this variable might be helpful in companion animal cardiac MRI or MDCTA[11,31,64-64].

Inclusion or exclusion of the papillary muscles into the ventricular volume has been used variably between authors and exclusion of the papillary muscles from the left ventricular volume will naturally result in small systematic differences in the quantitative values[60, 62, 66, 67]. In echocardiographic exams the papillary muscles are typically disregarded using Simpson's rule estimates and by definition in Teichholz estimates[68]. Automated threshold based 3D segmentation methods can be used to assess ventricular function and will usually

exclude the papillary muscles from the ventricular lumen as the attenuation of intraluminal contrast medium versus the myocardium is used for threshold settings[66].

We aimed to keep the contrast and saline chaser volume low in the MDCT part of our study to avoid volume overloading of the dogs; ventricular contrast achieved was adequate to depict the anatomy to semi-automatically outline the endocardial surfaces of the left and, despite the relatively small contrast volume used, also the right ventricle. However the ventricular enhancement was at the low end for recognition using automated threshold settings so these could not be consistently applied and planar measurements (Simpson method) were therefore performed in this study using the short axis planes for the left and transverse planes for the right heart. This is more time consuming for the evaluator and bears potential room for observer variance; this study used one evaluator to avoid introduction of inter-observer variation. The papillary muscles were consistently included in the ventricular volume in our study due to institutional preference. Overall the LVEDV reported in our study is slightly lower as reported by Sieslack13[28] whereas the stroke volumes reported are fairly similar. This may therefore relate to the inclusion of the papillary muscles but a difference caused by the anesthetic protocols used cannot be ruled out since they affect the cardiovascular system to differing degrees.

Systolic right ventricular function variables have not been investigated in companion animals using cross-sectional modalities but this gains progressive interest for evaluation in people[60, 69]. This study showed

also no difference between the two anesthetic protocols as well as imaging modality used for the assessment of RVEDV, RVESV, RVSV and RVEF and delivers an initial reference.

Overall, no difference was found for any of the evaluated planar variables using either anesthetic protocol within the modalities, MDCTA or MRI. This would make the use of the protocols interchangeable for evaluation of these variables within each modality. There was also a low bias in comparing MDCTA and MRI for all variables when the anesthesia protocols were combined. However, because our study was performed in healthy dogs, we cannot extrapolate our data to other species or to patients with cardiovascular diseases or abnormalities.

Placement of the measurements was overall easily performed, only over the caudal aspect of the left atrium mild flow-artifact from the pulmonary venous inflow made the delineation of the caudal atrial border difficult at times. However, the bias between the measurements acquired on MDCTA and MRI was only 0.3cm for this variable; though this should be considered as a possible disadvantage when using MRI to evaluate the caudal left atrial border.

As expected, the MRI and CT variables acquired using anesthesia protocols A and B produced different values to those acquired in the awake animals using echocardiography. Left end diastolic volumes were higher, end systolic volumes were lower; left ventricular stroke volume and ejection fractions were higher using echocardiography in the awake animals compared to any of the anesthesia modality combinations, even though there was overlap. These findings are

consistent with those found in previous studies in isoflurane-anesthetized dogs[70]. A recent study compared echocardiographic measurement of the left ventricular volume using the Teichholz and modified Simpson method to left ventricular volumes acquired using dual source CT and applying the Simpson method in seven propofol/isoflurane anesthetized dogs using medetomedine as premedication. In this study the left ventricular volumes using the modified Simpson method in echocardiography underestimated the volume both compared to echocardiographic measurement using the Teichholz method and measurements from the dual source CT studies using the modified Simpson method[14]. In a different study using ten propofol/isoflurane anesthetized dogs induced with diazepam and levomethadone showed a high correlation of the mean values for EDV and ESV measured from MDCT or echocardiographic exams, using the Simpson method as preferred calculation of the volumes[9,12]. Another study evaluated ten dogs using a non-specified anesthetic protocol for assessment of left ventricular volumes using three-dimensional echocardiography and magnetic resonance imaging did not find significant differences for EDV, ESV, and EF between the two modalities, but differences were found comparing to one or two dimensional echocardiographic measurements[12].

The IVSs measurement was larger when evaluated using echocardiography in the awake dogs, possibly indicating higher contractility in the awake compared to anesthetized dog as shown in previous reports in isoflurane-anesthetized dogs[70]; this effect was

present but weaker for LVPWs. Similarly, the fractional shortening was greater and LVIDs was lower in the awake dogs compared to either of our anesthesia protocols, most likely due to the background of isoflurane in all dogs[70]. The aortic and pulmonary artery diameter was larger in the awake versus anesthetized patients. Although previous reports have reported smaller aortic and pulmonic diameters in isoflurane-anesthetized dogs[41, 71], others have shown no change[70]. Even though blood pressure measurements were not acquired on the awake dogs, a reduction in systemic and pulmonary diameter is consistent with lower blood pressures associated with isoflurane anesthesia even though a modality specific alteration of acquisition of the variable cannot be fully ruled out.

The left atrial diameter was lower evaluated in the awake dogs compared to any of the anesthesia protocol–modality combinations. Mildly reduced cardiac contractility in the anesthetized dogs might explain this finding. Based on the difference in these measurements the LAAo ratio was additionally altered in the anesthetized animals; for the AoPA ratio there was greater overlap but also no predictive value for echocardiography was generated.

A previous study used seven isoflurane anesthetized normal beagles to compare anatomical measurements acquired using dual source CT to echocardiographic measurements and found overall good agreement except for the values of the interventricular wall and left ventricular posterior wall thickness in end diastole[41]. The authors of this study speculate that interference of anatomical structures such as the

papillary muscles or chorda tendinae in combination with lower far-field image quality in echocardiography compared to the high quality of the dual source CT images may be causative for this discrepancy. As clinical patients are unlikely to undergo an anesthetized echocardiogram before cross-sectional imaging a possible discrepancy of the values as described in our study may be considered. Alternatively evaluation of the cross-sectional measurements in the anesthetized animal compared to awake echocardiography in a larger patient group may show trends that may allow for prediction between the modalities in the future.

The main limitation of this study includes the low number of study subjects used; ideally a larger and more varied study population representing different dog breeds, sizes and chest morphologies might have been included. Echocardiography was not performed under anesthesia using the two study protocols as the primary aim of this study was to compare cardiac MRI and CT variables, yet including echocardiography under the same conditions may have helped to determine whether discrepancies in the cross-sectional variables relate to anesthetic protocol used or measurement method and is acknowledged as a limitation of the study. MRI studies took markedly longer to acquire than the MDCTA studies; availability of the respective modalities as well as the study question may determine the choice of modality for companion animal patients in the future, as a low bias was

present between the modalities in our study. Both modalities resulted in overall very good and diagnostic image quality.

References

1. Thomas W. Two-dimensional, real-time echocardiography in the dog. *Veterinary Radiology* 1984;25: 50-64.

2. Stepien RL, Hinchcliff KW, Constable PD, Olson J. Effect of endurance training on cardiac morphology in Alaskan sled dogs. *J Appl Physiol (1985)*. 1998;85: 1368-1375.

3. Cornell CC, Kittleson MD, Della Torre P, Haggstrom J, Lombard CW, Pedersen HD, et al. Allometric scaling of M-mode cardiac measurements in normal adult dogs. *Journal of veterinary internal medicine / American College of Veterinary Internal Medicine*. 2004;18: 311-321.

4. Buchanan JW. Selective angiography and angiocardiography in dogs with acquired cardiovascular disease. *Veterinary Radiology*. 1965;6: 5-20.

5. Buchanan JW, Patterson D.F. Selective Angography and Angiocardiography in Dogs with Congenital Cardiovascular disease. *Veterinary Radiology*. 1965;6: 21-39.

6. Chetboul V. Advanced techniques in echocardiography in small animals. *Vet Clin North Am Small Anim Pract*. 2010;40: 529-543.

7. Asferg C, Usinger L, Kristensen TS, Abdulla J. Accuracy of multi-slice computed tomography for measurement of left ventricular ejection fraction compared with cardiac magnetic resonance imaging and two-dimensional transthoracic echocardiography: a systematic review and meta-analysis. *Eur J Radiol*. 2012;81: e757-762.

8. Nasis A, Mottram PM, Cameron JD, Seneviratne SK. Current and evolving clinical applications of multidetector cardiac CT in assessment of structural heart disease. *Radiology*. 2013;267: 11-25.

9. Peters J, Lessick J, Kneser R, Wachter I, Vembar M, Ecabert O, et al. Accurate segmentation of the left ventricle in computed tomography images for local wall thickness assessment. *Med Image Comput Comput Assist Interv*. 2010;13: 400-408.

10. Tsang W, Bateman MG, Weinert L, Pellegrini G, Mor-Avi V, Sugeng L, et al. Accuracy of aortic annular measurements obtained from three-dimensional echocardiography, CT and MRI: human in vitro and in vivo studies. *Heart*. 2012;98: 1146-1152.

11. Alberti JF, de Diego JJ, Delgado RV, Riera JC, Torres RA. [State of the art: new developments in cardiac imaging]. *Rev Esp Cardiol (Engl Ed)*. 2012;65 Suppl 1: 24-34.

12. Achenbach S, Barkhausen J, Beer M, Beerbaum P, Dill T, Eichhorn J, et al. [Consensus recommendations of the German Radiology Society (DRG), the German Cardiac Society (DGK) and the German Society for Pediatric Cardiology (DGPK) on the use of cardiac imaging with computed tomography and magnetic resonance imaging]. *Rofo*. 2012;184: 345-368.

13. Al-Mohaissen MA, Kazmi MH, Chan KL, Chow BJ. Validation of Two-Dimensional Methods for Left Atrial Volume Measurement: A Comparison of Echocardiography with Cardiac Computed Tomography. *Echocardiography*. 2013.

14. Coon PD, Pollard H, Furlong K, Lang RM, Mor-Avi V. Quantification of left ventricular size and function using contrast-enhanced real-time 3D imaging with power modulation: comparison with cardiac MRI. *Ultrasound Med Biol*. 2012;38: 1853-1858.

15. Mai W, Weisse C, Sleeper MM. Cardiac magnetic resonance imaging in normal dogs and two dogs with heart base tumor. *Veterinary radiology & ultrasound : the official journal of the American College of Veterinary Radiology and the International Veterinary Radiology Association*. 2010;51: 428-435.

16. Petite AF, Kirberger RM. Mediastinum. In: Schwarz T, Saunders J (eds): *Veterinary Computed Tomography*. Chichester: Wiley-Blackwell, 2011;249-260.

17. Henninger W. Use of computed tomography in the diseased feline thorax. *The Journal of small animal practice*. 2003;44: 56-64.

18. Reetz JA, Buza EL, Krick EL. CT features of pleural masses and nodules. *Veterinary radiology & ultrasound : the official journal of the American College of Veterinary Radiology and the International Veterinary Radiology Association*. 2012;53: 121-127.

19. Marolf AJ, Gibbons DS, Podell BK, Park RD. Computed tomographic appearance of primary lung tumors in dogs. *Veterinary radiology & ultrasound : the official journal of the American College of Veterinary Radiology and the International Veterinary Radiology Association*. 2011;52: 168-172.

20. Prather AB, Berry CR, Thrall DE. Use of radiography in combination with computed tomography for the assessment of

noncardiac thoracic disease in the dog and cat. *Veterinary radiology & ultrasound : the official journal of the American College of Veterinary Radiology and the International Veterinary Radiology Association*. 2005;46: 114-121.

21. Armbrust LJ, Biller DS, Bamford A, Chun R, Garrett LD, Sanderson MW. Comparison of three-view thoracic radiography and computed tomography for detection of pulmonary nodules in dogs with neoplasia. *Journal of the American Veterinary Medical Association*. 2012;240: 1088-1094.

22. Schuller S, Fredericksen M, Schroder H, Meyer-Lindenberg A, Hewicker-Trautwein M, Nolte I. [Computer tomographic differentiation of intrathoracic neoplasms and inflammation in the dog]. *Berl Munch Tierarztl Wochenschr*. 2005;118: 76-84.

23. Henjes CR, Hungerbuhler S, Bojarski IB, Nolte I, Wefstaedt P. Comparison of multi-detector row computed tomography with echocardiography for assessment of left ventricular function in healthy dogs. *American journal of veterinary research*. 2012;73: 393-403.

24. Gilbert SH, McConnell FJ, Holden AV, Sivananthan MU, Dukes-McEwan J. The potential role of MRI in veterinary clinical cardiology. *Vet J*. 2010;183: 124-134.

25. Contreras S, Vazquez JM, Miguel AD, Morales M, Gil F, Lopez O, et al. Magnetic resonance angiography of the normal canine heart and associated blood vessels. *Vet J*. 2008;178: 130-132.

26. MacDonald KA, Kittleson MD, Garcia-Nolen T, Larson RF, Wisner ER. Tissue Doppler imaging and gradient echo cardiac magnetic

resonance imaging in normal cats and cats with hypertrophic cardiomyopathy. *Journal of veterinary internal medicine / American College of Veterinary Internal Medicine*. 2006;20: 627-634.

27. Meyer J, Wefstaedt P, Dziallas P, Beyerbach M, Nolte I, Hungerbuhler SO. Assessment of left ventricular volumes by use of one-, two-, and three-dimensional echocardiography versus magnetic resonance imaging in healthy dogs. *American journal of veterinary research*. 2013;74: 1223-1230.

28. Sieslack AK, Dziallas P, Nolte I, Wefstaedt P. Comparative assessment of left ventricular function variables determined via cardiac computed tomography and cardiac magnetic resonance imaging in dogs. *American journal of veterinary research*. 2013;74: 990-998.

29. Lee M, Park N, Lee S, Lee A, Jung J, Kim Y, et al. Comparison of echocardiography with dual-source computed tomography for assessment of left ventricular volume in healthy Beagles. *American journal of veterinary research*. 2013;74: 62-69.

30. Mahabadi AA, Achenbach S, Burgstahler C, Dill T, Fischbach R, Knez A, et al. Safety, efficacy, and indications of beta-adrenergic receptor blockade to reduce heart rate prior to coronary CT angiography. *Radiology*. 2010;257: 614-623.

31. McDonald KM, D'Aloia A, Parrish T, Mock J, Hauer K, Stillman AE, et al. Functional impact of an increase in ventricular mass after myocardial damage and its attenuation by converting enzyme inhibition. *J Card Fail*. 1998;4: 203-212.

32. Menke J, Unterberg-Buchwald C, Staab W, Sohns JM, Seif Amir Hosseini A, Schwarz A. Head-to-head comparison of prospectively triggered vs retrospectively gated coronary computed tomography angiography: Meta-analysis of diagnostic accuracy, image quality, and radiation dose. *Am Heart J*. 2013;165: 154-163 e153.

33. Hezzell MJ, Dennis SG, Humm K, Agee L, Boswood A. Relationships between heart rate and age, bodyweight and breed in 10,849 dogs. *The Journal of small animal practice*. 2013;54: 318-324.

34. Wess G MJ, Simak J, Hartman K. Use of Simpson's Method of Disc to Detect Early Echocardiographic Changes in Doberman Pinschers with Dilated Cardiomyopathy. *Journal of Veterinary Internal mMedicine*. 2010;24: 1069-1076.

35. Rosset A, Spadola L, Ratib O. OsiriX: an open-source software for navigating in multidimensional DICOM images. *J Digit Imaging*. 2004;17: 205-216.

36. Hergan K, Schuster A, Fruhwald J, Mair M, Burger R, Topker M. Comparison of left and right ventricular volume measurement using the Simpson's method and the area length method. *Eur J Radiol*. 2008;65: 270-278.

37. R Development Core Team. *R: A language and environment for statistical computing.* . Vienna: R Foundation for Statistical Computing, 2012.

38. Holm S. A simple sequentially rejective multiple test procedure. *Scandinavian Journal of Statistics*. 1979;17: 571-582.

39. Bland JM, Altman DG. Agreement between methods of measurement with multiple observations per individual. *J Biopharm Stat*. 2007;17: 571-582.

40. Hockings PD, Busza AL, Byrne J, Patel B, Smart SC, Reid DG, et al. Validation of MRI measurement of cardiac output in the dog: the effects of dobutamine and minoxidil. *Toxicol Mech Methods*. 2003;13: 39-43.

41. Park N, Lee M, Lee A, Lee S, Song S, Jung J, et al. Comparative study of cardiac anatomic measurements obtained by echocardiography and dual-source computed tomography. *J Vet Med Sci*. 2012;74: 1597-1602.

42. Pascoe PJ, Raekallio M, Kuusela E, McKusick B, Granholm M. Changes in the minimum alveolar concentration of isoflurane and some cardiopulmonary measurements during three continuous infusion rates of dexmedetomidine in dogs. *Vet Anaesth Analg*. 2006;33: 97-103.

43. Braz LG, Braz JR, Castiglia YM, Vianna PT, Vane LA, Modolo NS, et al. Dexmedetomidine alters the cardiovascular response during infra-renal aortic cross-clamping in sevoflurane-anesthetized dogs. *J Invest Surg*. 2008;21: 360-368.

44. Lin GY, Robben JH, Murrell JC, Aspegren J, McKusick BC, Hellebrekers LJ. Dexmedetomidine constant rate infusion for 24 hours during and after propofol or isoflurane anaesthesia in dogs. *Vet Anaesth Analg*. 2008;35: 141-153.

45. Uilenreef JJ, Murrell JC, McKusick BC, Hellebrekers LJ. Dexmedetomidine continuous rate infusion during isoflurane

anaesthesia in canine surgical patients. *Vet Anaesth Analg*. 2008;35: 1-12.

46. Ebner LS, Lerche P, Bednarski RM, Hubbell JA. Effect of dexmedetomidine, morphine-lidocaine-ketamine, and dexmedetomidine-morphine-lidocaine-ketamine constant rate infusions on the minimum alveolar concentration of isoflurane and bispectral index in dogs. *American journal of veterinary research*. 2013;74: 963-970.

47. Congdon JM, Marquez M, Niyom S, Boscan P. Cardiovascular, respiratory, electrolyte and acid-base balance during continuous dexmedetomidine infusion in anesthetized dogs. *Vet Anaesth Analg*. 2013;40: 464-471.

48. Steagall PV, Teixeira Neto FJ, Minto BW, Campagnol D, Correa MA. Evaluation of the isoflurane-sparing effects of lidocaine and fentanyl during surgery in dogs. *Journal of the American Veterinary Medical Association*. 2006;229: 522-527.

49. Aguado D, Benito J, Gomez de Segura IA. Reduction of the minimum alveolar concentration of isoflurane in dogs using a constant rate of infusion of lidocaine-ketamine in combination with either morphine or fentanyl. *Vet J*. 2011;189: 63-66.

50. Sano T, Nishimura R, Kanazawa H, Igarashi E, Nagata Y, Mochizuki M, et al. Pharmacokinetics of fentanyl after single intravenous injection and constant rate infusion in dogs. *Vet Anaesth Analg*. 2006;33: 266-273.

51. Grimm KA, Tranquilli WJ, Gross DR, Sisson DD, Bulmer BJ, Benson GJ, et al. Cardiopulmonary effects of fentanyl in conscious dogs and dogs sedated with a continuous rate infusion of medetomidine. *American journal of veterinary research*. 2005;66: 1222-1226.

52. Keating SC, Kerr CL, Valverde A, Johnson RJ, McDonell WN. Cardiopulmonary effects of intravenous fentanyl infusion in dogs during isoflurane anesthesia and with concurrent acepromazine or dexmedetomidine administration during anesthetic recovery. *American journal of veterinary research*. 2013;74: 672-682.

53. Seddighi R, Egger CM, Rohrbach BW, Cox SK, Doherty TJ. The effect of midazolam on the end-tidal concentration of isoflurane necessary to prevent movement in dogs. *Vet Anaesth Analg*. 2011;38: 195-202.

54. Jones DJ, Stehling LC, Zauder HL. Cardiovascular responses to diazepam and midazolam maleate in the dog. *Anesthesiology*. 1979;51: 430-434.

55. Heniff MS, Moore GP, Trout A, Cordell WH, Nelson DR. Comparison of routes of flumazenil administration to reverse midazolam-induced respiratory depression in a canine model. *Acad Emerg Med*. 1997;4: 1115-1118.

56. Bosiack AP, Mann FA, Dodam JR, Wagner-Mann CC, Branson KR. Comparison of ultrasonic Doppler flow monitor, oscillometric, and direct arterial blood pressure measurements in ill dogs. *J Vet Emerg Crit Care (San Antonio)*. 2010;20: 207-215.

57. Hou DJ, Tso DK, Davison C, Inacio J, Louis LJ, Nicolaou S, et al. Clinical utility of ultra high pitch dual source thoracic CT imaging of acute pulmonary embolism in the emergency department: Are we one step closer towards a non-gated triple rule out? *Eur J Radiol*. 2013;82: 1793-1798.

58. Saremi F, Grizzard JD, Kim RJ. Optimizing cardiac MR imaging: practical remedies for artifacts. *Radiographics : a review publication of the Radiological Society of North America, Inc*. 2008;28: 1161-1187.

59. Merin RG, Bernard JM, Doursout MF, Cohen M, Chelly JE. Comparison of the effects of isoflurane and desflurane on cardiovascular dynamics and regional blood flow in the chronically instrumented dog. *Anesthesiology*. 1991;74: 568-574.

60. Francois CJ, Fieno DS, Shors SM, Finn JP. Left ventricular mass: manual and automatic segmentation of true FISP and FLASH cine MR images in dogs and pigs. *Radiology*. 2004;230: 389-395.

61. Koren MJ, Devereux RB, Casale PN, Savage DD, Laragh JH. Relation of left ventricular mass and geometry to morbidity and mortality in uncomplicated essential hypertension. *Ann Intern Med*. 1991;114: 345-352.

62. Shors SM, Fung CW, Francois CJ, Finn JP, Fieno DS. Accurate quantification of right ventricular mass at MR imaging by using cine true fast imaging with steady-state precession: study in dogs. *Radiology*. 2004;230: 383-388.

63. Levy D, Garrison RJ, Savage DD, Kannel WB, Castelli WP. Prognostic implications of echocardiographically determined left

ventricular mass in the Framingham Heart Study. *The New England journal of medicine*. 1990;322: 1561-1566.

64. Devereux RB. Detection of left ventricular hypertrophy by M-mode echocardiography. Anatomic validation, standardization, and comparison to other methods. *Hypertension*. 1987;9: II19-26.

65. Devereux RB, Reichek N. Echocardiographic determination of left ventricular mass in man. Anatomic validation of the method. *Circulation*. 1977;55: 613-618.

66. Juergens KU, Seifarth H, Range F, Wienbeck S, Wenker M, Heindel W, et al. Automated threshold-based 3D segmentation versus short-axis planimetry for assessment of global left ventricular function with dual-source MDCT. *AJR American journal of roentgenology*. 2008;190: 308-314.

67. Fratz S, Schuhbaeck A, Buchner C, Busch R, Meierhofer C, Martinoff S, et al. Comparison of accuracy of axial slices versus short-axis slices for measuring ventricular volumes by cardiac magnetic resonance in patients with corrected tetralogy of fallot. *Am J Cardiol*. 2009;103: 1764-1769.

68. Folland ED, Parisi AF, Moynihan PF, Jones DR, Feldman CL, Tow DE. Assessment of left ventricular ejection fraction and volumes by real-time, two-dimensional echocardiography. A comparison of cineangiographic and radionuclide techniques. *Circulation*. 1979;60: 760-766.

69. Sanz J, Conroy J, Narula J. Imaging of the right ventricle. *Cardiol Clin*. 2012;30: 189-203.

70. Sousa MG, Carareto R, De-Nardi AB, Brito FL, Nunes N, Camacho AA. Effects of isoflurane on echocardiographic parameters in healthy dogs. *Vet Anaesth Analg*. 2008;35: 185-190.

71. Hettrick DA, Pagel PS, Warltier DC. Isoflurane and halothane produce similar alterations in aortic distensibility and characteristic aortic impedance. *Anesth Analg*. 1996;83: 1166-1172.

formatted refs

1. Thomas W. Two-dimensional, real-time echocardiography in the dog. *Veterinary Radiology* 1984;25: 50-64.

2. Stepien RL, Hinchcliff KW, Constable PD, Olson J. Effect of endurance training on cardiac morphology in Alaskan sled dogs. *J Appl Physiol (1985)*. 1998;85: 1368-1375.

3. Cornell CC, Kittleson MD, Della Torre P, Haggstrom J, Lombard CW, Pedersen HD, et al. Allometric scaling of M-mode cardiac measurements in normal adult dogs. *Journal of veterinary internal medicine / American College of Veterinary Internal Medicine*. 2004;18: 311-321.

4. Buchanan JW. Selective angiography and angiocardiography in dogs with acquired cardiovascular disease. *Veterinary Radiology*. 1965;6: 5-20.

5. Buchanan JW, Patterson D.F. Selective Angography and Angiocardiography in Dogs with Congenital Cardiovascular disease. *Veterinary Radiology*. 1965;6: 21-39.

6. Chetboul V. Advanced techniques in echocardiography in small animals. *Vet Clin North Am Small Anim Pract*. 2010;40: 529-543.

7. Gilbert SH, McConnell FJ, Holden AV, Sivananthan MU, Dukes-McEwan J. The potential role of MRI in veterinary clinical cardiology. *Vet J*. 2010;183: 124-134.

8. Mai W, Weisse C, Sleeper MM. Cardiac magnetic resonance imaging in normal dogs and two dogs with heart base tumor. *Veterinary radiology & ultrasound : the official journal of the American College of Veterinary Radiology and the International Veterinary Radiology Association*. 2010;51: 428-435.

9. Henjes CR, Hungerbuhler S, Bojarski IB, Nolte I, Wefstaedt P. Comparison of multi-detector row computed tomography with echocardiography for assessment of left ventricular function in healthy dogs. *American journal of veterinary research*. 2012;73: 393-403.

10. Contreras S, Vazquez JM, Miguel AD, Morales M, Gil F, Lopez O, et al. Magnetic resonance angiography of the normal canine heart and associated blood vessels. *Vet J*. 2008;178: 130-132.

11. MacDonald KA, Kittleson MD, Garcia-Nolen T, Larson RF, Wisner ER. Tissue Doppler imaging and gradient echo cardiac magnetic resonance imaging in normal cats and cats with hypertrophic cardiomyopathy. *Journal of veterinary internal medicine / American College of Veterinary Internal Medicine*. 2006;20: 627-634.

12. Meyer J, Wefstaedt P, Dziallas P, Beyerbach M, Nolte I, Hungerbuhler SO. Assessment of left ventricular volumes by use of one-, two-, and three-dimensional echocardiography versus magnetic resonance imaging in healthy dogs. *American journal of veterinary research*. 2013;74: 1223-1230.

13. Sieslack AK, Dziallas P, Nolte I, Wefstaedt P. Comparative assessment of left ventricular function variables determined via cardiac computed tomography and cardiac magnetic resonance imaging in dogs. *American journal of veterinary research*. 2013;74: 990-998.

14. Lee M, Park N, Lee S, Lee A, Jung J, Kim Y, et al. Comparison of echocardiography with dual-source computed tomography for assessment of left ventricular volume in healthy Beagles. *American journal of veterinary research*. 2013;74: 62-69.

15. Asferg C, Usinger L, Kristensen TS, Abdulla J. Accuracy of multi-slice computed tomography for measurement of left ventricular ejection fraction compared with cardiac magnetic resonance imaging and two-dimensional transthoracic echocardiography: a systematic review and meta-analysis. *Eur J Radiol*. 2012;81: e757-762.

16. Nasis A, Mottram PM, Cameron JD, Seneviratne SK. Current and evolving clinical applications of multidetector cardiac CT in assessment of structural heart disease. *Radiology*. 2013;267: 11-25.

17. Peters J, Lessick J, Kneser R, Wachter I, Vembar M, Ecabert O, et al. Accurate segmentation of the left ventricle in computed tomography images for local wall thickness assessment. *Med Image Comput Comput Assist Interv*. 2010;13: 400-408.

18. Tsang W, Bateman MG, Weinert L, Pellegrini G, Mor-Avi V, Sugeng L, et al. Accuracy of aortic annular measurements obtained from three-dimensional echocardiography, CT and MRI: human in vitro and in vivo studies. *Heart*. 2012;98: 1146-1152.

19. Alberti JF, de Diego JJ, Delgado RV, Riera JC, Torres RA. [State of the art: new developments in cardiac imaging]. *Rev Esp Cardiol (Engl Ed)*. 2012;65 Suppl 1: 24-34.

20. Achenbach S, Barkhausen J, Beer M, Beerbaum P, Dill T, Eichhorn J, et al. [Consensus recommendations of the German Radiology Society (DRG), the German Cardiac Society (DGK) and the German Society for Pediatric Cardiology (DGPK) on the use of cardiac imaging with computed tomography and magnetic resonance imaging]. *Rofo*. 2012;184: 345-368.

21. Al-Mohaissen MA, Kazmi MH, Chan KL, Chow BJ. Validation of Two-Dimensional Methods for Left Atrial Volume Measurement: A Comparison of Echocardiography with Cardiac Computed Tomography. *Echocardiography*. 2013.

22. Coon PD, Pollard H, Furlong K, Lang RM, Mor-Avi V. Quantification of left ventricular size and function using contrast-enhanced real-time 3D imaging with power modulation: comparison with cardiac MRI. *Ultrasound Med Biol*. 2012;38: 1853-1858.

23. Petite AF, Kirberger RM. Mediastinum. In: Schwarz T, Saunders J (eds): *Veterinary Computed Tomography*. Chichester: Wiley-Blackwell, 2011;249-260.

24. Henninger W. Use of computed tomography in the diseased feline thorax. *The Journal of small animal practice*. 2003;44: 56-64.

25. Reetz JA, Buza EL, Krick EL. CT features of pleural masses and nodules. *Veterinary radiology & ultrasound : the official journal of the*

American College of Veterinary Radiology and the International Veterinary Radiology Association. 2012;53: 121-127.

26. Marolf AJ, Gibbons DS, Podell BK, Park RD. Computed tomographic appearance of primary lung tumors in dogs. *Veterinary radiology & ultrasound : the official journal of the American College of Veterinary Radiology and the International Veterinary Radiology Association*. 2011;52: 168-172.

27. Prather AB, Berry CR, Thrall DE. Use of radiography in combination with computed tomography for the assessment of noncardiac thoracic disease in the dog and cat. *Veterinary radiology & ultrasound : the official journal of the American College of Veterinary Radiology and the International Veterinary Radiology Association*. 2005;46: 114-121.

28. Armbrust LJ, Biller DS, Bamford A, Chun R, Garrett LD, Sanderson MW. Comparison of three-view thoracic radiography and computed tomography for detection of pulmonary nodules in dogs with neoplasia. *Journal of the American Veterinary Medical Association*. 2012;240: 1088-1094.

29. Schuller S, Fredericksen M, Schroder H, Meyer-Lindenberg A, Hewicker-Trautwein M, Nolte I. [Computer tomographic differentiation of intrathoracic neoplasms and inflammation in the dog]. *Berl Munch Tierarztl Wochenschr*. 2005;118: 76-84.

30. Mahabadi AA, Achenbach S, Burgstahler C, Dill T, Fischbach R, Knez A, et al. Safety, efficacy, and indications of beta-adrenergic

receptor blockade to reduce heart rate prior to coronary CT angiography. *Radiology*. 2010;257: 614-623.

31. McDonald KM, D'Aloia A, Parrish T, Mock J, Hauer K, Stillman AE, et al. Functional impact of an increase in ventricular mass after myocardial damage and its attenuation by converting enzyme inhibition. *J Card Fail*. 1998;4: 203-212.

32. Menke J, Unterberg-Buchwald C, Staab W, Sohns JM, Seif Amir Hosseini A, Schwarz A. Head-to-head comparison of prospectively triggered vs retrospectively gated coronary computed tomography angiography: Meta-analysis of diagnostic accuracy, image quality, and radiation dose. *Am Heart J*. 2013;165: 154-163 e153.

33. Hezzell MJ, Dennis SG, Humm K, Agee L, Boswood A. Relationships between heart rate and age, bodyweight and breed in 10,849 dogs. *The Journal of small animal practice*. 2013;54: 318-324.

34. Wess G MJ, Simak J, Hartman K. Use of Simpson's Method of Disc to Detect Early Echocardiographic Changes in Doberman Pinschers with Dilated Cardiomyopathy. *Journal of Veterinary Internal mMedicine*. 2010;24: 1069-1076.

35. Rosset A, Spadola L, Ratib O. OsiriX: an open-source software for navigating in multidimensional DICOM images. *J Digit Imaging*. 2004;17: 205-216.

36. Hergan K, Schuster A, Fruhwald J, Mair M, Burger R, Topker M. Comparison of left and right ventricular volume measurement using the Simpson's method and the area length method. *Eur J Radiol*. 2008;65: 270-278.

37. R Development Core Team. *R: A language and environment for statistical computing.* . Vienna: R Foundation for Statistical Computing, 2012.

38. Holm S. A simple sequentially rejective multiple test procedure. *Scandinavian Journal of Statistics*. 1979;17: 571-582.

39. Bland JM, Altman DG. Agreement between methods of measurement with multiple observations per individual. *J Biopharm Stat*. 2007;17: 571-582.

40. Hockings PD, Busza AL, Byrne J, Patel B, Smart SC, Reid DG, et al. Validation of MRI measurement of cardiac output in the dog: the effects of dobutamine and minoxidil. *Toxicol Mech Methods*. 2003;13: 39-43.

41. Park N, Lee M, Lee A, Lee S, Song S, Jung J, et al. Comparative study of cardiac anatomic measurements obtained by echocardiography and dual-source computed tomography. *J Vet Med Sci*. 2012;74: 1597-1602.

42. Pascoe PJ, Raekallio M, Kuusela E, McKusick B, Granholm M. Changes in the minimum alveolar concentration of isoflurane and some cardiopulmonary measurements during three continuous infusion rates of dexmedetomidine in dogs. *Vet Anaesth Analg*. 2006;33: 97-103.

43. Braz LG, Braz JR, Castiglia YM, Vianna PT, Vane LA, Modolo NS, et al. Dexmedetomidine alters the cardiovascular response during infra-renal aortic cross-clamping in sevoflurane-anesthetized dogs. *J Invest Surg*. 2008;21: 360-368.

44. Lin GY, Robben JH, Murrell JC, Aspegren J, McKusick BC, Hellebrekers LJ. Dexmedetomidine constant rate infusion for 24 hours

during and after propofol or isoflurane anaesthesia in dogs. *Vet Anaesth Analg*. 2008;35: 141-153.

45. Uilenreef JJ, Murrell JC, McKusick BC, Hellebrekers LJ. Dexmedetomidine continuous rate infusion during isoflurane anaesthesia in canine surgical patients. *Vet Anaesth Analg*. 2008;35: 1-12.

46. Ebner LS, Lerche P, Bednarski RM, Hubbell JA. Effect of dexmedetomidine, morphine-lidocaine-ketamine, and dexmedetomidine-morphine-lidocaine-ketamine constant rate infusions on the minimum alveolar concentration of isoflurane and bispectral index in dogs. *American journal of veterinary research*. 2013;74: 963-970.

47. Congdon JM, Marquez M, Niyom S, Boscan P. Cardiovascular, respiratory, electrolyte and acid-base balance during continuous dexmedetomidine infusion in anesthetized dogs. *Vet Anaesth Analg*. 2013;40: 464-471.

48. Steagall PV, Teixeira Neto FJ, Minto BW, Campagnol D, Correa MA. Evaluation of the isoflurane-sparing effects of lidocaine and fentanyl during surgery in dogs. *Journal of the American Veterinary Medical Association*. 2006;229: 522-527.

49. Aguado D, Benito J, Gomez de Segura IA. Reduction of the minimum alveolar concentration of isoflurane in dogs using a constant rate of infusion of lidocaine-ketamine in combination with either morphine or fentanyl. *Vet J*. 2011;189: 63-66.

50. Sano T, Nishimura R, Kanazawa H, Igarashi E, Nagata Y, Mochizuki M, et al. Pharmacokinetics of fentanyl after single intravenous injection and constant rate infusion in dogs. *Vet Anaesth Analg*. 2006;33: 266-273.

51. Grimm KA, Tranquilli WJ, Gross DR, Sisson DD, Bulmer BJ, Benson GJ, et al. Cardiopulmonary effects of fentanyl in conscious dogs and dogs sedated with a continuous rate infusion of medetomidine. *American journal of veterinary research*. 2005;66: 1222-1226.

52. Keating SC, Kerr CL, Valverde A, Johnson RJ, McDonell WN. Cardiopulmonary effects of intravenous fentanyl infusion in dogs during isoflurane anesthesia and with concurrent acepromazine or dexmedetomidine administration during anesthetic recovery. *American journal of veterinary research*. 2013;74: 672-682.

53. Seddighi R, Egger CM, Rohrbach BW, Cox SK, Doherty TJ. The effect of midazolam on the end-tidal concentration of isoflurane necessary to prevent movement in dogs. *Vet Anaesth Analg*. 2011;38: 195-202.

54. Jones DJ, Stehling LC, Zauder HL. Cardiovascular responses to diazepam and midazolam maleate in the dog. *Anesthesiology*. 1979;51: 430-434.

55. Heniff MS, Moore GP, Trout A, Cordell WH, Nelson DR. Comparison of routes of flumazenil administration to reverse midazolam-induced respiratory depression in a canine model. *Acad Emerg Med*. 1997;4: 1115-1118.

56. Bosiack AP, Mann FA, Dodam JR, Wagner-Mann CC, Branson KR. Comparison of ultrasonic Doppler flow monitor, oscillometric, and direct arterial blood pressure measurements in ill dogs. *J Vet Emerg Crit Care (San Antonio)*. 2010;20: 207-215.

57. Hou DJ, Tso DK, Davison C, Inacio J, Louis LJ, Nicolaou S, et al. Clinical utility of ultra high pitch dual source thoracic CT imaging of acute pulmonary embolism in the emergency department: Are we one step closer towards a non-gated triple rule out? *Eur J Radiol*. 2013;82: 1793-1798.

58. Saremi F, Grizzard JD, Kim RJ. Optimizing cardiac MR imaging: practical remedies for artifacts. *Radiographics : a review publication of the Radiological Society of North America, Inc*. 2008;28: 1161-1187.

59. Merin RG, Bernard JM, Doursout MF, Cohen M, Chelly JE. Comparison of the effects of isoflurane and desflurane on cardiovascular dynamics and regional blood flow in the chronically instrumented dog. *Anesthesiology*. 1991;74: 568-574.

60. Francois CJ, Fieno DS, Shors SM, Finn JP. Left ventricular mass: manual and automatic segmentation of true FISP and FLASH cine MR images in dogs and pigs. *Radiology*. 2004;230: 389-395.

61. Koren MJ, Devereux RB, Casale PN, Savage DD, Laragh JH. Relation of left ventricular mass and geometry to morbidity and mortality in uncomplicated essential hypertension. *Ann Intern Med*. 1991;114: 345-352.

62. Shors SM, Fung CW, Francois CJ, Finn JP, Fieno DS. Accurate quantification of right ventricular mass at MR imaging by using cine

true fast imaging with steady-state precession: study in dogs. *Radiology*. 2004;230: 383-388.

63. Levy D, Garrison RJ, Savage DD, Kannel WB, Castelli WP. Prognostic implications of echocardiographically determined left ventricular mass in the Framingham Heart Study. *The New England journal of medicine*. 1990;322: 1561-1566.

64. Devereux RB. Detection of left ventricular hypertrophy by M-mode echocardiography. Anatomic validation, standardization, and comparison to other methods. *Hypertension*. 1987;9: II19-26.

65. Devereux RB, Reichek N. Echocardiographic determination of left ventricular mass in man. Anatomic validation of the method. *Circulation*. 1977;55: 613-618.

66. Juergens KU, Seifarth H, Range F, Wienbeck S, Wenker M, Heindel W, et al. Automated threshold-based 3D segmentation versus short-axis planimetry for assessment of global left ventricular function with dual-source MDCT. *AJR American journal of roentgenology*. 2008;190: 308-314.

67. Fratz S, Schuhbaeck A, Buchner C, Busch R, Meierhofer C, Martinoff S, et al. Comparison of accuracy of axial slices versus short-axis slices for measuring ventricular volumes by cardiac magnetic resonance in patients with corrected tetralogy of fallot. *Am J Cardiol*. 2009;103: 1764-1769.

68. Folland ED, Parisi AF, Moynihan PF, Jones DR, Feldman CL, Tow DE. Assessment of left ventricular ejection fraction and volumes by real-time, two-dimensional echocardiography. A comparison of

cineangiographic and radionuclide techniques. *Circulation*. 1979;60: 760-766.

69. Sanz J, Conroy J, Narula J. Imaging of the right ventricle. *Cardiol Clin*. 2012;30: 189-203.

70. Sousa MG, Carareto R, De-Nardi AB, Brito FL, Nunes N, Camacho AA. Effects of isoflurane on echocardiographic parameters in healthy dogs. *Vet Anaesth Analg*. 2008;35: 185-190.

71. Hettrick DA, Pagel PS, Warltier DC. Isoflurane and halothane produce similar alterations in aortic distensibility and characteristic aortic impedance. *Anesth Analg*. 1996;83: 1166-1172.

CHAPTER 7

General discussion

With this work we have been able to demonstrate the feasibility of pulmonary, coronary and cardiac CTA and to describe achievable exam quality in normal dogs.

Pulmonary computed tomographic angiography

Evaluation for pulmonary thromboembolism or pulmonary vascular anatomy is becoming increasingly relevant in advanced companion animal care.

Scintigraphic ventilation perfusion exams have been regarded the gold standard for detection of pulmonary perfusion defects in veterinary medicine.[1] Unfortunately, these exams have somewhat limited applicability in veterinary practice due to the limited availability of the equipment and radioactive tracers, almost exclusively to academic institutions, and applicability due to the use of radioactive tracers that may require special housing for the examined patients. Therefore, relatively few studies have focused on pulmonary perfusion evaluation using scintigraphic studies in the past,[2-9] but the dog is frequently used in an experimental model, currently specifically for testing different labeling agents.[3,4]

Fluoroscopic guided pulmonary angiography is most commonly used for the evaluation and ballooning treatment of pulmonary arterial stenotic disease.[1,5-7]

The accessibility of the equipment is often limited to specialist institutions and, if performed as specific pulmonary angiography, the

invasive nature of the exam may limit the applicability in critical patients with suspected thromboembolism.

Due to the non-invasive nature and accessibility of further thoracic (and possibly abdominal) anatomy, CT exams are now commonly included in the companion animal workup. CTA can be performed either as a specific exam or in addition to standard CT exam. Our study gives the first detailed description of the normal canine pulmonary 64-MDCTA anatomy.[8] We describe a focal variation in the diameter of the right cranial pulmonary artery that should be taken into consideration when evaluating the pulmonary arteries for normalcy. A peripheral right pulmonary artery stenosis has been described in a puppy using non-selective CTA, but clinical signs of dyspnea and additional cardiac and main pulmonary artery changes were observed in this patient, whereas the dogs in our study were normal.[9]

Several studies have used the pulmonary arteries as internal reference to evaluate the lobar bronchi for normalcy in dogs and cats,[10-12] but normal pulmonary arterial size has not been described in companion animals beyond the echocardiographic measurements of the main pulmonary artery.[13,14]

In our study we are able to translate the echocardiographic measurement of the aorta to pulmonary artery diameter ratio to CTA studies,[13,14] but prediction of the corresponding measurement using echocardiography on the awake dog was not possible.[8]

Even though the discrepancy between the measurements was fairly

small, this should be considered when applying CTA exams for evaluation of the MPA and aorta. The use of anesthetic drugs and the rapidly injected contrast bolus might alter the cardiovascular status and could possibly lead to temporary alteration in vessel diameter. Prior studies report lower peak velocity across the aortic and pulmonic valve in isoflurane anesthetized dogs[15] and reduced aortic diameter using isoflurane.[16]

Alternatively, modality inherent differences of image acquisition and -generation may explain this discrepancy; such that the outline of the borders of the structures for placing the measurement might be slightly different when created by the ultrasound beam being reflected at tissues of different impedance rather than contrast medium outlining the lumen of the structure during CTA. Spatial resolution should only have had a minor impact: the MDCTA study used 1.25mm reconstructed slice thickness with 0.625mm spacing and the display field of view was set at 12cm using a 512 x 512 matrix, resulting in pixel dimensions of 0.23mm. While all CTA exams were judged diagnostic in our study, mild variations in post contrast attenuation in the main pulmonary artery occurred. High density objects such as mineral/bone or intravascular contrast medium can cause a blooming artefact especially when reviewed using a narrow window width setting and potentially lead to altered border definition.[15]

Exams in our study were reviewed using window width and level setting optimized by the examiner per subject, this could possibly be standardized in further studies.

A further reason to consider for the discrepancy would be that the echocardiographic measurements were performed by a cardiologist and the CTA measurements were performed by a radiologist. Interoperator variance may have had an impact on placing the measurements, though this effect is also considered minor as placement of measurements was discussed during study planning and echocardiographic images and measurements were reviewed by the radiologist. Yet, displaying the echocardiographic images during evaluation of the CTA exams and matching the CTA planes exactly to the plane and measurement placement yielded on echocardiographic exam may give further information on the observed discrepancy. No trend was identified in our study that would explain a systematic error between the measurements using echocardiography and CTA. Further studies evaluating the aorta to main pulmonary artery ratio as well as lobar and possibly sublobar pulmonary arterial size in a varied population of normal dogs and cats between echocardiography and CTA may be helpful to further investigate if a different ratio value may need to be used to differentiate normalcy from disease when performing pulmonary CTA.

In addition there is no value for normalcy reported for the lobar and possibly sublobar pulmonary arterial size in dogs beyond the evaluation for symmetry with veins and the radiographic measurements comparing to rib size.[17]

This could be especially helpful in detecting and grading changes relating to pulmonary hypertension associated with primary lung

disease[18] or parasitic disease.[19-21]

While our study used a standard bolus design and different reconstruction slice thickness to evaluate the detectability of main, lobar and sublobar pulmonary artery branches,[8] other studies have focused on the optimization of contrast bolus design with regards to contrast medium concentration[22] and bolus volume respective to scan duration[23] for optimal depiction of the pulmonary arteries in dogs. In addition, test bolus and bolus tracking techniques have been compared for computed tomographic angiography in normal beagles.[24] First successful reports of pulmonary CTA appear now in the veterinary literature, describing pulmonary thromboembolism using CTA in veterinary patients[25,26] as well as experimental models,[27] each study using different acquisition protocols and contrast bolus design and timing.

Defining standards for optimized CT acquisition and contrast injection / contrast enhancement parameters that can be uniformly applied will be essential to successfully implement pulmonary CTA for diagnostic workup in the companion animal patient population. This will aid to further evaluate the prevalence of pulmonary thromboembolism in veterinary patients, which is likely underdiagnosed without the use of pulmonary arterial CTA. This might be challenging compared to humans as our veterinary population markedly varies in size and will likely demand more individualized protocols compared to human patients.

Coronary artery computed tomographic angiography

Prior veterinary studies have relied on selective angiography exams to depict the coronary arteries or echocardiography to show the ostium of the coronary arteries.

Normalcy[6] and aberrant anatomy of the coronary artery anatomy[28-34] has been shown using both modalities in dogs. Also the most commonly observed anomaly involving pulmonary artery (i.e. pulmonic stenosis) concurrent with aberrant right coronary artery anatomy is usually evaluated using specific angiography under fluoroscopic guidance, often with sequential ballooning procedure.[33,35-38] The canine model has been used for investigation of experimental coronary artery stenosis using CTA, yet mostly with the focus on myocardial perfusion defects rather than depiction of the coronary anatomy.[39-41]

In our studies we were able to demonstrate feasibility of depiction of the normal canine coronary arteries and provide the first detailed description of the canine coronary anatomy using CTA.[42,43] Even though the canine coronary arteries are smaller compared to these vessels in adult human patients and the heart rate achieved with the given anesthetic protocols did not reach the recommended target heart rate < 65bpm, the canine coronary arteries were easily localized in our study.

Predominant artefact noted in our study was blur of the vessel margins. As the image resolution was optimized for the given equipment achieving 0.625mm slice thickness, this represents a limit of the achievable resolution using this modality that may need to be an

accepted limitation in future application of these studies. It may place a limitation on the utilization of CTA for depicting small luminal stenosis or endothelial irregularities especially in the more distal portions of the vessels but based on our current work this should not interfere with anatomical localization of the vessels as needed to determine aberrant anatomy. From a practical standpoint this concept will be important when reconstructing the studies to set the DFOV around the anatomy in question (i.e. the heart) to minimize pixel dimensions.

Iterative reconstruction algorithms now become available on MDCT equipment and can help to reduce image noise which may possibly address the encountered blur artefact.[44] Iterative reconstruction algorithms are also being evaluated to achieve reduced dose[45] and reduce dose of iodine needed,[46] which could find application in veterinary patients.

Vasodilators are routinely used in human patients especially in the evaluation of obstructive coronary artery disease to allow for optimal depiction of the coronary arteries.[47-49]

Our study demonstrated no difference in the detection of the coronary artery segment length or diameter using nitroprusside and good anatomical depiction was achieved without the use of a vasodilator.[42] In fact, hypotension was produced when using nitroprusside and as importance for coronary imaging in dogs will likely lie in the depiction of the anatomy rather than assessing luminal patency compared to

humans,[50,51] the use of vasodilators may likely be omitted as done for our second study population.

Motion artefact is an important factor that can result in non-diagnostic studies and therefore a regular heart rate as well as down-regulation of the heart to 65pbm is utilized in human patients. The concept of heart rate regulation was central to this work and different anesthetic protocols were utilized, neither consistently achieving the target heart rate that is lower than normal physiological canine heart rate.
Motion artefact was commonly seen in our study and it was concluded that this relates to the higher heart rate in our study subjects over the recommended 65bpm. Motion of the heart can lead to blurring of vessel margins. Therefore, the optimal interval of the cardiac cycle is selected to evaluate the specific coronary artery segments; our study has shown that overall the late diastolic phase is generating the images with least motion yet there are differences between the exact interval used for the segments but also between individual dogs. Using this optimal selection minimized motion induced blur such that main occurrence of blur was attributed to limits of spatial resolution as indicated above. Retrospectively gated studies allow for reconstruction and review of the entire cardiac cycle and may be indicated to perform until more experience on predictable diagnostic quality depiction of the coronary arteries is established in clinical patients on the expense of a higher radiation dose used. The prospectively gated technique acquires images only in preselected cardiac cycle intervals, usually including less than a

quarter of the cardiac cycle and may be prone to introduce more motion induced blur compared to the retrospectively gated method.
For the purpose of our studies the motion artefact did however not interfere with the anatomical localization of the vessels making the coronary CTA a feasible exam especially in the workup of breeds prone to aberrant coronary arteries relating to pulmonic stenosis[30,31] We speculate that, similar as in pediatric medicine, the excursion of the heart due to motion is lower at higher heart rate compared to a heart rate just above the recommended 65bpm, hence diagnostic quality study quality was achieved.[52,53] This is essential in further implementation of this technique, that with CT equipment used similar as in this study anesthetic or sedative protocols tailored to the patients needs are likely adequate rather than targeted lowering of the heart rate. Arrhythmias were not observed in our study population and would be expected to have a possibly detrimental effect on study quality if present in clinical patients; hence anti-dysrhythmic medication may be indicated but further studies are needed to assess this in clinical patients.

In human patients motion artefact is a major factor to impact the diagnostic accuracy of cardiac computed tomographic coronary angiography and motion correction algorithms are investigated to remedy affected segments for evaluation.[54]
In addition to the heart rate, regular heart rhythm is important to allow for optimal image acquisition as irregular heart rhythm can interfere with the gating software and produce motion artefact on the images.

Class II or IV antidysrythmic medications such as beta-blocker or calcium channel blocker are commonly administered in humans prior to coronary CTA to reduce and regulate heart rate but may also have contraindications in certain patients.[55,56]

The dogs in our first study population[42] showed no arrhythmias or rapid changes in heart rate during the anesthesia whilst receiving esmolol, a class II beta blocker. In our second study population[43] no beta blocker was used but focus was laid on reduction of heart rate by means of the anesthesia protocols. Where the heart rate was overall lower compared to our first study and no specific arrhythmias were observed, there was variation in heart rate seen during the overall anesthesia as well as image acquisition time. One dog specifically showed rapid increase of the heart rate immediately after contrast bolus injection. Especially any effect of the contrast medium injection may have been obscured by the use of the beta blocker in the first study population. Overall incidence of contrast reactions in dogs undergoing CT examinations is low[57] but changes in heart rate and blood pressure have been reported using iodinated contrast media in dogs.[58]

Even though without the use of antidysrythmic medication diagnostic study quality was achieved in all study subjects, these agents may be a consideration in patients with known arrhythmias or to possibly avoid rapid changes in heart rate from the effects of contrast media.

Veterinary patients will need to be sedated or anesthetized to undergo the coronary CTA exam to allow for compliance for positioning on the

CT table during the exam. It would be the logical consequence to adjust the anesthetic or sedative protocol to optimize image quality by reducing and regulating the heart rate. It may not be physiologically feasible to reduce the heart rate to <65bpm in dogs as this lays below the normal range for canine heart rate, especially in dogs with thoracic cardiovascular disease. Yet based on our study results diagnostic exams can be expected to succeed even at higher heart rate.

We did not find a significant difference using the two study protocols[43] with regards to image quality and heart rate between the protocols yet the blood pressure was higher using protocol B involving dexmedetomedine. Anesthetic protocols tailored to the individual patients needs aiming for lower heart rate without necessarily achieving the recommended <65bpm are likely feasible to achieve diagnostic coronary CTA exams in patients with suspicion for aberrant coronary arteries, if similar CT equipment and protocols are used. Applying coronary CTA in affected patients will be helpful to evaluate the impact of this diagnostic tool on patient care and further disease definition. Especially as with specific contrast bolus design such as for a triple rule out study the left and right heart as well as the pulmonary and systemic thoracic arterial system can be depicted, further understanding of the anatomic changes associated with aberrant coronary artery conformation may be generated.

Cardiac computed tomographic angiography

In the final part of the thesis, planar and volumetric cardiac measurements were analyzed using two different anesthetic protocols for ECG gated cardiac CTA.[59] These measurements are currently most commonly generated in the awake companion animal patient using echocardiography, but especially in the workup of congenital but also acquired heart disease the application of CTA may aid advanced patient care and understanding of disease processes and surgical planning.

The standard planar and volumetric cardiac measurements used in echocardiography were easily adapted for the CTA exams. Where as in echocardiography several individual image planes are recorded and some measurements can already be acquired while the patient is examined, the necessary CT image planes are reconstructed on a workstation by the evaluator after the CT exam has been completed. It is therefore important to ensure that the exam is of diagnostic quality while the patient is still in CT, such that repeat exams could be performed if needed. In our study population mild motion artefact was seen during systole but this did not interfere with application of the measurements and may be expected at the achieved heart rates between 66 – 98.6bpm with both anesthetic protocols used. Also, no difference was found using either of the two applied anesthetic protocols for the generated planar and volumetric measurements. There was however very limited predictability of the values generated from comparable measurements using echocardiography; only left

ventricular end diastolic volume using protocol B (dexmedetomidine) was comparable to the value generated using awake echocardiographic exam.

The reason for this may be multifactorial, the most impactful likely being the anesthetized state of the dogs altering cardiac function and with that possibly also likely the given cyclic morphology (i.e. wall thickness measurements) for CTA compared to the awake state for echocardiography. Other factors to take into consideration are the rapidly injected contrast bolus and differences of image acquisition or volume calculation inherent to the modalities. Especially comparing to the volumetric measurements for echocardiography where a calculation for estimations are used,[60,61] CTA provides a more direct measurement with less of an estimative factor.

A recent study has attempted to use non-ECG gated CT measurements for comparison to echocardiographic measurements.[62] Only equivalence between the measurements of the aortic annulus was seen between echocardiographic and non-ECG gated CT exam whereas the other measurements could not be translated. The results of this study support the need for advanced CT equipment with ECG gating to produce relevant cardiac CTA exams.

64-MDCT dual source cardiac CTA exams were compared to echocardiographic measurements in normal dogs in a study by Park et al 2012.[63] The dogs in this study underwent awake echocardiography and then were anesthetized for repeat echocardiogram and CTA using medetomedine for induction and isoflurane maintenance for both

exams. Planar measurements similar to our study were applied to the CTA as well as the two echocardiographic exams. Overall no significant differences were found between the results from measurements of the awake and anesthetized echocardiogram as well as anesthetized echocardiogram and CTA. Only the interventricular septal thickness and left ventricular posterior wall thickness did not fall within the 95% confidence interval when comparing anesthetized echocardiographic and CTA results. The authors speculate that this difference was possibly due to the image plane acquired using echocardiography, that may have included papillary muscles or chordae tendinae, were as the CT images provided high quality images with minimal motion artefact. In our study we found poor predictability of the echocardiographic measurements acquired in the awake dogs compared to the CTA measurements acquired in the anesthetized dogs using both anesthetic protocols. The difference in the results may be explained by the use of the different anesthetic protocols in our study. In addition, in the study by Park et al[63] the CTA planes were generated based on the echocardiographic image in the same study subject, which might have allowed for more identical placement of the measurements between both studies. In our study the echocardiographic images were not used to align the CTA planes but the cardiac MRI images were used for alignment for the CTA image planes. This might further explain the difference between awake echocardiogram and anesthetized CTA results in our study.

Further studies applying planar measurements in veterinary patients with cardiac disease using possibly also different anesthetic protocols will be needed to assess impact on patient care and disease understanding. Exploration of the translatability of anesthetized or sedated CTA results to echocardiographic measurements in the awake patient will be relevant for implementation of these exams in veterinary patients.

Left ventricular function has been studied using cardiac CTA in comparison to echocardiography as well as MRI based measurements of left ventricular function using an anesthetic protocol of levomethadon, diazepam and propofol for induction and isoflurane for maintenance of anesthesia. The study comparing cardiac CTA and echocardiography, both acquired in anesthetized dogs, found good correlation of the assessed parameters of ESV, EDV and EF.[64] It is difficult to compare these results to our study as the echocardiogram was performed in awake dogs in our study, representing the typical clinical situation, where the dogs were anesthetized in the study by Henjes et al.[64] Despite the different anesthetic protocol used in the study by Henjes et al[64] overall comparable results with regards to the CT analysis in our study. A further study comparing cardiac CT and cardiac MRI showed similar variables for both left ventricular volume and function parameters,[65] similar as reported in our study. This study used again the same anesthetic protocol as described above. Additional research from the same group quantified right ventricular volume in

dogs comparing three-dimensional echocardiography and computed tomography to magnetic resonance imaging as a reference standard in anesthetized dogs. The anesthetic protocol used included again levomethadon, diazepam and propofol for induction and isoflurane was used for maintenance of anesthesia. In this study cardiac computed tomography overestimated and echocardiography underestimated right ventricular volume compared to the values generated using MRI.[66] Our study did not include right ventricular volume estimation using echocardiography but compared CT and MRI generated right ventricular end systolic and – diastolic volumes as well as stroke volume and ejection fraction. No predictable trend of overestimation of the right ventricular volume using CT with either of the protocols nor difference between anesthetic protocols and modality was found in our study. Therefore, the overestimation of right ventricular volume as described by Sieslack et al[66] may not be translatable at this time but further investigation of the discrepancy between the studies may be needed. The discrepancy to our results could relate to different anesthetic protocols used or different evaluation software and methods used. In addition, tracing the outline of the right ventricular endocardial border is more challenging than the left ventricular endocardial border due to presence of the moderator bands and trabeculae and no standards for evaluation of the right ventricular volume using cross sectional modality exams have been established in dogs.

Further correlation of planar and volumetric measurements in patients with cardiac disease using echocardiography and cardiac CTA will be helpful to determine if the discrepancy we saw between awake echocardiogram and anesthetized CTA is a persistent finding or specific to our study conditions, or if the use of different anesthetic or sedative protocols can minimize this difference to ease translatability between the modalities.

Reports of non-gated MDCTA for patients with structural cardiac or thoracic vascular disease such as pericardial effusion or congenital abnormalities appear in the literature,[67-69] yet systematic analyses of cardiac CTA for specific cardiac diseases and especially for assessment of cardiac function in veterinary patients are to be generated in future studies.

We conclude that we have been able to produce substantial baseline data for use of pulmonary, coronary and cardiac CTA in dogs. Further application of the MDCTA techniques in companion animal patients with comparison to current standard imaging modalities used will determine utility of MDCTA in veterinary medicine.

References

1. Koblik P, Hornof, W, Harnagel S, Fisher, PA comparison of pulmonary angiography, digital subtraction angiography, and 99mTc-DTPAM/AA ventilation-perfusion scintigraphy for detection of experimental pulmonary emboli in the dog. *Veterinary Radiology* 1989;30:159-168.

2. Liska WD, Poteet BA. Pulmonary embolism associated with canine total hip replacement. *Vet Surg* 2003;32:178-186.

3. Ji S, Fang W, Dong N, et al. Detection of thromboembolism with (9)(9)mTc-labeled F(ab)(2) fragment of anti-glycoprotein IIIa chimeric monoclonal antibody in beagle canines. *Thrombosis research* 2012;130:703-708.

4. Morris TA, Marsh JJ, Chiles PG, et al. Single photon emission computed tomography of pulmonary emboli and venous thrombi using anti-D-dimer. *Am J Respir Crit Care Med* 2004;169:987-993.

5. Caivano D, Birettoni F, Fruganti A, et al. Transthoracic echocardiographically-guided interventional cardiac procedures in the dog. *J Vet Cardiol* 2012;14:431-444.

6. Buchanan JW. Selective angiography and angiocardiography in dogs wtih congenital cardiovascular disease. *Veterinary Radiology* 1965;6:21-39

7. Buchanan JW. Selective angiography and angiocardiography in dogs with acquired cardivascular disease. *Veterinary Radiology* 1965;6:5-20.

8. Drees R, Frydrychowicz A, Keuler NS, et al. Pulmonary angiography with 64-multidetector-row computed tomography in normal dogs. *Vet Radiol Ultrasound* 2011;52:362-367.
9. MacGregor JM, Winter MD, Keating J, et al. Peripheral pulmonary artery stenosis in a four-month-old West Highland White Terrier. *Vet Radiol Ultrasound* 2006;47:345-350.
10. Cannon MS, Wisner ER, Johnson LR, et al. Computed tomography bronchial lumen to pulmonary artery diameter ratio in dogs without clinical pulmonary disease. *Vet Radiol Ultrasound* 2009;50:622-624.
11. Reid LE, Dillon AR, Hathcock JT, et al. High-resolution computed tomography bronchial lumen to pulmonary artery diameter ratio in anesthetized ventilated cats with normal lungs. *Vet Radiol Ultrasound* 2012;53:34-37.
12. Szabo D, Sutherland-Smith J, Barton B, et al. Accuracy of a computed tomography bronchial wall thickness to pulmonary artery diameter ratio for assessing bronchial wall thickening in dogs. *Vet Radiol Ultrasound* 2015;56:264-271.
13. Boon JA. Manual of Veterinary Echocardiography. In, 2nd edition ed Wiley & Blackwell; 2011:153ff.
14. Bussadori C, DeMadron E, Santilli RA, et al. Balloon valvuloplasty in 30 dogs with pulmonic stenosis: effect of valve morphology and annular size on initial and 1-year outcome. J *Vet Intern Med* 2001;15:553-558.
15. Sousa MG, Carareto R, De-Nardi AB, et al. Effects of isoflurane on echocardiographic parameters in healthy dogs. *Vet Anaesth Analg* 2008;35:185-190.

16. Hettrick DA, Pagel PS, Warltier DC. Isoflurane and halothane produce similar alterations in aortic distensibility and characteristic aortic impedance. *Anesth Analg* 1996;83:1166-1172.

17. Oui H, Oh J, Keh S, et al. Measurements of the pulmonary vasculature on thoracic radiographs in healthy dogs compared to dogs with mitral regurgitation. *Vet Radiol Ultrasound* 2015;56:251-256.

18. Johnson VS, Corcoran BM, Wotton PR, et al. Thoracic high-resolution computed tomographic findings in dogs with canine idiopathic pulmonary fibrosis. *J Small Anim Pract* 2005;46:381-388.

19. Takahashi A, Yamada K, Kishimoto M, et al. Computed tomography (CT) observation of pulmonary emboli caused by long-term administration of ivermectin in dogs experimentally infected with heartworms. *Veterinary parasitology* 2008;155:242-248.

20. Seiler GS, Nolan TJ, Withnall E, et al. Computed tomographic changes associated with the prepatent and early patent phase of dirofilariasis in an experimentally infected dog. *Vet Radiol Ultrasound* 2010;51:136-140.

21. Dennler M, Makara M, Kranjc A, et al. Thoracic computed tomography findings in dogs experimentally infected with Angiostrongylus vasorum. *Vet Radiol Ultrasound* 2011;52:289-294.

22. Habing A, Coelho JC, Nelson N, et al. Pulmonary angiography using 16 slice multidetector computed tomography in normal dogs. *Vet Radiol Ultrasound* 2011;52:173-178.

23. Makara M, Dennler M, Kuhn K, et al. Effect of contrast medium injection duration on peak enhancement and time to peak enhancement of canine pulmonary arteries. *Vet Radiol Ultrasound* 2011;52:605-610.
24. Cassel N, Carstens A, Becker P. The comparison of bolus tracking and test bolus techniques for computed tomography thoracic angiography in healthy beagles. *J S Afr Vet Assoc* 2013;84:E1-9.
25. Ngwenyama TR, Herring JM, O'Brien M, et al. Contrast-enhanced multidetector computed tomography to diagnose pulmonary thromboembolism in an awake dog with pyothorax. *J Vet Emerg Crit Care (San Antonio)* 2014;24:731-738.
26. Goggs R, Chan DL, Benigni L, et al. Comparison of computed tomography pulmonary angiography and point-of-care tests for pulmonary thromboembolism diagnosis in dogs. *J Small Anim Pract* 2014;55:190-197.
27. Jung J, Chang J, Oh S, et al. Computed tomography angiography for evaluation of pulmonary embolism in an experimental model and heartworm infested dogs. *Vet Radiol Ultrasound* 2010;51:288-293.
28. Visser LC, Scansen BA, Schober KE. Single left coronary ostium and an anomalous prepulmonic right coronary artery in 2 dogs with congenital pulmonary valve stenosis. *J Vet Cardiol* 2013;15:161-169.
29. Waterman MI, Abbott JA. Novel coronary artery anomaly in an English Bulldog with pulmonic stenosis. *J Vet Intern Med* 2013;27:1256-1259.

30. Buchanan JW. Pathogenesis of single right coronary artery and pulmonic stenosis in English Bulldogs. *J Vet Intern Med* 2001;15:101-104.

31. Buchanan JW. Pulmonic stenosis caused by single coronary artery in dogs: four cases (1965-1984). *J Am Vet Med Assoc* 1990;196:115-120.

32. Kittleson M, Thomas W, Loyer C, et al. Single coronary artery (type R2A). *J Vet Intern Med* 1992;6:250-251.

33. Estey C. A case of valvular pulmonic stenosis and an aberrant coronary artery in a Brittany spaniel. *Can Vet J* 2011;52:541-543.

34. Minami T, Wakao Y, Buchanan J, et al. A case of pulmonic stenosis with single coronary artery in a dog. *Nihon Juigaku Zasshi* 1989;51:453-456.

35. Pereira M. SS, Copeland H., Lopez-Alvarez J., Summerfield N., Cripps P., Dukes-McEwan J. Balloon Valvuloplasty for treatment of pulmonic stenosis in English Bulldogs with an aberrant coronary artery. *J Vet Intern Med* 2010;24:354-359.

36. Johnson MS, Martin M. Results of balloon valvuloplasty in 40 dogs with pulmonic stenosis. *J Small Anim Pract* 2004;45:148-153.

37. Fonfara S, Martinez Pereira Y, Swift S, et al. Balloon valvuloplasty for treatment of pulmonic stenosis in English Bulldogs with an aberrant coronary artery. *J Vet Intern Med* 2010;24:354-359.

38. Fonfara S, Martinez Pereira Y, Dukes McEwan J. Balloon valvuloplasty for treatment of pulmonic stenosis in English Bulldogs with an aberrant coronary artery--2 years later. *J Vet Intern Med* 2011;25:771.

39. Lardo AC, Cordeiro MA, Silva C, et al. Contrast-enhanced multidetector computed tomography viability imaging after myocardial infarction: characterization of myocyte death, microvascular obstruction, and chronic scar. *Circulation* 2006;113:394-404.

40. Lautamaki R, George RT, Kitagawa K, et al. Rubidium-82 PET-CT for quantitative assessment of myocardial blood flow: validation in a canine model of coronary artery stenosis. *Eur J Nucl Med Mol Imaging* 2009;36:576-586.

41. George RT, Ichihara T, Lima JA, et al. A method for reconstructing the arterial input function during helical CT: implications for myocardial perfusion distribution imaging. *Radiology* 2010;255:396-404.

42. Drees R, Frydrychowicz A, Reeder SB, et al. 64-multidetector computed tomographic angiography of the canine coronary arteries. *Vet Radiol Ultrasound* 2011;52:507-515.

43. Drees R, Johnson RA, Pinkerton M, et al. Effects of two different anesthetic protocols on 64-MDCT coronary angiography in dogs. *Vet Radiol Ultrasound* 2015;56:46-54.

44. Naoum C, Blanke P, Leipsic J. Iterative reconstruction in cardiac CT. *J Cardiovasc Comput Tomogr* 2015;9:255-263.

45. Nakagawa M, Ozawa Y, Sakurai K, et al. Image quality at low tube voltage (70 kV) and sinogram-affirmed iterative reconstruction for computed tomography in infants with congenital heart disease. *Pediatr Radiol* 2015;45:1472-1479.

46. Qi L, Wu SY, Meinel FG, et al. Prospectively ECG-triggered high-pitch 80 kVp coronary computed tomography angiography with 30 mL of 270 mg I/mL contrast material and iterative reconstruction. *Acta Radiol* 2015, epub ahead of print.

47. Takx RA, Sucha D, Park J, et al. Sublingual Nitroglycerin Administration in Coronary Computed Tomography Angiography: a Systematic Review. *Eur Radiol* 2015, epub ahead of print.

48. Chun EJ, Lee W, Choi YH, et al. Effects of nitroglycerin on the diagnostic accuracy of electrocardiogram-gated coronary computed tomography angiography. *J Comput Assist Tomogr* 2008;32:86-92.

49. Decramer I, Vanhoenacker PK, Sarno G, et al. Effects of sublingual nitroglycerin on coronary lumen diameter and number of visualized septal branches on 64-MDCT angiography. *Am J Roentgenol* 2008;190:219-225.

50. Liu SK TL, Tappe JP, Fox PR. Clinical and pathological findings in dogs with atherosclerosis. *J Am Vet Med Assoc* 1986;189:227-232.

51. Schulma-Marcus K DI, Truong QA. State of the art updates ofn cardiac computed tomography angiogrpahy for assessing coronary artery disease. *Curr Treat Options Cardiovasc* 2015;17:398.

52. Duan X, Yu T, Wang F, et al. Anomalous origin of the left coronary artery from the pulmonary artery in infants: imaging findings and clinical implications of cardiac computed tomography. *J Comput Assist Tomogr* 2015;39:189-195.

53. Walsh R, Nielsen JC, Ko HH, et al. Imaging of congenital coronary artery anomalies. *Pediatr Radiol* 2011;41:1526-1535.

54. Carrascosa P, Deviggiano A, Capunay C, et al. Effect of intracycle motion correction algorithm on image quality and diagnostic performance of computed tomography coronary angiography in patients with suspected coronary artery disease. *Acad Radiol* 2015;22:81-86.

55. Kahn M CK, Gutierrez FR, Haalla S, Woodard PK, Saeed IM. Contraindications and side effects of commonly used medications in coronary CT. *Int J Cardiovasc Imaging* 2011;27:441-449.

56. Panny HK AWJ, Fishman EK. Beta-Blockers for cardiac CT: a primar for the radiologist. *Am J Roentgenol* 2006;186:S341-345.

57. Vance A, Nelson M, Hofmeister EH. Adverse reactions following administration of an ionic iodinated contrast media in anesthetized dogs. *J Am Anim Hosp Assoc* 2012;48:172-175.

58. Pollard RE, Puchalski SM, Pascoe PJ. Hemodynamic and serum biochemical alterations associated with intravenous administration of three types of contrast media in anesthetized dogs. *Am J Vet Res* 2008;69:1268-1273.

59. Drees R, Johnson RA, Stepien RL, et al. Quantitative Planar and Volumetric Cardiac Measurements Using 64 Mdct and 3t Mri Vs. Standard 2d and M-Mode Echocardiography: Does Anesthetic Protocol Matter? *Vet Radiol Ultrasound* 2015, epub ahead of print.

60. Stepien RL HK, Constable PD, Olson J. Effect of endurance training on cardiac morphology in Alaskan sled dogs. *J Appl Physiol* 1985;1998:1368-1375.

61. Al-Mohaissen MA, Kazmi MH, Chan KL, et al. Validation of two-dimensional methods for left atrial volume measurement: a comparison of echocardiography with cardiac computed tomography. *Echocardiography* 2013;30:1135-1142.

62. Laborda-Vidal P, Maddox TW, Navarro-Cubas X, et al. Comparison between echocardiographic and non-ECG-gated CT measurements in dogs. *Vet Rec* 2015;176:335.

63. Park N, Lee M, Lee A, et al. Comparative study of cardiac anatomic measurements obtained by echocardiography and dual-source computed tomography. *J Vet Med Sci* 2012;74:1597-1602.

64. Henjes CR, Hungerbuhler S, Bojarski IB, et al. Comparison of multi-detector row computed tomography with echocardiography for assessment of left ventricular function in healthy dogs. *Am J Vet Res* 2012;73:393-403.

65. Sieslack AK, Dziallas P, Nolte I, et al. Comparative assessment of left ventricular function variables determined via cardiac computed tomography and cardiac magnetic resonance imaging in dogs. *Am J Vet Res* 2013;74:990-998.

66. Sieslack AK, Dziallas P, Nolte I, et al. Quantification of right ventricular volume in dogs: a comparative study between three-dimensional echocardiography and computed tomography with the reference method magnetic resonance imaging. *BMC Vet Res* 2014;10:242.

67. Scollan KF, Bottorff B, Stieger-Vanegas S, et al. Use of multidetector computed tomography in the assessment of dogs with pericardial effusion. *J Vet Intern Med* 2015;29:79-87.

68. Markovic LE, Kellihan HB, Roldan-Alzate A, et al. Advanced multimodality imaging of an anomalous vessel between the ascending aorta and main pulmonary artery in a dog. J Vet Cardiol 2014;16:59-65.

69. Cuddy LC, Maisenbacher HW, Vigani A, et al. Computed tomography angiography of coarctation of the aorta in a dog. *J Vet Cardiol* 2013;15:277-281.

SUMMARY

Cardiovascular disorders are a common origin of presentation in dogs. The diagnosis of cardiovascular disorders relies mainly on traditional imaging modalities (radiography or echocardiography). Until now, thoracic CTA has found limited implementation in the diagnostic workup of companion animals while it has an enormous diagnostic potential. Additionally, advanced CT equipment allowing image acquisition at high speed and resolution and gated to the cardiac cycle is becoming available in veterinary institutions and evaluation of the feasibility and capability of thoracic CTA in companion animals is needed.

In the **first chapter**, the technical and practical aspects of thoracic cardiovascular CTA are reviewed in light of the currently available veterinary literature and future opportunities given utilizing MDCT in companion animal patients with suspected thoracic cardiovascular disease.

In the **second chapter**, the scientific aim of this work is formulated: to evaluate the feasibility of pulmonary and coronary CTA as well as functional cardiac CTA in dogs and to define the limitations and opportunities with regards to achievable image quality, also in light of anesthetic protocols and comparable diagnostic modalities used for diagnosis of cardiac disorders.

In the **third chapter**, pulmonary angiography using 64-multidetector-row computed tomography (MDCT) was used to evaluate pulmonary artery anatomy, and determine the sensitivity of pulmonary artery segment visualization in four Beagle dogs using images reconstructed to 0.625mm and retro-reconstructed to 1.25, and 2.5mm slice thickness. Morphologically, characteristic features included a physiological focal narrowing in the right cranial pulmonary artery in all dogs. While the right cranial pulmonary artery divided into two equally sized branches, only a single left cranial (cranial portion) lobar artery was present. Compared to 1.25 and 2.5mm retro-reconstructions, 0.625mm reconstructions allowed for detection of significantly ($P \leq 0.05$) more pulmonary artery segments and sharper depiction of vessel margins. Clinical applications such as prevalence and significance of diameter changes, and detection of pulmonary arterial thrombembolism on lobar and sublobar level, remain to be established.

In the **fourth chapter**, canine coronary artery angiography was performed in four anesthetized healthy dogs using 64-multidetector computed tomography (MDCT). Esmolol, a β-1 adrenergic receptor antagonist, and sodium nitroprusside, an arteriolar and venous dilator, were administered to enhance visualization of the coronary arteries by reducing heart rate and creating vasodilation. The left main coronary artery with its three main branches and the right coronary artery were visualized and subdivided in 13 segments for evaluation. Optimal reconstruction interval, expressed as percentage of the R-to-R interval,

was determined at 5% in 2.9%, 35% in 1%, 75% in 21.2%, 85% in 43.3%, and 95% in 31.7% of the segments. Overall image quality was good to excellent in 55.7%. Artifacts (blur, motion, stair step) did not interfere with anatomic depiction of the arteries. Cross sectional anatomy of the coronary arteries as evaluated from the coronary CTA agreed well with gross anatomic evaluation and published information. The use of esmolol did not lead to the target heart rate of 60 to 65 beats per minute (bpm). Nitroprusside had no significant effect on visualized length or diameter of the coronary artery branches. Coronary CTA is useful for the anatomic depiction of coronary artery branches in the dog.

In the **fifth chapter,** the effects of two different clinically applicable anesthetic protocols on cardiovascular parameters and 64-MDCTA quality on 10 healthy dogs were compared. Scan protocols and bolus volumes were standardized. Heart rate during image acquisition did not differ between protocols (P = 1), with 80.6 ± 7.5bpm for protocol A and 79.2 ± 14.2bpm for protocol B. Mean blood pressure was significantly higher (P > 0.05) using protocol B (protocol A 62.8 ± 9.1 vs protocol B 72.4 ± 15.9 mmHg). R-R intervals allowing for the best depiction of the individual coronary artery segments were found in the end diastolic period and varied between the 70-95% interval. Diagnostic quality had higher scores for more proximal segments and lower for more distal segments, respectively. No significant differences were identified between the two protocols for optimal reconstruction interval,

diagnostic quality and measured length of individual segments or proximal diameter of the coronary arteries (P = 1). Both anesthetic protocols yielded diagnostic quality coronary 64-MDCTA exams in healthy dogs.

In the **sixth chapter,** the effects of two different anesthetic protocols on cardiac measurements in 10 healthy beagle dogs using 64-MDCTA, 3T MRI and standard awake echocardiography was tested. Both anesthetic protocols used propofol for induction and isoflurane for anesthetic maintenance. In addition, protocol A used midazolam/fentanyl and protocol B used dexmedetomedine as premedication and constant rate infusion during the procedure. Significant elevations in systolic and mean blood pressure were present when using protocol B. There was overall good agreement between the variables of cardiac size and systolic function generated from the MDCTA and MRI exams and no significant difference was found when comparing the variables acquired using either anesthetic protocol within each modality. Systolic function variables generated using 64-MDCTA and 3T MRI were only able to predict the left ventricular end diastolic volume as measured during awake echocardiogram when using protocol B and 64-MDCTA. For all other systolic function variables, prediction of awake echocardiographic results was not possible (P = 1). Planar variables acquired using MDCTA or MRI did not allow prediction of the corresponding measurements generated using echocardiography in the awake patients (P=1).

Summary

SAMENVATTING

Cardiovasculaire aandoeningen zijn een veel voorkomende oorzaak van klachten bij honden. Het diagnostisch proces van cardiovasculaire aandoeningen maakt vooral gebruik van traditionele beeldvormingsmethoden zoals radiografie en echografie. Tot nu toe werd thorax computer tomografie angiografie (CTA) weinig gebruikt in het diagnostisch proces bij gezelschapsdieren, terwijl dit nochtans een enorm diagnostisch potentieel heeft. Bijkomend is met een gespecialiseerd systeem voor computer tomografie (CT) zeer snelle beeldacquisitie mogelijk, met een hoge resolutie en connectie met de hartcyclus. Deze systemen zijn in toenemende mate beschikbaar in diergeneeskundige instellingen, en er is duidelijk nood aan een evaluatie van de capaciteiten en de praktische haalbaarheid van thorax CTA bij gezelschapsdieren. Dit werk poogt hier een antwoord op te bieden.

In het **eerste hoofdstuk** van dit doctoraat worden de technische en praktische aspecten van thoracale cardiovasculaire CTA gekaderd in de beschikbare diergeneeskundige literatuur. Vervolgens worden de toekomstmogelijkheden voor het gebruik van multi-detector computer tomografie (MDCT) toegelicht voor wat betreft gezelschapsdieren met een vermoeden van een thoracale cardiovasculaire aandoening.

De wetenschappelijke doelstellingen van dit doctoraat worden beschreven in het **tweede hoofstuk**. De eerste doelstelling van dit

werk is het evalueren van de haalbaarheid van pulmonaire en coronale CTA en functionele cardio CTA bij honden en het definiëren van de beperkingen en mogelijkheden op het vlak van beeldkwaliteit en anesthesieprotocollen in vergelijking met gelijkaardige diagnostische modaliteiten.

In het **derde hoofdstuk** wordt pulmonaire angiografie met behulp van 64-MDCT in detail bestudeerd bij 4 beagle honden . De anatomie van de pulmonaire arterie, en de sensitiviteit van de pulmonaire arterie segmentvisualisatie worden beschreven. Hiervoor werden de beelden gereconstrueerd tot 0.625 mm en retro-gereconstrueerd tot respectievelijk 1.25 mm, en 2.5mm snededikte. Op morfologisch vlak was onder meer een karakteristieke fysiologische vernauwing van de rechter craniale pulmonaire arterie bij alle honden zichtbaar. In tegenstelling tot de rechter craniale pulmonaire arterie, die splitst in twee takken van gelijke grootte, werd telkens slechts één linker craniale lobaire arterie vastgesteld. In vergelijking met de 1.25 mm en de 2.5 mm retro-reconstructies, werden bij de 0.625 mm reconstructies significant meer ($P \leq 0.05$) pulmonaire arteriële segmenten gedetecteerd en waren de vaatwanden scherper afgetekend. Mogelijke klinische toepassingen zoals de prevalentie, oorsprong en de consequenties van diameterveranderingen, alsook de detectie van pulmonaire arteriële thromboëmbolismen op lobair en sublobair niveau zijn voorlopig nog niet gangbaar in de praktijk.

In het **vierde hoofdstuk** wordt coronaire arteriële angiografie met behulp van 64-MDCT uitgevoerd op vier gezonde, geanesthesieerde honden. Esmolol, een β-1 adrenergische receptor antagonist en sodium nitroprusside, een arteriolaire en veneuze dilatator, werden toegediend teneinde de visualisatie van coronaire arteries te verbeteren door het reduceren van de hartslag en het creëren van vasodilatatie. De linker grote coronaire arterie met drie grote takken en de rechter coronaire arterie werden ter evaluatie gevisualiseerd en onderverdeeld in 13 segmenten. Het optimale reconstructie interval, uitgedrukt als een percentage van het RR-interval ('ECG-gating'), werd vastgelegd op 5% in 2.9%, 35% in 1%, 75% in 21.2%, 85% in 43.3%, en 95% in 31.7% van de segmenten. De algemene beeldkwaliteit was goed tot uitstekend in 55.7% van de gevallen. Artefacten gaven geen interferentie met de anatomische weergave van de arteries. De cross-sectionele anatomie van de coronaire arteries uit de coronaire CTA, vertoonde een goede correlatie met de gemiddelde anatomische evaluatie en reeds gepubliceerde informatie. Het gebruik van esmolol leidde niet tot het bedoelde hartritme van 60-65 slagen per minuut (bpm). Nitroprusside had geen significant effect op de lengte of diameter van de coronaire arteriële takken. De resultaten van deze studie tonen aan dat coronaire CTA van nut is voor de anatomische weergave van de coronaire arteriële takken bij de hond.

In het **vijfde hoofdstuk** worden de effecten van twee verschillende anesthesieprotocollen voor cardiovasculaire parameters en 64-MDCTA

kwaliteit vergeleken bij 10 gezonde honden. Scanprotocollen en bolusvolumes werden tijdens het onderzoek gestandaardiseerd. Er was geen verschil in hartritme tijdens de beeldacquisitie tussen de protocollen (P = 1), met 80.6 ± 7.5bpm voor protocol A en 79.2 ± 14.2bpm voor protocol B. De gemiddelde bloeddruk was significant hoger (P<0.05) bij protocol B (protocol A: 62.8 ± 9.1 vs protocol B: 72.4 ± 15.9 mmHg). RR-intervals voor de beste visualisatie van de individuele coronaire arteriële segmenten was in de eind diastolische fase en varieerden tussen het 70-95% interval. De diagnostische kwaliteit bleek hoger voor de proximale segmenten en lager voor de distale segmenten. Geen significante verschillen werden gevonden tussen de twee protocollen voor het optimaal reconstructie interval, de diagnostische kwaliteit en de gemeten lengte van de individuele segmenten of de proximale diameter van de coronaire arteries (P = 1). Beide anesthesieprotocollen leverden diagnostisch kwaliteitsvolle coronaire 64-MDCTA onderzoeken op bij gezonde honden.

In het **zesde hoofdstuk** worden de effecten van twee verschillende anesthesieprotocollen op hartmetingen met behulp van 64-MDCTA, 3T MRI en standaard echocardiografie bij tien gezonde Beagle honden in wakkere toestand getest. Beide anesthesieprotocollen gebruikten propofol voor de inductie en isofluraan voor het onderhouden van de anesthesie. Bijkomend gebruikte protocol A midazolam/fentanyl en protocol B dexmedetomedine als premedicatie en continu infuus tijdens de procedure. Significante verhogingen in de systolische en gemiddelde

bloeddruk waren merkbaar tijdens protocol B. Over het algemeen was er een goede overeenkomst tussen de hartvariabelen en de systolische functie gegenereerd door MDCTA en MRI onderzoeken. Er werd geen significant verschil gevonden bij het vergelijken van variabelen die voorkwamen bij beide protocollen binnen elke modaliteit. Systolische functionele variabelen verkregen door 64-MDCTA en 3T MRI waren enkel voorspellend voor het linker ventriculair eind diastolisch volume zoals gemeten tijdens de echografie in wakkere toestand met protocol B. Voor de overige systolische functies was een voorspelling van de resultaten van de echografie in wakkere toestand niet mogelijk (P=1). Planaire variabelen verkregen door MDCTA of MRI lieten geen voorspelling toe van de corresponderende metingen die gegenereerd werden bij de echografie in wakkere toestand (P=1).

CURRICULUM VITAE

Curriculum vitae

Randi Drees was born on December 2nd, 1975, in Überlingen, Germany. She studied veterinary medicine at the Freie Universität Berlin from 1995 to 2001. Supported by a two year stipend of the Sonnenfeld Stiftung Berlin she pursued her thesis with the title 'Peripheral washout sign in coloncarcinoma CC531 in rats in a collaboration with the Institut für Veterinäranatomie of Fachbereich Veterinärmedizin at the Freie Universität Berlin and the Institute for Radiologie Campus Charité Mitte at the Humboldt Universität zu Berlin, completed in 2005. After two years in private practice Randi moved to the United States in 2005 to pursue a four-year residency with the American College of Veterinary Radiology and the European College of Diagnostic Imaging at the University of Wisconsin-Madison, becoming board certified with both colleges in 2008. Randi then pursued an alternative residency in Veterinary Radiation Oncology with the American College of Veterinary Radiology also at University of Wisconsin-Madison, becoming board certified in 2012. Randi stayed on at University of Wisconsin-Madison's Veterinary Medicine Teaching Hospital as a clinical instructor and then assistant professor in Diagnostic Imaging and Radiation Oncology, eventually becoming section head of the Diagnostic Imaging section. In 2013 Randi relocated to the United Kingdom to take up a senior lectureship at the Royal Veterinary Colleges Queen Mother Hospital for Small Animals where she now serves as head of the Diagnostic Imaging Service.

Her special interests lay in cross-sectional imaging focussing on vascular and oncological applications.

Curriculum vitae

Randi Drees is author or co-author of many scientific publications in international journals and book chapters and an active as speaker at national or international veterinary scientific and educational events.

Publications

1. Snyder CJ, Soukup JW, Drees R, Tabone TJ. Caudal mandibular bone height and buccal cortical bone thickness measured by computed tomography in healthy dogs. Vet Surg. 2015;18 – epub ahead of print
2. Fenn J, Drees R, Volk HA, Decker S. Inter- and intraobserver agreement for diagnosing presumptive ischemic myelopathy and acute noncompressive nucleus pulpous extrusion in dogs using magnetic resonance imaging. Vet Radiol Ultrasound. 2015;25 – epub ahead of print
3. Drees R, Johnson RA, Stepien RL, Munoz Del Rio A, Saunders JH, François CJ. Quantitative planar and volumetric cardiac measurement using 64 MDCT and 3T MRI vs standard 2D and M-Mode echocardiography: does anesthetic protocol matter? Vet Radiol Ultrasound. 2015;56(6), 638-57.
4. Soukup JW, Drees R, Koenig LJ, Snyder CJ, Hetzel S, Miles CR, Schwarz T. Comparison of the diagnostic image quality of the canine maxillary dentoalveolar structures obtained by cone beam computed tomography and 64-multidetector row computed tomography. J Vet Dent. 2015;32(2):80-6.
5. Peek A, Pinkerton M, Bentley E, Drees R Cavernous Sinus Syndrome in a Holstein Bull. Vet Opthalmol. 2015;18(2):164-7.
6. Oliveira CR, Henzler MA, Johnson RA, Drees, R. Assessment of respiration-induced displacement of canine abdominal organs in

dorsal and ventral recumbency using multislice computed tomography. Vet Radiol Ultrasound. 2015;56(2):133-43.

7. Drees R, Johnson R, Francois C, Saunders J. Effects of two different anesthetic protocols on cardiac flow measured by two dimensional phase contrast MRI. Vet Radiol Ultrasound. 2015;56(2):168-75.
8. Drees R, Johnson R, Francois C, Saunders J. Effects of two different anesthetic protocols on 64-MDCT coronary angiography in dogs. Vet Radiol Ultrasound. 2015;56(1):46-54.
9. Bell L, Johnson K, Fain S, Wentland D, Drees R, Johnson R, Baumann G, Francois C, Nagle SK. Simultaneous MRI of Lung Structure and Perfusion in a single Breathhold. J Magn Reson Imaging. 2015;41(1):52-9.
10. Nevitt BN, Langan JN, Adkesson MJ, Mitchell MA, Henzler M, Drees R.Comparison of air sac volume, lung volume and lung densities determined by use of computed tomography in conscious and anesthetized Humboldt penguins (Spheniscus humboldti) positioned in ventral, dorsal and right lateral recumbency. Am J Vet Res. 2014;75(8):739-45.
11. Budgeon C, Mans C, Stein J, Drees R, Robat C, Pinkerton M, Tamara Chamberlin T, McAnulty JF, Imai DM. Malignant trichoepithelioma of the ear canal in a pet rabbit (Oryctolagus cuniculus). J Am Vet Med Assoc 2014;15;245(2):227-31.
12. Drees R, Francois C, Saunders J. Invited Review: Computed tomographic Angiography (CTA) of the thoracic cardiovascular

system in companion animals. Vet Radiol Ultrasound. 2014;55(3):229-40.

13. Darrow BG, Mans C, Drees R, Schwarz T, Pinkertion ME, Sladky KK.Pulmonary blastomycosis in a domestic ferret (mustela putorius furo). J Exotic Pet Med, 2014;23, Issue 2, 158–64.
14. Markovic LE, Kellihan HB, Roldán-Alzate A, Drees R, Bjorling DE, Francois CJ. Advanced multimodality imaging of an anomalous vessel between the ascending aorta and main pulmonary artery in a dog. J Vet Cardiol. 2014;16(1):59-65.
15. Imai DM, Miller JL, Leonard BC, Bach JF, Drees R, Steinberg H, Teixiera LBC. Visceral leiomyopathy associated with intestinal pseudo-obstruction in a Bengal cat (Felix catus x Prionailurus bengalensis). Vet Pathol epub ahead of print
16. Rossi F, Caleri E, Bacci B, Drees R, Groth A, Hammond G, Vignoli M, Schwarz T. CT features of basihyoid ectopic thyroid carcinoma in dogs. Vet Radiol Ultrasound. 2013;54(6), 575-81.
17. Mans C, Drees R, Sladky KK, Hatt JM, Kircher PR. Effects of body position and extension of the neck and extremities on lung volume measured via computed tomography in red-eared slider turtles (Trachemys scripta elegans). J Am Vet Med Assoc. 2013;15;243(8):1190-6.
18. Hoey S, Keller D, Chamberlin T, Pinkerton M, Waller K, Drees RP. Pulmonary-tracheobronchial prolapse in a new Caledonian giant gecko (Rhadocodactylus Leachianus). Vet Radiol Ultrasound. 2013; 54(6), 630-3.

19. Hoey S, Drees R, Hetzel S. Evaluation of the gastrointestinal tract in dogs using computed tomography. Vet Radiol Ultrasound. 2013;54(1):25-30.
20. Sumner JP, Hardie RJ, Henningson JN, Drees R, Markel MD, Bjorling D. Evaluation submucosally injected polyethylene glycol-based hydrogel and bovine cross–linked collagen in the canine urethra using cystoscopy, magnetic resonance imaging and histopathology. J Vet Surg. 2012;41(6):655-63.
21. Rodriguez-Ramos Fernandez J, Thomas NJ, Dubielzig RR, Drees R Osteosarcoma of the maxilla with concurrent osteoma in a southern sea otter (Enhydra lutris nereis). J Vet Comp Pathol. 201;147(2-3):391-6.
22. Sim RS, Pinkerton ME, Naranjo C, Drees R, Rodriguez-Ramos Fernandez J, Sanchez-Migallon Guzman D. Hepatocellular carcinoma in a black-tailed prairie dog (Cynomys ludivicans) Consulta Veterinary. Journal, Special, 2011;403-6.
23. Sander W, Sanchez-Migallon Guzman D, Keller D, Danielson D, Rodriguez-Ramos Fernandez J, Drees R, Naranjo C, Webb JL. Surgical amputation of a forelimb osteosarcoma in a domestic ferret (Mustela putorius). Consulta Veterinary Journal. 2011;413-417.
24. Drees R, Frydrychowicz AP, Reeder SB, Pinkerton ME, Johnson R. 64 Slice Multi-detector Computed Tomographic Angiography of the Canine Coronary Arteries. Vet Radiol Ultrasound. 201;52(5):507-515.

25. Drees R, Frydrychowicz AP, Keuler N, Reeder SB, Johnson R. Pulmonary Angiography with 64 slice multidetector computed tomography (MDCT) in dogs: Pulmonary arterial anatomy and sensitivity of artery visualization. Vet Radiol Ultrasound. 2011;52(4):362-7.
26. Drees R, Perrier M, Vetter JR, Brounts S, Schwarz T. Magnification Radiography in the horse to blur our superimposed structures Wien. Tierärztl. Mschr. - Vet Med Austria. 2011;98,160–5.
27. Rodriguez-Ramos Fernandez J, Pinkerton ME, Heisey, DM, Drees R, Schneider J, Stickney L, Hofmeister EK, Sanchez-Migallon Guzman Elodontomas in captive red-backed voles (Myodes gapperi) J Zoo Wildlife Med. 2010.41(3):555-61.
28. Saam DE, Drees R, Gonzalez OD. What's your diagnosis? Chondrosarcoma in a dog. J Am Vet Med Assoc 2010;327(1):33-4.
29. Dennison SE, Drees R, Rylander H, Pettigrew R, Milovancev M, Keuler NS, Schwarz T. Comparison of conventional myelography, survey-, intravenously and intrathecally contrast-enhanced computed tomography in dogs with suspected cervical and thoracolumbar spinal cord compression. Vet Radiol & Ultrasound 2010;51:254-8.
30. Rao D, Rylander H, Drees R, Schwarz T, Steinberg H. Granular cell tumor in a lumbar spinal nerve of a dog. J Vet Diag Investi. 2010;22:4.

31. Drees R, Forrest LJ, Chappell R. Comparison of computed tomography and magnetic resonance imaging for the evaluation of canine intranasal neoplasia. J Small Anim Pract 2009;50:1-7.
32. Koch C, Drees R, Hartmann F, McGuirk S, Prichard MA. Nocardia arthriditis infection in the distal metaphysis of the metatarsal bone III and IV of a heifer J Am Vet Med Assoc. 2009;234:669-673.
33. Drees R, Dennison SE, Keuler NS, Schwarz T. Computed tomographic imaging protocol for the canine cervical and lumbar spine. Vet Radiol Ultrasound 2009;50:74-9.
34. Drees R, Hünigen H, Wagner S, Schnorr J, Plendl J, Taupitz M. Peripheral washout phenomenon in and animal tumor model: comparison of dynamic magnetic resonance imaging using a small molecular contrast medium with histology Vet Comp Oncol 2008;6:151-61.
35. Schnorr J, Wagner S, Abramjuk C, Drees R, Schink T, Schellenberger E, Pilgrim H, Hamm B, Taupitz M. Focal liver lesions: SPIO-, Gadolinium-, and Ferucarbotran-enhanced dynamic T1-weighted and delayed T2-weighted MR imaging in rabbits. Radiology. 2006;240:90-100.

Oral presentations at national or international meetings

1. Drees R, Johnson RA, Stepien RL, Munoz Del Rio A, Saunders JH, Francois CJ. (2013) Comparison of two different anesthetic protocols for two-dimensional cardiac measurements using 64

MDCT and 3T magnetic resonance imaging. ACVR Annual scientific conference, Savannah, GA, October 2013.

2. Drees R, Johnson RA, Stepien RL, Munoz Del Rio A, Saunders JH, Francois CJ. (2013) Comparison of two different anesthetic protocols for volumetric cardiac function measurements using 64 MDCT and 3T magnetic resonance imagingECVDI Annual scientific conference, Cascais, Portugal, September 2013..
3. Oliveira CR, Drees R, Henzler MA. (2012) Assessment of respiratory induced displacement of canine abdominal structures in dorsal versus ventral recumbency using computed tomographic imaging.ACVR Annual scientific conference, Las Vegas, NV, October 18-21, 2012.
4. Stein JE, Drees R. (2012) Computed tomographic features of presumptively normal abdominal lymph nodes in dogs. ACVR Annual scientific conference, Las Vegas, NV, October 18-21, 2012.
5. Hoey S, Drees R, Yu X. (2011) Evaluating gastrointestinal wall thickness and diameter in normal dogs using computed tomography. EVDI Annual Scientific Conference, London, UK, August 30-31, 2011.
6. Schwarz T, Pot S, Bentley E, Marques AIC, Smith S, Drees R. (2011) Diagnostic imaging features of canine infraorbital cysts. EVDI Annual Scientific Conference, London, UK, August 30-31, 2011.
7. Mans C, Drees R, Sladky KK, Hatt JM, Kircher PR. (2011) Effect of body position, leg and neck extension, and sedation on lung volume in red-eared slider turtles (Trachemys scripta elegans). 43nd

Annual Conference of the American Association of Zoo Veterinarians (AAZV). Kansas City, MO, October 23-28, 2011.

8. Drees R, Frydrychowicz AP, Reeder SB, Pinkerton ME, Johnson R .(2010) Imaging of the Coronary Arteries Using 64-Slice MDCT Angiography in the dog Annual ScientificMeeting of the American College of Veterinary Radiology, Asheville, NC, USA, August 15-19, 2010.
9. Clapp SK, Drees, R. (2010) Measurement of normal canine Adrenal Gland size on transverse plane in CT Annual ScientificMeetng of the American College of Veterinary Radiology, Asheville, NC, USA, August 15-19, 2010.
10. Drees, R, Frydrychowicz AP, Keuler, NK, Reeder SB, Johnson, R. (2010) Pulmonary Angiography with 64-slice MDCT in dogs: Pulmonary Arterial Anatomy and Sensitivity of Artery Visualization 16th EVDI annual conference, Giessen, Germany, July 20-24, 2010.
11. Drees, R, Frydrychowicz AP, Reeder SB, Pinkerton ME, Johnson R. (2010) Canine Coronary Artery Angiography using 64-slice MDCT 16th EVDI annual conference, Giessen, Germany, July 20-24, 2010.
12. Drees, R, Pot S, Bentley E, Schwarz T. (2010) Diagnostic imaging features of cystic lesions associated with the nasolacrimal system in five dogs. ECVO Annual Scientific Meeting, Berlin, Germany, May 27-29, 2010.
13. Drees R, Perrier M, Brounts S, Schwarz T. (2009) Magnification Radiography in large animal patients 15th Congress of the IVRA, Buzios, RJ, Brazil, July 26-31, 2009

14. Drees R, Dennison SE, Keuler NS, Schwarz T. (2008) Computed tomographic imaging protocol for the canine cervical and lumbar spine. 15th EAVDI / EVDI annual scientific conference, Svolvær, Norway, August 6-9, 2008.
15. Drees R, Dennison S, Schwarz T. (2007) Establishment of a computed tomographic protocol for the canine cervical and lumbar spine. ACVR annual scientific conference, Chicago, Il, USA, November 27 – December 1, 2007.
16. Drees R, Forrest LJ, Chappell R. (2007) Comparison of pre and post contrast computed tomography and magnetic resonance imaging for the evaluation of canine nasal neoplasia. ACVR annual scientific conference, Chicago, Il, USA, November 27 – December 1, 2007.
17. Drees R, Hünigen H, Wagner S, Schnorr J, Plendl J, Taupitz M. (2005) Peripheral washout sign in colon carcinoma CC531 in rats: introduction of an animal model by magnetic resonance imaging and histology. ACVR annual scientific conference, Chicago, Il, USA, November 29 – December 3, 2005.
18. Drees R, Schnorr J, Plendl J, Hünigen H. (2004) Peripheral washout in a malignant rat tumor model Annual Meeting of the German Society for Microcirculation and Vascular Biology, Berlin, Germany, October 7-9, 2004.
19. Hünigen H, Bisplinghoff P, Plendl J, Drees R, Schnorr J (2004). Physiologische und pathologische Angiogenese: Gelbkörperanbildung und Tumorwachstum im Vergleich (Physiological and pathological angiogenesis: Comparison of

development of corpus luteum and tumor growth). 15. Symposium Fachgruppe Physiologie und Biochemie der Deutschen Veterinärmedizinischen Gesellschaft, Berlin, Germany, March 2004.

20. Hünigen H, Drees R, Schnorr J, Plendl J. (2004) Angiogenesis and interstitial pressure in a rat tumour model. 25. Congress of the European Association of Veterinary Anatomists, Oslo, Norway, July 28-31st, 2004.

THANK YOU NOTE

Even though I pursued this work as a primary author, none of this would have been possible without the help of the many inspirational individuals who I am very humbled to have worked alongside in the past years.

First I would like to thank Jimmy Saunders as promoter of my thesis who sparked the first curiosity in pursuing my research interest in this topic in form of a PhD thesis. Jimmy has provided extremely insightful mentoring to me throughout this work as well as in the wider ECVDI framework that I am very grateful for.

At the School of Medicine and Public health at the University of Wisconsin-Madison I would like to thank in chronological order the following individuals: Scott Reeder for being receptive to the veterinarian knocking at his door and helping me in the first phase of the research project. Scott introduced me to Alex Frydrychowicz, who taught me to navigate the first canine coronaries I had ever seen on a CTA exam and provided essential input for the first two original manuscripts; writing research publications has become so much easier utilizing the wisdom I have gleamed from him. Alejandro Munoz del Rio who was able to help tame the statistical beast with outstanding expertise and a good sense of humor; and through whom I have discovered a new level of sophistication in responding to reviewer comments. Last but very much not the least I would like to thank Chris Francois for this outstanding guidance and input in the main stages of the research project; his expertise and enthusiasm are unparalleled and continue to be a great inspiration for me. I would also like to thank the

technical staff at WIMR for their assistance with the scans over the years.

At the School of Veterinary Medicine at the University of Wisconsin-Madison, Becky Johnson has been my rock from the very beginning thoughts about this research all the way through completion of the projects. Her knowledgeable and always prompt and efficient input as well as her 'can do' attitude were a key factor in making any of this possible and she provided an inspirational role model for me. I would like to thank Rebecca Stepien for her assistance with echocardiograms and critical input for manuscript writing. Marie Pinkerton for her fantastic assistance with the gross examinations. Mary Behan, Lauren Trepanier and Lisa Forrest as members of my research mentoring committee who encouraged and supported me to carve out my niche in the clinical and research world, which I am extremely grateful for.

In my current team I would like to thank Richard Lam and Chris Lamb for listening, their critical discussions and continuous inspiration.

I would like to provide a special thank you to the members of my PhD jury at the Faculty of Veterinary Medicine at the University of Ghent: Pascale Smets, Katrien Vanderperren, Catherine Delesalle and Ingeborgh Polis; as well as the Virginia Luis-Fuentes from the RVC and Chris Francois from UW Madison; the projects seemed completed and manuscripts had gone through many peer review rounds; yet the jury's detailed review and constructive input has provided the opportunity to give this work the final polish and has provided wonderful food for thought for possible future work.

Thank you note

I am grateful to my family Inge, Ulrich, Anneke, Martje, Lasse and Martin for encouraging and supporting me on my endeavors across the pond and channel. Also my friends in Germany, the USA, England and across the world who provided balance and the necessary sense of humor, and especially Jamie and LC for their company.

As this chapter of my education comes to a close, many new avenues have opened through the experiences made and more so through the inspirational people I met and continue to be surrounded by across the globe, leaving me excited for new endeavors.

Thank you all.

Randi Drees